

**UCSF**

**UC San Francisco Electronic Theses and Dissertations**

**Title**

Active-Site Inhibition of the Mammalian Target of Rapamycin

**Permalink**

<https://escholarship.org/uc/item/5bb6h5np>

**Author**

Feldman, Morris Eli

**Publication Date**

2009

Peer reviewed|Thesis/dissertation

Active-Site Inhibition of the Mammalian Target of Rapamycin

by

Morris Eli Feldman

DISSERTATION

Submitted in partial satisfaction of the requirements for the degree of

DOCTOR OF PHILOSOPHY

in

Biophysics

in the

GRADUATE DIVISION

of the

UNIVERSITY OF CALIFORNIA, SAN FRANCISCO

Copyright 2009  
by  
Morris Eli Feldman

To Chanda

## Acknowledgments

I thank my academic advisor, Dr. Kevan Shokat, for his support and guidance throughout my graduate school experience. I am grateful for Kevan's advice and constant willingness to help me think clearly and straightforwardly about scientific research. Kevan brought unflagging enthusiasm for my projects to all of our meetings together. His insights allowed me to appreciate the larger importance and value of my research. I also appreciate how Kevan demonstrated that engagement with science is compatible with a rich family life. Lab events with Kevan and his wife and children allowed me to see that it is possible to enjoy family and lead a world-class scientific lab at the same time.

In the Shokat lab, I was fortunate to work among a generous and kind group of talented people; I thank everyone in the Shokat lab. I am especially indebted to former lab members and graduate students Matt Simon and Zack Knight. Working with Matt provided an enlightening introduction to organic chemistry, a fruitful collaboration on the engrailed project and a continuing friendship. Working with Zack taught me how to approach scientific problems directly and efficiently. I thank Beth Apsel for her help with the TOR inhibitor project. Arvin Dar, Dorothea Fiedler, Dusty Maly and Eli Zunder provided invaluable scientific advice and were always available to exchange ideas or just relax and talk. I especially want to thank Valerie Ohman who keeps the Shokat lab functioning in multiple ways; I am grateful for Valerie's administrative support which allowed me to focus on science.

I thank Drs. Davide Ruggero and Jack Taunton for serving on my Thesis committee; their advice and insight was critical to my success. I was supported from 2006-2008 by a generous fellowship from the ARCS Foundation.

## **Chapter Specific Acknowledgments**

### **Chapter 1**

Chapter 1 has been submitted for inclusion in the book *PI3K in Health and Disease*. The book is being edited by Christian Rommel, Bart Vanhaesebroeck and Peter Vogt, and will be published by Springer New York, Heidelberg as a volume in their Current Topics CTMI series. Kevan Shokat coauthored this chapter.

### **Chapter 2**

Most of Chapter 2 was previously published in PLoS Biology, Feb. 10, 2009, 7(2):e38; Morris E. Feldman, Beth Apsel, Aino Uotila, Robbie Loewith, Zachary A. Knight, Davide Ruggero and Kevan M. Shokat. The sections dealing with PKC and RSK were not previously published (2.2.4 and 2.2.6). Beth performed the proliferation assays. Aino and Robbie performed the mTORC1 and mTORC2 assays. Zack, Davide and Kevan provided experimental advice and help writing and editing the manuscript. I performed all the other experiments in this chapter. I wish to thank Jack Taunton for suggesting the Sin1<sup>-/-</sup> experiments and Bing Su for providing the Sin1<sup>-/-</sup> MEFs. I thank Aya Pusic for providing primary MEFs and for experimental advice. I thank Arvin Dar for performing the JAK kinase assay, and William Weiss and Maria Barna for advice on this manuscript. I thank Chao Zhang and Dorothea Fiedler for providing BX-795.

### **Chapter 3**

Chapter 3 is based a paper published in Cell, May 19, 2006, 125(4):733-747; Zachary A. Knight, Beatriz Gonzalez, Morris E. Feldman, Eli R. Zunder, David D. Goldenberg, Olusegun Williams, Robbie Loewith, David Stokoe, Andras Balla, Balazs Toth, Tamas Balla, William A. Weiss, Roger L. Williams and Kevan M. Shokat. Zack synthesized and tested the kinase inhibitors, and performed the western blots. I performed the lipid labeling and glucose uptake assays.

### **Chapter 4**

Chapter 4 is based on a protocol published in Nature Protocols, Oct. 4, 2007, 2:2459-2466; Zachary A. Knight, Morris E. Feldman, Andras Balla, Tamas Balla and Kevan M. Shokat. Zack invented the membrane capture kinase assay and supervised the experiments. Adras and Tamas provided purified PI4-K. I designed and wrote the image analysis software called *Spot*. I also performed and analyzed the kinase assays shown in this chapter. We thank James Hurley for the generous gift of PI(5)P4-KII $\beta$ .

### **Chapter 5**

Chapter 5 was previously published in ACS Chemical Biology, Dec. 15, 2006, 1(12):755-760; Matthew D. Simon, Morris E. Feldman, Daniel Rauh, Ann E. Maris, David E. Wemmer and Kevan M. Shokat. Matt synthesized the modified DNA, performed the phage display selections and the EMSA assays. I performed the CD experiments and expressed untagged engrailed protein. Matt and I together performed the crysatalligraphy. Ann and David provided assistance with data collection and interpretation of the structure. Daniel helped with data collection and solving the structures. I thank Luke Rice and Chris Waddling for training and assistance with crystallography and structure refinement, the ALS 8.3.1

beamline, Janet Chung and Irene Gomez Pinto in the James lab at UCSF for assistance with large scale purification of the DNA strands, the Frankel lab at UCSF for use of their DNA synthesizer, Gregory Weiss and Ken Sato for assistance setting up the phage selections, Carl Pabo for a critical discussion of this work and Robert Grant for providing unpublished structure factors for the Q50A HD mutant.



# Active-Site Inhibition of the Mammalian Target of Rapamycin

Morris Eli Feldman

Cell signaling pathways direct cell growth and differentiation during development and the improper growth and proliferation of cancer cells largely by directing the transcription of genes and the translation of these transcripts into proteins. Chapters 1 and 2 address the cellular properties of a new class of inhibitors of the mammalian Target of Rapamycin (mTOR) kinase. mTOR sits at the hub of an important growth factor sensing pathway and its activity controls the translation of proteins important for cell growth and proliferation. Rapamycin is a small molecule natural product and an allosteric inhibitor of mTOR which is commonly used as an immunosuppressant and is being investigated for the treatment of cancer. Rapamycin has even been shown to extend lifespan in mice. New inhibitors that target the active site of mTOR have very different cellular effects than rapamycin and may prove useful in the treatment of human diseases and cancer. Chapter 3 examines the effects of isoform specific PI3-K inhibitors on insulin signaling. Discovering specific inhibitors of protein and lipid kinases requires testing many inhibitors against many kinases. When we assay kinases *in vitro*, we use a nitrocellulose membrane to capture the phosphorylated substrate. Chapter 4 describes an image analysis program specifically designed to analyze membrane capture kinase assays. Chapter 5 investigates the adaptability of the highly conserved interface between a homeodomain transcription factor and its target gene. Homeodomain transcription factors are highly conserved regulators of metazoan body development that control development by binding to DNA and regulating the transcription of their target genes. Adaptability of homeodomain transcription factor binding is examined in Chapter 5 through the biochemical, biophysical and structural characterization of an adapted mutant of the engrailed homeodomain.

# Contents

Acknowledgments . . . . .	iv
Abstract . . . . .	viii
Contents . . . . .	ix
List of Figures . . . . .	xiii
List of Tables . . . . .	xv
<b>1 Insights into mTOR Signaling From a New Generation of TOR Kinase Domain Inhibitors (TORKinibs)</b>	<b>1</b>
1.1 Two TOR Complexes and Rapamycin Studies in <i>S. cerevisiae</i> . . . . .	2
1.2 A Single Mammalian TOR in Two Complexes (mTORC1 & mTORC2) . . . . .	4
1.3 Regulation of AGC Kinases through Hydrophobic Motif Phosphorylation by TOR . . . . .	7
1.4 TORC1 Substrate 4EBP-1, a Key Regulator of Cap-Dependent Translation . . . . .	9
1.5 mTOR is Upstream and Downstream of Akt . . . . .	11
1.6 Rapamycin Induces Feedback Activation of Akt . . . . .	12
1.7 mTOR Inhibitors for Cancer . . . . .	13
1.8 Active-Site Inhibitors of mTOR . . . . .	15
1.9 TORKinibs and Akt . . . . .	16
1.10 Cell Proliferation and Rapamycin-Resistant mTORC1 . . . . .	20
1.11 Reexamination of Rapamycin's Inhibition of mTORC1 . . . . .	23
1.11.1 Models for Substrate Specific Inhibition of mTOR by Rapamycin . . . . .	24
1.12 Using Inhibitors of mTOR to Treat Cancer . . . . .	26
References . . . . .	27

<b>2 Active-Site Inhibitors of mTOR Target Rapamycin-Resistant Outputs of mTORC1 and mTORC2</b>	<b>38</b>
2.1 Introduction . . . . .	40
2.2 Results . . . . .	42
2.2.1 Specific Active-Site Inhibition of mTOR by the TORKinibs PP242 and PP30 . . . . .	42
2.2.2 Inhibition of mTORC2 and Akt Phosphorylation by TORKinibs . .	44
2.2.3 Akt Substrate Phosphorylation is Only Modestly Inhibited by PP242	48
2.2.4 PKC-HM Phosphorylation . . . . .	49
2.2.5 PP242 Does Not Have an Obvious Effect on Actin Stress Fibers . .	51
2.2.6 RSK Phosphorylation . . . . .	52
2.2.7 PP242 Inhibits Proliferation More Completely than Rapamycin . .	53
2.2.8 Rapamycin-Resistant mTORC1 . . . . .	54
2.2.9 Inhibition of Translation by TORKinibs . . . . .	58
2.2.10 Inhibition of mTORC1 and mTORC2 In Vivo . . . . .	61
2.3 Discussion . . . . .	62
2.4 Materials and Methods . . . . .	64
References . . . . .	70

<b>3</b>	<b>Molecular and Cellular Response to Isoform Specific PI3-K Inhibition</b>	<b>78</b>
3.1	Introduction . . . . .	79
3.2	PI3-K Inhibitors . . . . .	82
3.3	The Role of PI3-K Isoforms in Insulin Signaling . . . . .	83
3.4	p110 $\alpha$ Is the Primary Insulin Responsive PI3-K in Adipocytes and Myotubes	83
3.5	Functional Inhibition of Glucose Transport . . . . .	88
3.6	p110 $\alpha$ /p110 $\delta$ Set a Phenotypic Threshold in Myo- tubes, but not Adipocytes . . . . .	88
3.7	Materials and Methods . . . . .	90
	References . . . . .	93
<b>4</b>	<b><i>Spot</i>: Software for the Analysis of Kinase Assays</b>	<b>97</b>
4.1	Kinases and Kinase Inhibitors . . . . .	98
4.2	Potency and Selectivity of Kinase Inhibitors . . . . .	99
4.3	Low Throughput Kinase Assays . . . . .	100
4.4	Kinase Assays by Substrate Capture on Nitrocellulose . . . . .	101
4.5	Image Processing Approaches used by <i>Spot</i> . . . . .	102
	4.5.1 Finding the Spots . . . . .	103
	4.5.2 Refining the Spot Locations . . . . .	103
	4.5.3 Arraying the Spots . . . . .	104
4.6	Using <i>Spot</i> to Analyze a Kinase Assay . . . . .	105
4.7	Obtaining <i>Spot</i> . . . . .	107
	References . . . . .	107

<b>5</b>	<b>The Structure and Properties of a Re-Engineered Homeodomain Protein–DNA Interface</b>	<b>109</b>
5.1	Introduction . . . . .	110
5.2	Design and Synthesis of Derivatized Nucleosides . . . . .	112
5.3	Phage-Display Selections . . . . .	115
5.4	Biochemical Analysis of a Selected Mutant . . . . .	116
5.5	Structural Analysis of the Selected Mutant in Complex with DNA . . . . .	119
5.6	Analysis of the Stability of the Selected Mutant . . . . .	124
5.7	Conclusions . . . . .	125
5.8	Materials and Methods . . . . .	125
	References . . . . .	130
	<b>Appendix</b>	<b>135</b>
	Morpholino-Pyridine Inhibitors of the PI3-K Family . . . . .	135

# List of Figures

1.1	Representative Inhibitors of mTOR and/or PI3-K . . . . .	6
1.2	Important Phosphorylation Sites on Akt . . . . .	8
1.3	The PI3-K⇒Akt⇒mTOR Pathway . . . . .	11
2.1	Inhibition of mTORC2 by TORKinibs . . . . .	44
2.2	Time Course for Inhibition of Akt Phosphorylation by PP242 . . . . .	45
2.3	PP242 Does Not Inhibit T308-P on S473A Akt . . . . .	46
2.4	PP242 Does Not Inhibit Akt T308-P in Sin1 <sup>-/-</sup> . . . . .	47
2.5	Akt Substrate Phosphorylation upon PP242 Treatment . . . . .	48
2.6	PKC-HM Phosphorylation . . . . .	50
2.7	PP242 Does Not Affect Actin Stress Fibers . . . . .	51
2.8	mTOR Does Not Phosphorylate p90-RSK . . . . .	52
2.9	TORKinibs Block Cell Proliferation More Completely Than Rapamycin . . . . .	54
2.10	PP242 but Not Rapamycin Inhibits p-4EBP1 at T36/45 . . . . .	55
2.11	Like PP242, PP30 also Inhibits p-4EBP1 at T36/45 . . . . .	56
2.12	PP242 Inhibits Rapamycin-Resistant mTORC1 . . . . .	57
2.13	PP242 Inhibits Assembly of the Translation Initiation Complex . . . . .	58
2.14	PP242 Inhibits Cap-Dependent Translation . . . . .	59
2.15	PP242 Inhibits Protein Synthesis . . . . .	60
2.16	PP242 Inhibits Rapamycin-Resistant mTOR <i>In Vivo</i> . . . . .	61
3.1	Phosphoinositide Synthetic Pathway . . . . .	80
3.2	Inhibitors of p110 $\alpha$ Block Activation of Akt . . . . .	85
3.3	Deacylation of Phosphoinositides . . . . .	86
3.4	HPLC Analysis of Phosphoinositides . . . . .	86

3.5	Phosphoinositides in Cells Treated with PI3-K Inhibitors . . . . .	87
3.6	Glucose Uptake is Blocked by Inhibitors of p110 $\alpha$ but not p110 $\beta$ . . . . .	88
3.7	p110 $\beta$ Sets a Threshold for p110 $\alpha$ Activity in Myotubes . . . . .	89
4.1	Dose-Response Curve . . . . .	99
4.2	Example Lipid Kinase Assay on Nitrocellulose . . . . .	101
4.3	Substrate Specificity of Lipid Kinases . . . . .	102
4.4	Screenshot of <i>Spot</i> . . . . .	105
5.1	Homeodomain Mutants that Bind Modified DNA . . . . .	113
5.2	HD $\Phi$ Prefers Modified DNA . . . . .	117
5.3	Dissection of HD $\Phi$ . . . . .	118
5.4	HD $\Phi$ Requires High PEG-400 to Crystallize . . . . .	119
5.5	Structures of HD $\Phi$ Bound to Modified and Unmodified DNA . . . . .	121
5.6	Conformation of Lys50 . . . . .	122
5.7	HD $\Phi$ Prefers TAATCC <u>C</u> over TAATCG <u>C</u> . . . . .	123
5.8	Stability of HD Mutants . . . . .	124

## List of Tables

1.1	Properties of Selected TORKinibs . . . . .	21
2.1	<i>In Vitro</i> IC <sub>50</sub> Values for PP242 and PP30 . . . . .	43
2.2	PP242 and PP30 Inhibit mTORC1 and mTORC2 . . . . .	43
3.1	IC <sub>50</sub> Values for Selected PI3-K Inhibitors against Lipid Kinases . . . . .	82
5.1	Binding Affinities and Thermal Stabilities for HD Mutants . . . . .	118
5.2	Crystallographic Data and Refinement . . . . .	120



# Chapter 1

## Insights into mTOR Signaling From a New Generation of TOR Kinase Domain Inhibitors (TORKinibs)

### Abstract

mTOR (mammalian Target of Rapamycin) is the hub of the phosphoinositide 3-Kinase (PI3-K)⇒Akt⇒mTOR pathway, which is one of the most commonly mutated pathways in cancer. PI3-Ks and mTOR are related kinases which share an evolutionarily related kinase domain although the former is a lipid kinase and the latter is a protein kinase. As a result of their similar ATP sites, the prototypical PI3-K inhibitors LY294002 and wortmannin inhibit both kinases, although the compounds have been primarily thought of as inhibitors of PI3-Ks. The widespread use of these reagents to understand PI3-K signaling and the likelihood that many of their effects are confounded by dual inhibition of PI3-K and mTOR make it essential to develop selective mTOR inhibitors in part to understand the unique cellular effects of inhibition of this key downstream component in the growth factor pathway.

Rapamycin has historically provided a means for selective mTOR inhibition, yet it is not a typical ATP competitive inhibitor, making its effects difficult to reconcile with LY294002 and wortmannin. Several groups have recently reported pharmacological agents which inhibit mTOR but not PI3-K, providing a new pharmacological approach to selective mTOR inhibition. The TOR kinase domain inhibitors of mTOR have been termed TORKinibs to distinguish their mode of action from rapamycin and its analogs (rapalogs). These inhibitors bind to the ATP binding site of the kinase domain of mTOR and as a result inhibit both mTOR complexes, TORC1 (rapamycin sensitive) and TORC2 (rapamycin resistant). These molecules have allowed a reinvestigation of mTOR and in particular a reinvestigation of the mechanistic basis for incomplete proliferative arrest of cells by Rapamycin. A consensus has quickly emerged from the study of various TORKinibs that Rapamycin is ineffective at blocking cell proliferation because it only partially inhibits the activity of mTORC1. The profound anti-proliferative effect of TORKinibs, suggests that as the molecules enter the clinic they may be successful in the treatment of cancers where rapamycin has failed.

## **1.1 Two TOR Complexes and Rapamycin Studies in**

### ***S. cerevisiae***

Immediately after the discovery of TOR as the target of rapamycin in yeast [1, 2], it was recognized that some essential functions of TOR are resistant to rapamycin. TOR is a serine threonine kinase related to PI3-K. Yeast have two genes coding for TOR, TOR1 and TOR2 [3, 4]. Rapamycin blocks the growth of wild-type yeast, yet mutation of a conserved amino acid in either of the two yeast genes for TOR allows them to grow in the presence of rapamycin. The ability of rapamycin to block yeast growth also requires the presence of the proline isomerase FPR1. Rapamycin inhibits wild-type TOR by nucleating the formation of a ternary complex containing FPR1, rapamycin and TOR, and the formation of this complex

prevents TOR from phosphorylating its substrates. The resistance alleles of TOR1 and TOR2 prevent the formation of this inhibitory complex [5]. Yet TOR1 and TOR2 are not redundant because, of the two yeast TOR genes, TOR2 is essential, while TOR1 can be deleted. This presents a paradox because mutation of either TOR1 or TOR2 leads to rapamycin resistance, yet only TOR2 is essential. Resolving this paradox, led to the recognition that TOR possess rapamycin resistant functions.

Understanding how yeast can have two target of rapamycin genes, TOR1 and TOR2, yet only one of these genes, TOR2, is essential, revealed that some functions of TOR2 are resistant to rapamycin. The logic for this conclusion is as follows. TOR2 is an essential gene in yeast and if rapamycin inhibited all the functions of TOR2, then treating yeast with rapamycin would be equivalent to deletion of TOR2. Yet treating yeast with rapamycin and deleting TOR2 are not equivalent because rapamycin-resistance mutations in TOR1 allows yeast to grow in the presence of rapamycin, but not in the absence of the essential TOR2. Treating yeast with rapamycin is therefore not equivalent to deleting the essential TOR2. Thus TOR2 must have an essential function that is unaffected by rapamycin. Mutation of TOR1 is sufficient to allow yeast to grow in the presence of rapamycin, because mutant TOR1 can provide the essential TOR functions that are usually sensitive to rapamycin, while wild-type TOR2 continues to provide TOR functions that are resistant to rapamycin.

TOR was found to belong to two protein complexes TORC1 and TORC2 and the rapamycin resistant functions of TOR were ascribed to TORC2. While activity of both TOR complexes is required for yeast growth, rapamycin can only inhibit TORC1 [6]. TOR2 is essential because it can participate in either TOR complex, while TOR1 can only belong to the rapamycin sensitive TORC1 and is excluded from TORC2. Rapamycin-FPR1 inhibits TOR by binding to FKBP-Rapamycin Binding Domain (FRB) of TOR. TORC2 is resistant to rapamycin because one of the components of TORC2 likely occludes the FRB domain of TOR and prevents the binding of rapamycin-FPR1. Although these elegant yeast experiments

clearly established that TORC2 is resistant to rapamycin, they don't exclude the possibility that TORC1 also has rapamycin resistant functions. Even though it is widely assumed that rapamycin is a complete inhibitor of TORC1, the experiments in yeast that identified rapamycin-resistant functions of TORC2 leave open the possibility that TORC1 also has functions that are resistant to rapamycin, but are nonetheless dependent on catalytic activity rather than a scaffolding function.

## **1.2 A Single Mammalian TOR in Two Complexes (mTORC1 & mTORC2)**

TOR is conserved in all eukaryotes examined so far, including mammals. Mammals have a single TOR gene called mTOR for mammalian TOR [7–11], yet like yeast TOR, mTOR belongs to two protein complexes, mTORC1 and mTORC2 [6, 12, 13]. The major components of mTORC1 are mTOR, LST8 and Raptor. mTORC2 also contains mTOR and LST8, but instead of Raptor, mTORC2 contains Rictor and the additional component Sin1. Like yeast TORC1, mTORC1 is sensitive to rapamycin because rapamycin mediates the formation of an inhibitory complex between the FRB of mTOR and a proline isomerase FKBP-12, the mammalian ortholog of the yeast FPR1. Rapalogs such as CCI-779 [14] and RAD001 [15] are analogs of rapamycin that exhibit better pharmacokinetic properties than rapamycin, but share the same basic pharmacological mechanism. The discovery of rapamycin resistant functions of TOR was greatly facilitated by the discovery of TOR in yeast which has two genes for TOR, with only TOR2 participating in TORC2. If yeast had a single TOR gene like mammals, or if TOR1 and TOR2 were completely redundant, the discovery of rapamycin resistant functions of TOR would have been much more difficult. Conversely, the ease by which rapamycin resistant functions were associated with TORC2 and the finding that mTORC2 is similarly resistant to rapamycin has limited the search for rapamycin resistant

functions of mTORC1, and it has been widely assumed, without any experimental evidence, that rapamycin is a complete inhibitor of mTORC1. The key finding made clear by using TORKinibs, is that mTORC1 has important functions that are resistant to rapamycin, and rapamycin-resistance is therefore distributed between both mTOR complexes. By analogy, yeast TORC1 may also possess rapamycin resistant functions, though these have not yet been described.

mTORC2 is resistant to inhibition by rapamycin, although, as discussed below, long term treatment with rapamycin can prevent the assembly of mTORC2 in some cell lines [16]. The inhibition of mTORC2 assembly by rapamycin may explain why mTORC2 is resistant to acute treatment with rapamycin. Upon long term treatment with rapamycin, it is thought that newly synthesized mTOR binds to rapamycin—FKBP before it has a chance to be incorporated into mTORC2. Once bound by rapamycin—FKBP, mTOR can no longer be incorporated into mTORC2, probably because binding of rapamycin—FKBP to the FRB domain of mTOR prevents the subsequent association of one of the core components of mTORC2 such as Sin1 or Rictor. The binding of rapamycin—FKBP to mTOR therefore appears to be mutually exclusive to the binding of Sin1 and/or Rictor. Sin1 and/or Rictor probably use the FRB domain as part of their binding surface to mTOR and therefore they can't bind to mTOR when the FRB domain is already occupied. Conversely, Sin1 and/or Rictor probably prevent the association of rapamycin—FKBP with mTORC2 by covering the FRB domain of mTOR, thereby rendering mTORC2 resistant to rapamycin.

The two mTOR complexes regulate cell growth by phosphorylating members of the AGC (protein kinase A/protein kinase G/protein kinase C) kinase family [30]. mTORC1 also phosphorylates eIF4E-Binding protein (4EBP) [31, 32] a regulator of Cap-dependent translation, which is not an AGC kinase. Because rapamycin only inhibits mTORC1, it was widely assumed that active site inhibitors of mTOR (TORKinibs, Fig 1.1) would slow cell growth more effectively than rapamycin through dual inhibition of mTORC1/mTORC2 [33].

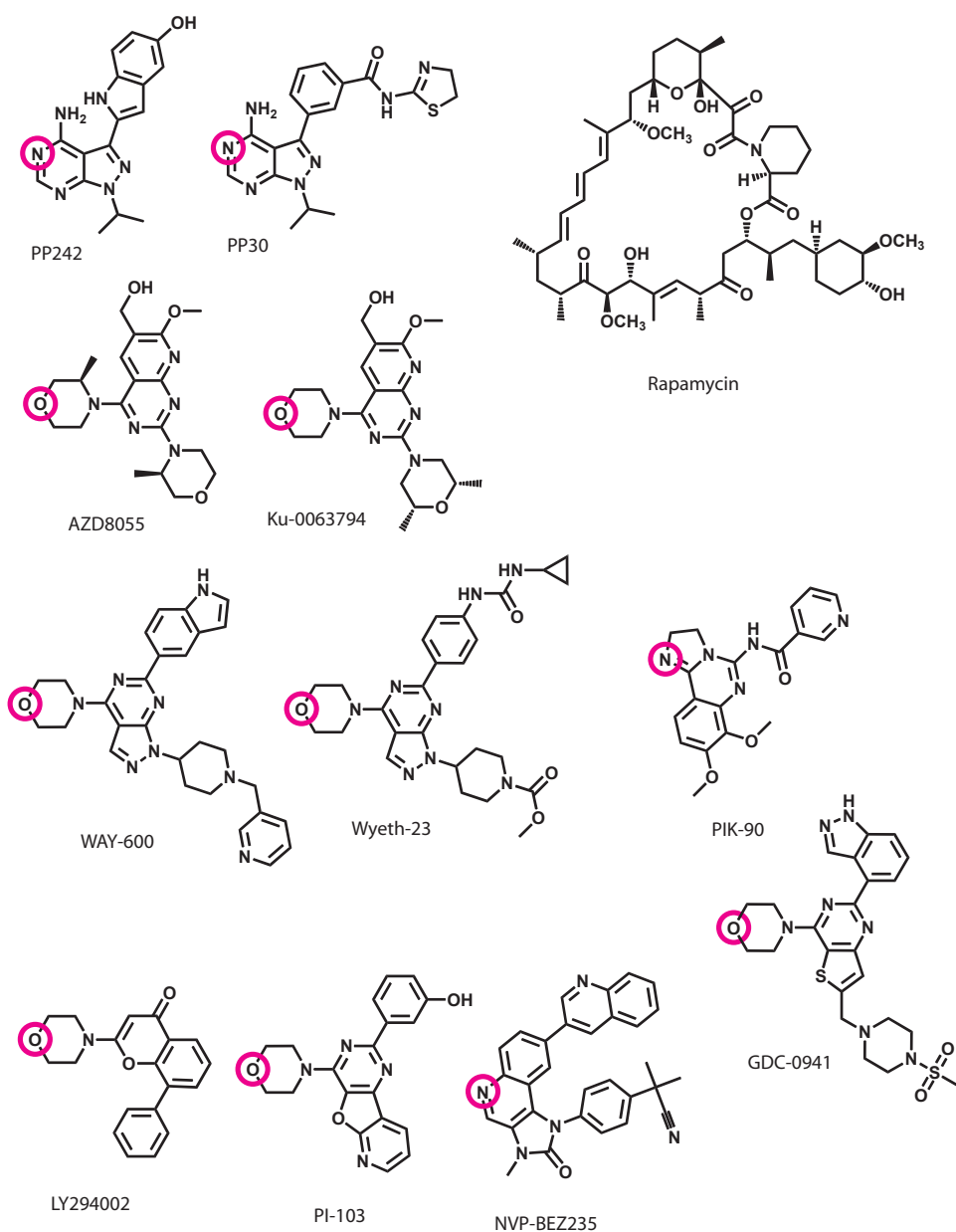


Figure 1.1: Representative inhibitors of mTOR and/or PI3-K.

Rapamycin is an allosteric inhibitor of mTOR, while the other inhibitors are active-site inhibitors of mTOR and/or PI3-K. The hinge-binding hydrogen bond acceptor is shown in red (see text). PP242, PP30 [17], AZD8055 [18], Ku-0063794 [19], WAY-600 [20, 21] and Wyeth-23 [22] are all TORKinibs, that is specific active-site inhibitors of mTOR. Torin1 could not be included because its structure has not been released [23]. LY294002 [24, 25], PI-103 [26] and NVP-BEZ235 [27] are dual inhibitors of mTOR and PI3-K. PIK-90 [26] and GDC-0941 [28, 29] are inhibitors of PI3-K which do not target mTOR.

Surprisingly, TORKinibs show enhanced antiproliferative activity as compared to rapamycin through their effect on mTORC1 [17, 19, 23]. TORKinibs revealed that rapamycin resistant functions of mTOR are not limited to mTORC2, and mTORC1 activity is partially resistant to rapamycin. These rapamycin resistant activities will be examined below after we discuss the known substrates of mTOR and its regulation as the hub of the PI3-K $\Rightarrow$ Akt $\Rightarrow$ mTOR pathway.

### **1.3 Regulation of AGC Kinases through Hydrophobic Motif Phosphorylation by TOR**

Regulation of AGC kinase phosphorylation by mTOR has been thoroughly reviewed [30], and we will focus our discussion on p70 S6-Kinase (S6K), Akt and Serum and Glucocorticoid induced Kinase (SGK) because these are the best validated AGC kinase substrates of mTOR and furthermore these three kinase are all activated by phosphorylation in response to growth factor stimulation of PI3-K. Active SGK and Akt phosphorylate a number of pro-survival and anti-apoptotic substrates such as FoxO, Glycogen Synthase Kinase (GSK) and BAD. S6K phosphorylates ribosomal protein S6, an important biomarker for PI3-K pathway activation. It also phosphorylates IRS1 resulting in feedback inhibition of PI3-K as discussed in section 1.6. In addition, S6K probably phosphorylates components of the preinitiation complex for protein synthesis, including eIF4B. Translation initiation is discussed below in section 1.4.

AGC kinases share a 30 amino acid stretch of sequence homology C-terminal to their kinase domains. At the end of this region of C-terminal homology, AGC kinases often contain a phosphorylation site within a stretch of hydrophobic residues called the hydrophobic motif (HM). Because its phosphorylation and activation is acutely sensitive to rapamycin, S6K was one of the earliest discovered substrates of mTOR. mTOR phosphorylates the hydrophobic motif of S6K at T389 [34]. Another important hydrophobic motif phosphorylation is S473

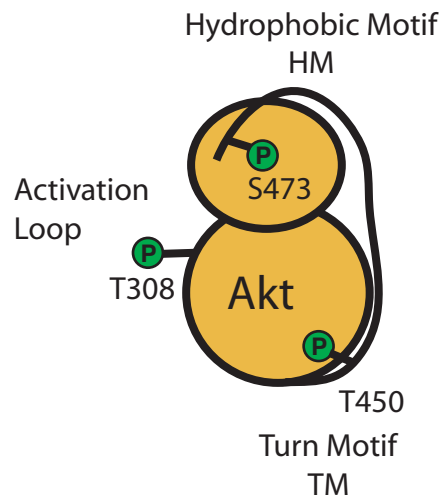


Figure 1.2: Important phosphorylation sites on Akt. Other AGC kinases are phosphorylated on homologous sites.

on Akt (Fig 1.2). Because the phosphorylation of Akt is not acutely sensitive to rapamycin, it was not initially recognized that mTOR was the kinase for S473-P on Akt and several other putative kinases for S473 on Akt were proposed [35]. RNAi targeting of Rictor revealed that the rapamycin-resistant mTOR Complex 2 is the HM kinase for Akt [36]. Cells from knockout mice lacking mTORC2 have confirmed that phosphorylation of Akt at S473 is dependent on mTORC2 [37–39]. SGK is highly related to Akt and it is also phosphorylated by mTORC2 [40]. Further experiments will be required to determine if the HMs of other AGC kinases are also phosphorylated by mTOR. These studies will be greatly helped by the ability to acutely inhibit mTOR using TORKinibs.

HM phosphorylation by mTOR can directly increase the activity of AGC kinases. Once phosphorylated, the hydrophobic motif of an AGC kinase binds to a docking site on the N-lobe of its own kinase domain. Binding of a phosphorylated hydrophobic motif to the kinase N-lobe, orders the kinase active site [41] and increases the activity of the kinase by 5 to 10 fold in the case of Akt [42].

HM phosphorylation is however, not the most important determinant of kinase activity. Activation loop phosphorylation by PDK1 is more critical for kinase activity than hydropho-



bic motif phosphorylation (Fig 1.3). For example, the activity of Akt with T308 (Fig 1.2) mutated to alanine is 100 fold lower than the wild-type kinase [42]. mTOR however, cooperates with PDK1 to activate AGC kinases. Unlike most AGC kinases, PDK1 lacks the C-terminal hydrophobic motif. Despite lacking a hydrophobic motif, PDK1 still possesses a binding site for phosphorylated hydrophobic motifs on the N-lobe of its kinase domain. The hydrophobic motif binding site in PDK1 is called the PIF pocket and it can interact with the phosphorylated hydrophobic motifs of its kinase substrates. For example, hydrophobic motif phosphorylation of S6K by mTOR creates a binding site for PDK1 on S6K, thereby priming S6K for activation loop phosphorylation by PDK1. Using cells in which the PDK1 PIF pocket was mutated to no longer bind to phosphorylated HMs, it was found that S6K, RSK and SGK all require prior hydrophobic motif phosphorylation to prime them for activation loop phosphorylation by PDK1 [43]. In contrast, phosphorylation of the activation loop of Akt at T308 was retained in cells with the mutant PIF pocket, suggesting that activation loop phosphorylation Akt by PDK1 does not require priming hydrophobic motif phosphorylation by mTOR. The turn motif (TM) is a third conserved phosphorylation site on AGC kinases. The TM is located between the kinase domain and the HM. Phosphorylation of the TM stabilizes the binding of the HM to the kinase N-lobe [44]. TM phosphorylation of Akt at T450 (Fig 1.2) is absent in cells that lack mTORC2. Lacking TM phosphorylation, Akt is unstable in these cells and associates chaperones such as HSP90. Unlike the highly regulated HM and activation loop phosphorylations, TM phosphorylation is constitutive [45, 46].

## **1.4 TORC1 Substrate 4EBP-1, a Key Regulator of Cap-Dependent Translation**

In addition to S6K, mTORC1 is known to phosphorylate 4EBP, a key regulator of cap-dependent translation [31, 32]. Most proteins are translated from mRNAs through 5' cap-

dependent translation rather than internal ribosome entry site (IRES) dependent translation [47]. The up regulation of cap-dependent translation is emerging as a key feature of the oncogenic program resulting from oncogene/tumor suppressor induced activation of the Ras $\Rightarrow$ MAPK and the PI3-K $\Rightarrow$ Akt $\Rightarrow$ mTOR pathways which are the two most commonly activated signaling pathways in cancer [48–50]. 4EBP binds to the major mRNA 5' cap binding protein eIF4E and inhibits the ability of eIF4E to nucleate the formation of the translation preinitiation complex. Phosphorylation of 4EBP by mTOR releases 4EBP from eIF4E, relieving the inhibition of eIF4E by exposing a surface on eIF4E for the binding of eIF4G (Fig 1.3). eIF4G is a large scaffolding protein which recruits the remaining preinitiation complex members including eIF3, the 40S subunit of the ribosome and a helicase composed of eIF4A and the helicase cofactor eIF4B. Once formed, the entire preinitiation complex, known as eIF4F, scans forward through the 5' untranslated region (UTR) of the mRNA to find the start codon and begin translating the mRNA. The helicase activity provided by eIF4A and eIF4B allows the preinitiation complex to unwind the secondary structure of 5' UTRs that would otherwise stall the scanning process and preventing translation initiation. Some messages are poorly translated by resting cells because they contain highly structured 5' UTRs that are difficult to unwind. For example, the 5' UTRs of some key oncogenic proteins such as VEGF, ODC, HIF1 $\alpha$  are highly structured [51]. The 5' UTRs of these messages probably evolved as an extra barrier to their translation so that these oncogenic messages would not be inappropriately translated by resting cells. Translation of these oncogenic messages likely requires high levels of translation initiating activity which may account for the need to upregulate cap-dependent translation as part of the oncogenic program downstream of oncogenic events within the RAS $\Rightarrow$ MAPK and PI3-K $\Rightarrow$ Akt $\Rightarrow$ mTOR pathways.

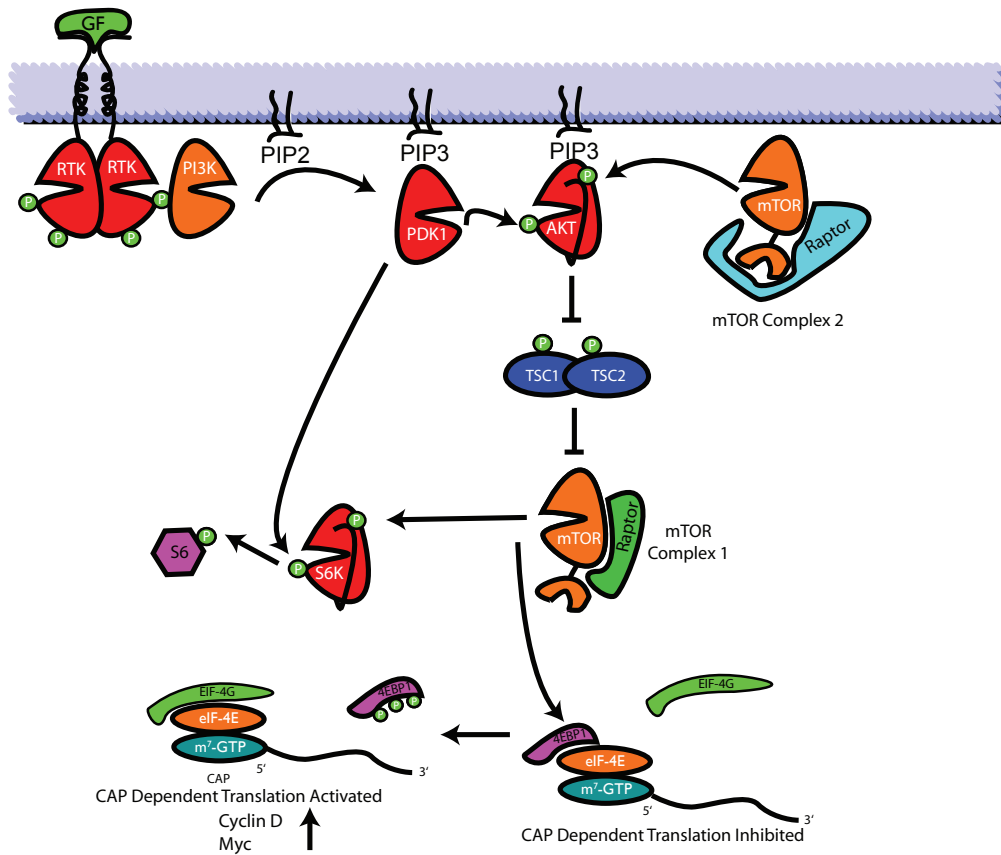


Figure 1.3: The PI3-K⇒Akt⇒mTOR pathway.

Note especially that mTORC2 is upstream of Akt, while mTORC1 is downstream and activated by Akt.

## 1.5 mTOR is Upstream and Downstream of Akt

The discovery that Akt is phosphorylated by mTORC2 was exciting because mTORC1 was already known to be regulated in part by Akt activity (Fig 1.3). The regulation of Akt by mTORC2, therefore places mTOR both upstream and downstream of Akt within the critical oncogenic PI3-K⇒Akt⇒mTOR pathway. Prior to the discovery of Akt's regulation by mTORC2, an analysis of the molecular basis of Tuberous Sclerosis had shown that Akt is a major regulator of mTORC1 [52]. Tuberous sclerosis is a genetic disorder caused by the loss of either of the tuberous sclerosis genes TSC1 or TSC2. Loss of TSC1 or TSC2 causes

the growth of benign tumors throughout the body and it characterized at the molecular level by constitutively active mTORC1 leading to the hyperphosphorylation of S6K, S6 and 4EBP. The TSC1/2 complex is therefore a negative regulator of mTORC1. TSC2 is a GTPase activating protein (GAP) for the GTPase Rheb which when bound to GTP is an activator of mTORC1. TSC2 promotes the hydrolysis GTP in Rheb to GDP. TSC2 is not stable on its own, but must form a complex with TSC1 in order to be stable. Loss of either TSC1 or TSC2 therefore leads to an accumulation of GTP::Rheb which activates mTORC1. TSC2 is a substrate of Akt. Phosphorylation of TSC2 by Akt inhibits the ability of TSC2 to act as a GAP for Rheb and similar to loss of the TSC1/2 complex, leads to an accumulation of GTP::Rheb and activation of mTORC1. In wild-type cells with an intact TSC1/2 complex, Akt activates mTOR by phosphorylating TSC2, while in cells that lack TSC1/2, mTORC1 is constitutively activated even in the absence of growth factor stimulation of Akt through upstream PI3-K activation.

## **1.6 Rapamycin Induces Feedback Activation of Akt**

In addition to providing insight into the regulation of mTORC1 by Akt, studying Tuberous Sclerosis also revealed a mechanism by which activated mTORC1 inhibits upstream activation of PI3-K and Akt. In cells lacking the TSC1/2 complex, mTORC1 is constitutively active and S6K is constitutively phosphorylated as discussed above. In addition to hyperactivation of mTORC1 and its downstream substrates, cells lacking TSC1/2 show a deficit in Akt phosphorylation and activity [53]. Conversely, cells treated with the mTORC1 inhibitor rapamycin, which strongly inhibits S6K phosphorylation by mTORC1, often show an increase in the phosphorylation of Akt [54]. Active S6K phosphorylates IRS1, an important adapter that allows certain receptor tyrosine kinases such as the insulin receptor and the insulin like growth factor receptors (IGF) to activate PI3-K. Serine/Threonine phosphorylation of

IRS1 by S6K targets IRS1 for degradation and therefore inhibits the activation of PI3-K by RTKs such as the insulin receptor and IGF-1 [55]. Highly active S6K in TSC1/2 null cells phosphorylates IRS1, targeting IRS1 for degradation and limiting the ability of some RTKs to activate PI3-K and Akt. By inhibiting mTORC1 and S6K, rapamycin has the opposite effect of relieving feedback inhibition of IRS1 from S6K. Rapamycin treatment therefore often results in more efficient activation of PI3-K by RTKs, leading to hyperphosphorylation of Akt. Because IRS1 scaffolds the upstream activators of the MAPK pathway including Grb2, SOS and Ras, rapamycin treatment can also cause hyperactivation of the MAPK pathway [56, 57]. Hyperactivation of both Akt and the MAPK pathway in response to rapamycin treatment for cancer may actually accelerate the progression of the cancer in some cases.

## **1.7 mTOR Inhibitors for Cancer**

The oncogenic potential of the PI3-K $\Rightarrow$ Akt $\Rightarrow$ mTOR pathway became clear as the PIP3 phosphatase PTEN was identified as the second most commonly mutated tumor suppressor [58] after p53 and sequencing efforts identified activating mutations in PI3-K driving a wide variety of cancers [59]. The activation of mTORC1 downstream of PI3-K, suggested that mTOR inhibitors and in particular inhibitors of mTORC1, such as rapamycin, would be effective anti-cancer therapies. Several findings challenged this assumption. First of all, although rapamycin and analogs of rapamycin developed to alter the pharmacokinetic properties of rapamycin (rapalogs) have been evaluated for the treatment of a broad variety of cancers, so far rapamycin has only been approved for the treatment of renal cell carcinoma. Rapamycin's lack of broad efficacy as a cancer therapeutic was generally thought to stem from its inability to inhibit mTORC2, however in some cell lines, long-term rapamycin treatment appeared to act as a dual inhibitor of mTORC1/2, by blocking the assembly

mTORC2 in addition to directly inhibiting mTORC1 [16]. The ability of rapamycin to act as a dual inhibitor of mTORC1/2 challenged the explanation that it was a poor anti-cancer therapeutic because it didn't inhibit mTORC2 and suggested that despite the compelling logic of the PI3-K $\Rightarrow$ Akt $\Rightarrow$ mTOR pathway, mTOR might not be a good target for cancer treatment. Furthermore the fact that rapamycin is extremely well tolerated when taken as an immunosuppressant [60] suggested that it did not possess the type of potent anti-proliferative activities of an anti-cancer therapeutic.

Although the failure of rapamycin to effectively treat many types of cancers suggested that mTOR might not be a good target for cancer therapy, the surprising *in vitro* efficacy of inhibitors targeting both PI3-K and the active site of mTOR challenged this view [27, 61]. At the very least, these studies argued that inhibition of mTOR in addition to PI3-K might be important in the treatment of cancer and they left open the possibility that active site inhibitors of mTOR alone might be powerful anti-proliferative agents. Although mTOR is a protein kinase, it is a member of the PI3-K family of lipid kinases and small molecule inhibitors of the active-site of PI3-K often inhibit the active site of mTOR as well. Indeed, the classic pan-PI3-K inhibitor LY294002 (Fig 1.1) inhibits both mTOR and PI3-K with similar potency [24]. Many of the cellular functions attributed to PI3-K using LY294002 may therefore be due to active-site inhibition of mTOR or at least dual inhibition of PI3-K and mTOR. A structurally similar but much more potent PI3-K inhibitor, PI-103, also inhibits PI3-K and mTOR [26] and the clinical PI3-K inhibitor NVP-BEZ235 also targets mTOR [27]. PI-103 showed surprising efficacy in the inhibition of glioma cell proliferation *in vitro* through its dual inhibition of PI3-K and mTOR [61]. In this study, PI-103 was better at inhibiting cell proliferation than the pure PI3-K inhibitor PIK-90. It was unclear however how a pure active-site inhibitor of mTOR would compare with a pure PI3-K inhibitor.

## 1.8 Active-Site Inhibitors of mTOR

The placement of mTORC2 upstream of Akt and mTORC1 downstream of Akt suggested that an active-site inhibitor which targets mTORC1 and mTORC2 should be efficacious in cancer. Although long term treatment with rapamycin can inhibit mTORC2 [16], this affect is limited to a minority of cell lines and it is unclear whether it could be relied on to inhibit mTORC2 in cancer cells *in vivo*. Because of the highly compelling pathway logic and as a hedge against the possibility that dual PI3-K/mTOR inhibitors might be poorly tolerated in the clinic, much effort was recently invested to develop specific inhibitors of the mTOR active site. These efforts are coming to light with the recent release of multiple papers documenting the effect of specific active-site inhibitors of mTOR [17–23], see also Chapter 2.

Structures of these inhibitors are shown in Figure 1.1. Except for the pyrazolopyrimidines, PP242 and PP30 (Chapter 2, all the ATP site inhibitors of mTOR described so far share the aryl-morpholine pharmacophore of LY294002. The inhibitors from Astra-Zeneca (AZD8055 and Ku-0063794) contain two morpholines. It is interesting that the morpholine continues to be a critical pharmacophore in both the AZ and Wyeth series, which can be traced directly back to Eli Lilly's initial 1994 report of LY294002 [25]. Just two years after the first report of LY294002, Abraham and colleagues reported that LY294002 was also an inhibitor of mTOR [24]. The fact that it required almost 13 years for selective mTOR inhibitors to be reported is quite surprising considering the increasing appreciation of the importance of mTOR in the past decade. One potential explanation for this slow pace of inhibitor discovery was the availability of rapamycin and its amazing potency and selectivity for mTOR, and the difficulty of carrying out biochemical assays of mTOR kinase activity in a highthroughput assay.

Although no crystal structure has been reported for the kinase domain of mTOR, based on the published structure of LY294002 and other drugs bound to the related PI3-K $\gamma$  [62] we can make a tentative guess about the orientation of each drug in the mTOR binding site. A key feature is an H-bond acceptor (morpholine ether oxygen circled in red) in the AZ and Wyeth series, which is predicted to bind to the N-H bond of Val2240 in mammalian mTOR. Interestingly, the morpholines in the AZ series contain alkyl substitutions compared to LY294002 which may enhance binding to mTOR or diminish binding to the PI3-K. The binding orientation of PP242 can be predicted based on a similar analysis to structures of the related PP102 bound to PI3-K $\gamma$ . In this case the pyrimidine ring N-1 supplies the H-bond acceptor function of the morpholine ether oxygen in the other series. In the PP242 series, the hydroxy-indole function exerts critical interactions in the so-called affinity pocket of mTOR. Small modifications of this heterocycle, cause severe diminution of binding affinity or selectivity within the PI3-K/mTOR family [63].

Initial work with the active site inhibitors *in vitro* quickly led to a re-evaluation of the mechanism of action of rapamycin and a new understanding for the partial effect of rapamycin as an anti-proliferative [17, 19, 23] and anti-cancer agent [18, 20–22]. These studies revealed that the problem with rapamycin was not that it missed mTORC2, but that it only partially inhibits mTORC1. This has refocused our attention on the importance of mTORC1, 4EBP1 and protein translation in the treatment of cancer.

## 1.9 TORKinibs and Akt

Because it was expected that TORKinibs would differ from rapamycin in their ability to inhibit mTORC2, the effect of TORKinibs on the mTORC2 dependent phosphorylation of Akt phosphorylation at S473 was examined. S473-P is potently inhibited by TORKinibs in all cell lines examined so far [17–23]. Preliminary *in vivo* experiments, showed inhibition of



S473-P in fat and liver of mice following acute administration of PP242 [17]. Unexpectedly, S473-P in skeletal muscle appeared resistant to inhibition by PP242. Consistent with the possible resistance of muscle S473-P to TORKinibs, a muscle specific knockout of the rictor, which is required for the formation of mTORC2, shows only partial rather than complete loss of S473-P [64]. These results suggest that in muscle a kinase other than mTOR, such as DNA-PK, might play a role in the phosphorylation of Akt on S473, but these tissue specific effects of TORKinibs need to be repeated using multiple inhibitors.

When studies using RNAi discovered that mTORC2 was the kinase for S473-P on Akt, it was seen that disabling mTORC2 using RNAi also caused a loss of T308-P in most of the cell lines examined [36, 65]. In contrast, subsequent genetic knockout of integral mTORC2 components such as Rictor, SIN1 and LST8 led to inhibition of S473-P with no effect on T308-P [37–39]. In MEFs derived from mice lacking mTORC2, both basal and growth factor stimulated phosphorylation of T308-P was largely unperturbed. Closer examination revealed that, in addition to S473, these cells also lacked TM phosphorylation of Akt at T450. Loss of TM-P reduced the stability of Akt leading to its association with HSP90 and causing its expression level to be somewhat variable [45, 46].

Whereas, all current TORKinib studies see potent *in vitro* inhibition of S473-P, the influence of TORKinibs on T308-P varies. Inhibition of mTOR using the TORKinibs PP242 and PP30, led to a reduction in T308-P, but the EC<sub>50</sub> for inhibition of T308-P was 4-fold weaker than for inhibition of S473 [17]. To confirm that the weaker inhibition of T308-P wasn't due to an off target of PP242 or PP30, it was shown that these TORKinibs had no effect on T308-P in Sin1<sup>-/-</sup> cells. Sin1<sup>-/-</sup> cells lack mTORC2 and S473-P, but retain T308-P. Because these cells lack the TORKinib target mTORC2 and already show a complete loss of Akt S473-P, the only way TORKinibs could affect T308-P is through inhibition of an off target. The TORKinibs, PP242 and PP30 had no effect on T308-P in Sin1<sup>-/-</sup> cells, while in matching wild-type cells with mTORC2 and S473-P they inhibited

S473-P and T308-P. In a conceptually identical experiment, the TORKinib Torin1 had no effect on the phosphorylation of T308 in *mLST8<sup>-/-</sup>* cells which like *Sin1<sup>-/-</sup>*, also lack mTORC2 [23]. Furthermore, another TORKinib, Ku-0063794, had no effect on T308-P in *Rictor<sup>-/-</sup>*, *mLST8<sup>-/-</sup>* and *Sin1<sup>-/-</sup>* cells which all lack mTORC2, but it inhibited T308-P in wild-type MEFs where mTORC2 is intact [19]. The lack of an effect of TORKinibs on T308-P in cells lacking mTORC2 suggests that in WT cells the inhibition of T308-P is due indirectly to inhibition of mTORC2's phosphorylation of S473-P of Akt.

In wild-type cells where mTORC2 is present, S473-P and T308-P appear to be somewhat tethered, such that inhibition of S473-P also inhibits T308-P, though to a lesser extent [66]. The partial dependence of T308-P on S473-P might be because PDK1 finds it easier to phosphorylate Akt when it is already phosphorylated on T308, perhaps due to an interaction between the PIF pocket of PDK1 and S473-P. Alternately S473-P might protect T308-P from dephosphorylation. In either case, in cells that lack mTORC2, the dependence of T308-P on S473-P is apparently lost through an unknown compensatory mechanism.

The pharmacological finding that T308-P is linked to S473-P underscores the importance of deciphering the logic of complex kinase signaling pathways using specific kinase inhibitors rather than genetic knockouts. Genetic knockouts of a key survival kinase such as mTORC2, often generate a complex phenotype that is not due primarily to loss of the kinase activity being studied [67]. Instead the phenotype generated by a kinase knockout is often an amalgam of effects due to loss of the scaffolding role of the kinase protein itself and compensatory signaling changes within the kinase network. Together these effects obscure the phenotype that would be seen if the kinase activity were acutely inhibited. Important aspects of kinase signaling often become apparent only once a network is probed using specific inhibitors. Even studying kinase signaling using specific inhibitors is not without peril because when a kinase inhibitor binds into the active site of a kinase it alters the conformation of the kinase, sometimes leading to unexpected consequences. For instance

the binding of inhibitors to the active site of Akt alters the conformation of Akt leading to massive hyperphosphorylation of Akt on both S473 and T308 [68]. If simply altering the conformation of a kinase using a small molecule can distort the logic of a kinase pathway, removing a kinase entirely may have a correspondingly greater effect on a kinase pathway.

Although the studies mentioned above with PP242, PP30 and Ku-0063794 found a tethering between S473-P and T308-P in a variety of wild-type cell lines [17, 19] and even *in vivo* [17], studies using AZD8055 [18] and WAY-600 [21] see a striking lack of effect of TORKinibs on T308-P, even at concentrations much higher than required to affect S473-P. Whether the differences are due to inherent differences in the pharmacological properties of the molecules or simply differences in experimental setup such as choice of cell line will require directly comparing all the current TORKinibs in a side by side experiment. Comparing the effects from multiple compounds with different structures that all target a single kinase is a very effective way to avoid pitfalls when using kinase inhibitors. Although the results obtained with a single compound might be spurious because they are due to the inhibition of a known or perhaps unknown off target, the compendium of results obtained using two or more compounds increases the likelihood that the effects seen in the experiment are due to inhibition of the intended target. In this regard it is scientifically irresponsible when research with new pharmacological agents is presented without releasing the structure of these new molecules [23]. The report of the activity of a small molecule, without revealing its structure prevents the fundamental requirement of all science, the replication of results. As testament to this principle, a subsequent study using Torin1, whose structure has not been published, used PP242 to buttress their findings [69]. Luckily for those in the mTOR field, multiple TORKinibs have been structurally reported (Fig 1.1), even two from major pharmaceutical companies. Just as most journals require the release of protein structure coordinates, all journals must require the release of the structure of pharmacological agents used in a study. The patent process allows for the free circulation of new inventions while

protecting commercial interests. Rather than opposing disclosure of chemical structures in scientific literature, authors should secure patent protection for their inventions prior to publication if they have commercial interests.

Despite differing in their affect on T308-P, all TORKinibs cause some inhibition of Akt substrate phosphorylation. In the case of PP242 and Ku-0063794, their inhibition of Akt substrate phosphorylation generally tracks with their inhibition of Akt at T308 [17, 19]. Using AZD8055 and WAY-600, although no inhibition of Akt T308-P was seen, these molecules inhibited Akt substrate phosphorylation at concentrations slightly higher than those required to inhibit S473 [18, 21].

## **1.10 Cell Proliferation and Rapamycin-Resistant**

### **mTORC1**

Across multiple cell lines, rapamycin causes a potent ( $EC_{50}$  1-10 nM), but only partial (40-60%) inhibition in cell proliferation. Prior to the introduction of TORKinibs, it was assumed that rapamycin could only partially inhibit cell proliferation because it could not inhibit mTORC2. Reassuringly, cell proliferation is in most cases completely inhibited by TORKinibs, at concentrations that are not substantially higher than the biochemical  $EC_{50}$  for inhibition mTOR as judged by the phosphorylation of S473 on Akt or T389 on S6K. Surprisingly however, the proliferation of cells lacking mTORC2, including *Sin1<sup>-/-</sup>* [17], *Rictor<sup>-/-</sup>* [23] and *mLST8<sup>-/-</sup>* [19] MEFs is only partially sensitive to rapamycin, while TORKinibs fully inhibit the proliferation of these cells (Table 1.1). The presence of mTORC2 is therefore not required for rapamycin and a TORKinib to have a differential effect on cell proliferation, suggesting that rapamycin and TORKinibs differ in their effects on mTORC1, and indicating that important activities of mTORC1 are resistant to rapamycin.

Compound	Chemical Class	<i>In Vitro</i> IC <sub>50</sub> $\mu$ M ([ATP] $\mu$ M)		Cell Proliferation		Reference
		mTOR	p110 $\alpha$	EC <sub>50</sub> $\mu$ M	Cell Line	
PP242	Pyrazolopyrimidine	0.008 (10)	1.96 (10)	0.6	WT & Sin1 <sup>-/-</sup> MEFs	[17]
PP30	Pyrazolopyrimidine	0.080 (10)	3 (10)	6	WT & Sin1 <sup>-/-</sup> MEFs	[17]
Torin1	Unknown	0.003 (10)	1.8 (10)	< 0.25	WT & Rictor <sup>-/-</sup> MEFs	[23]
Ku-0063794	Morpholino-pyridopyrimidine	0.010 (100)	> 10 (1000)	< 3	WT & mLST8 <sup>-/-</sup> MEFs	[19]
AZD8055	Morpholino-pyridopyrimidine	0.00013 (20?)	3.6 (20?)	0.05 0.05 0.02	U87-MG A549 H838	[18]
WAY-600	Morpholino-pyrazolopyrimidine	0.009 (100)	1.96 (100)	0.6–2.5	Multiple Tumor Lines	[20, 21]
Wyeth-23	Morpholino-pyrazolopyrimidine	0.00045 (100)	0.7 (100)	0.04	LNcap	[22]

Table 1.1: Properties of selected TORKinibs.

S6K and 4EBP1 are the best characterized substrates of mTOR and naturally their phosphorylation was examined in cells treated with TORKinibs. Surprisingly, whereas S6K-P was potently inhibited by rapamycin and TORKinibs, 4EBP1 phosphorylation was fully inhibited only by TORKinibs, but not rapamycin. A pair of threonine phosphorylations on 4EBP1, T37/46, which were known to be quite resistant to rapamycin [70, 71], were found to be highly sensitive TORKinibs. It had been previously asserted that because T37/46 were constitutively phosphorylated they were therefore partially resistant to rapamycin, perhaps because only a small amount of mTOR activity might be required to maintain their phosphorylation [72]. The sensitivity of T37/46-P and S6K-P to TORKinibs is nearly identical however, suggesting that rapamycin is simply not a good inhibitor of mTOR's phosphorylation of 4EBP1 at T37/46. In this way, rapamycin is acting as a substrate specific inhibitor of mTOR in that it inhibits mTOR's phosphorylation of S6K but not 4EBP. 4EBPs have a major role in the regulation of cap-dependent translation and across a wide range of assays it was found that treating cells with TORKinibs, inhibited cap-dependent translation and total protein synthesis to a much greater extent than rapamycin. The greater inhibition of 4EBP-P and cap-dependent translation could therefore account for the much greater ability of TORKinibs to block cell proliferation when compared with rapamycin. It is also possible that other substrates of mTORC1 are, like 4EBP, resistant to rapamycin and the combined inhibition of 4EBP-P as well as other rapamycin-resistant substrates of mTORC1 accounts for the profound antiproliferative effects of TORKinibs. In addition, studies showing that TORKinibs can inhibit cell proliferation to a greater extent than rapamycin even in the absence of mTORC2, were only performed on MEFs. It is likely that in other cell types and especially in cancer cells with activated PI3-K and Akt, that the full inhibition of mTORC1 by a TORKinib will cooperate with inhibition of mTORC2 to fully inhibit cell proliferation. Luckily, by targeting the active site of mTOR, TORKinibs naturally inhibit the all the activity of mTORC1 and mTORC2.

Despite the general finding that rapamycin is only a partial inhibitor of cell proliferation, at very high concentrations, rapamycin is able to completely inhibit proliferation of some cell lines [73]. Typically, cell proliferation slows by approximately 40% in cells treated with 1-10 nM rapamycin. Increasing the concentration of rapamycin above 10 nM causes no further decrease in cell proliferation until around 10-50  $\mu$ M when cell proliferation is suddenly affected once again and cell proliferation is often fully inhibited by these micromolar concentrations of rapamycin. Surprisingly the inhibition of cell proliferation by micromolar concentrations of rapamycin is independent of FKBP12. Micromolar concentrations of rapamycin therefore inhibit mTOR through a distinct mode of action from nanomolar rapamycin which depends on binding FKBP12 to mTOR. Like the inhibition of mTOR by TORKinibs, micromolar, but not nanomolar rapamycin causes a large decrease in protein translation. Micromolar rapamycin and TORKinibs both cause a strong decrease in protein synthesis and cell proliferation suggesting that micromolar rapamycin, like TORKinibs, may be acting as a complete inhibitor of mTORC1. Reaching micromolar concentrations may be possible and actually achieved when cancer patients are treated with rapalogs having enhanced pharmacokinetic properties such as RAD001. It is possible that some of the promising effects observed with rapalogs as anti-cancer agents may depend on reaching micromolar rather than nanomolar concentrations with these agents.

## **1.11 Reexamination of Rapamycin's Inhibition of mTORC1**

At nanomolar concentrations, rapamycin is a substrate specific inhibitor of mTORC1, fully inhibiting S6K while only partially inhibiting 4EBP. Furthermore, protein translation is largely unaffected by nanomolar rapamycin and cell proliferation is only partially inhibited. In contrast, TORKinibs and probably micromolar rapamycin act as direct and complete

inhibitors of mTORC1. Through complete inhibition of mTORC1, TORKinibs cause full dephosphorylation of 4EBP, strong inhibition of protein synthesis and full inhibition of cell proliferation. It is unclear exactly how rapamycin—FKBP binding to the FRB domain of mTOR prevents mTOR from phosphorylating S6K. Similarly, it is unclear how 4EBP phosphorylation can escape inhibition by rapamycin. However, knowing that rapamycin inhibits mTORC1 in a substrate specific fashion, helps to narrow the possible models for how rapamycin inhibits mTOR. Several models are presented below to explain the partial inhibition of mTORC1 by rapamycin.

### **1.11.1 Models for Substrate Specific Inhibition of mTOR by Rapamycin**

One model for the inhibition of S6K phosphorylation by mTOR asserts that rather than directly inhibiting the kinase activity of mTOR, binding of rapamycin—FKBP to the FRB domain of mTOR occludes the association of mTOR with its substrates [5]. Within the framework of this model, the inhibition of S6K, but not 4EBP phosphorylation by rapamycin can be explained if binding of rapamycin—FKBP to the FRB domain of mTORC1 only interferes with the binding and phosphorylation of S6K, but has a minimal effect on the phosphorylation of the smaller substrate 4EBP.

Just as Rictor or Sin1 probably protects mTORC2 from inhibition by rapamycin, there may exist a subtype of mTORC1 whose FRB is protected from rapamycin by an as yet undiscovered protein partner. This subtype of mTORC1, which we will hypothetically name mTORC1 $\beta$ , may be primarily responsible for the phosphorylation of 4EBP, while the hypothetical mTORC1 $\alpha$ , which is fully sensitive to rapamycin, is responsible for the phosphorylation of S6K. This model might be verified through the discovery of new protein co-factors of mTORC1.



Binding of rapamycin to the FRB domain of TOR is conserved through evolution from yeast to mammals. The conservation of rapamycin binding is probably not due to an evolutionary need to conserve the ability of mTOR to bind rapamycin. Instead, the conservation of rapamycin binding probably reflects the need for the FRB domain of mTOR to perform an important cellular role and conservation of this cellular role has constrained the evolution of mTOR and inadvertently conserved its binding to rapamycin. Rapamycin's binding surface with TOR is highly hydrophobic, suggesting that the FRB domain of TOR might be involved in lipid binding. A solution structure of PA bound to the FRB of mTOR has been solved by NMR [74], and experiments suggest that mTORC1 is regulated might be regulated in part through activation by PA [75, 76]. The conserved binding site on mTOR for rapamycin, may reflect the constraint that mTOR maintain a binding site for PA through evolution. PA is generated by the hydrolysis of phosphatidylcholine by phospholipase D, or by the phosphorylation of diacyl-glycerol (DAG), by diacylglycerol kinase, or by the acylation of lysophosphatidic acid (LPA) by LPA acyltransferase (LPAAT) [76]. Phospholipase D is probably responsible for the bulk production of PA and phospholipase D can be inhibited by n-butanol and to lesser extent sec-butanol while it is unaffected by tert-butanol. S6K phosphorylation is inhibited by n-butanol, but less so by sec-butanol and unaffected by tert-butanol, suggesting a pathway in which PA produced by phospholipase D either activates mTOR or cooperates with other inputs to mTOR to facilitate its phosphorylation of S6K. For instance, binding of mTOR to PA might localize it to a membrane compartment where S6K is present and waiting to be phosphorylated. Rapamycin by binding to the FRB domain of mTOR, likely occludes binding of PA and may prevent the PA dependent activation or localization of mTOR. Rapamycin might primarily affect mTOR's phosphorylation of S6K, while having less effect on 4EBP, if the pathway activating mTOR to phosphorylated 4EBP doesn't rely on PA. For instance, while S6K might require PA binding to mTOR to properly associate mTOR and S6K, mTOR's phosphorylation of

4EBP might not require membrane association. By being regulated independently of PA, mTOR's phosphorylation of 4EBP would escape inhibition by rapamycin.

## 1.12 Using Inhibitors of mTOR to Treat Cancer

The assignment of antiproliferative effects from active-site TOR inhibitors to mTORC1 over mTORC2, while interesting, is a rather academic enterprise, because there is no specific inhibitor of mTORC2. A specific inhibitor of mTORC2 would undoubtedly be highly interesting and might well prove useful for some cancers as suggested by genetic studies in which eliminating mTORC2 [66] block the development of cancer in the mouse. But, such an inhibitor would likely require inhibiting protein–protein interactions necessary for the assembly of mTORC2 or allosterically inhibiting mTORC2 without affecting mTORC1. Given that our ability to discover specific inhibitors of protein-protein interactions and allosteric inhibitors is still in its infancy, it is unlikely we will soon see the discovery of a specific inhibitor of mTORC2 with the potency and pharmacological properties needed for even preclinical work. Instead, the compelling question right now is what type of inhibitor (PI3-K, dual PI3-K/mTOR, isoform specific PI3-K, TORKinib or Rapamycin) from our current arsenal of potent inhibitors will be the best for treating each subtype of cancer.

Of the many other hallmarks of cancer [77], hyperproliferation is often the basis for targeting cancer using conventional chemotherapy. In this sense, mTOR inhibitors seem to follow a similar logic. However, while conventional chemotherapy targets cancer cells by targeting hyperproliferating cells in general, mTOR inhibitors present a slightly different logic; they seek to inhibit the pathways that drive cell proliferation. By blocking the proliferation of cancer cells, TORKinibs may even antagonize conventional chemotherapy because chemotherapy relies on hyperproliferation to distinguish between cancer and non-cancer cells. Alternately, because the PI3-K $\Rightarrow$ Akt $\Rightarrow$ mTOR pathway drives cell survival,

inhibitors of mTOR and/or PI3-K may synergize with chemotherapeutic agents that cause or activate apoptosis. Careful awareness and evaluation of these possibilities is critical as TORKinibs are brought into the clinic.

## References

- 1) Cafferkey R, Young PR, McLaughlin MM, Bergsma DJ, Koltin Y, Sathé GM, Faucette L, Eng WK, Johnson RK, and Livi GP, “Dominant missense mutations in a novel yeast protein related to mammalian phosphatidylinositol 3-kinase and VPS34 abrogate rapamycin cytotoxicity,” *Mol Cell Biol*, vol. 13, no. 10, pp. 6012–23, 1993.
- 2) Heitman J, Movva NR, and Hall MN, “Targets for cell cycle arrest by the immunosuppressant rapamycin in yeast,” *Science*, vol. 253, no. 5022, pp. 905–9, 1991.
- 3) Helliwell SB, Wagner P, Kunz J, Deuter-Reinhard M, Henriquez R, and Hall MN, “TOR1 and TOR2 are structurally and functionally similar but not identical phosphatidylinositol kinase homologues in yeast,” *Mol Biol Cell*, vol. 5, no. 1, pp. 105–18, 1994.
- 4) Kunz J, Henriquez R, Schneider U, Deuter-Reinhard M, Movva NR, and Hall MN, “Target of rapamycin in yeast, TOR2, is an essential phosphatidylinositol kinase homolog required for G1 progression,” *Cell*, vol. 73, no. 3, pp. 585–96, 1993.
- 5) Zheng XF, Florentino D, Chen J, Crabtree GR, and Schreiber SL, “TOR kinase domains are required for two distinct functions, only one of which is inhibited by rapamycin,” *Cell*, vol. 82, no. 1, pp. 121–30, 1995.

- 6) Loewith R, Jacinto E, Wullschleger S, Lorberg A, Crespo JL, Bonenfant D, Oppliger W, Jenoe P, and Hall MN, "Two TOR complexes, only one of which is rapamycin sensitive, have distinct roles in cell growth control," *Mol Cell*, vol. 10, no. 3, pp. 457–68, 2002.
- 7) Brown EJ, Albers MW, Shin TB, Ichikawa K, Keith CT, Lane WS, and Schreiber SL, "A mammalian protein targeted by G1-arresting rapamycin-receptor complex," *Nature*, vol. 369, no. 6483, pp. 756–8, 1994.
- 8) Chen Y, Chen H, Rhoad AE, Warner L, Caggiano TJ, Failli A, Zhang H, Hsiao CL, Nakanishi K, and Molnar-Kimber KL, "A putative sirolimus (rapamycin) effector protein," *Biochem Biophys Res Commun*, vol. 203, no. 1, pp. 1–7, 1994.
- 9) Chiu MI, Katz H, and Berlin V, "RAPT1, a mammalian homolog of yeast Tor, interacts with the FKBP12/rapamycin complex," *Proc Natl Acad Sci U S A*, vol. 91, no. 26, pp. 12 574–8, 1994.
- 10) Sabatini DM, Erdjument-Bromage H, Lui M, Tempst P, and Snyder SH, "RAFT1: a mammalian protein that binds to FKBP12 in a rapamycin-dependent fashion and is homologous to yeast TORs," *Cell*, vol. 78, no. 1, pp. 35–43, 1994.
- 11) Sabers CJ, Martin MM, Brunn GJ, Williams JM, Dumont FJ, Wiederrecht G, and Abraham RT, "Isolation of a protein target of the FKBP12-rapamycin complex in mammalian cells," *J Biol Chem*, vol. 270, no. 2, pp. 815–22, 1995.
- 12) Kim DH, Sarbassov DD, Ali SM, King JE, Latek RR, Erdjument-Bromage H, Tempst P, and Sabatini DM, "mTOR interacts with raptor to form a nutrient-sensitive complex that signals to the cell growth machinery," *Cell*, vol. 110, no. 2, pp. 163–75, 2002.
- 13) Sarbassov DD, Ali SM, Kim DH, Guertin DA, Latek RR, Erdjument-Bromage H, Tempst P, and Sabatini DM, "Rictor, a novel binding partner of mTOR, defines a

- rapamycin-insensitive and raptor-independent pathway that regulates the cytoskeleton,” *Curr Biol*, vol. 14, no. 14, pp. 1296–302, 2004.
- 14) Rini B, Kar S, and Kirkpatrick P, “Temsirolimus,” *Nat Rev Drug Discov*, vol. 6, no. 8, pp. 599–600, 2007.
  - 15) Sedrani R, Cottens S, Kallen J, and Schuler W, “Chemical modification of rapamycin: the discovery of SDZ RAD,” *Transplant Proc*, vol. 30, no. 5, pp. 2192–4, 1998.
  - 16) Sarbassov DD, Ali SM, Sengupta S, Sheen JH, Hsu PP, Bagley AF, Markhard AL, and Sabatini DM, “Prolonged rapamycin treatment inhibits mTORC2 assembly and Akt/PKB,” *Mol Cell*, vol. 22, no. 2, pp. 159–68, 2006.
  - 17) Feldman ME, Apsel B, Uotila A, Loewith R, Knight ZA, Ruggero D, and Shokat KM, “Active-site inhibitors of mTOR target rapamycin-resistant outputs of mTORC1 and mTORC2,” *PLoS Biol*, vol. 7, no. 2, p. e38, 2009.
  - 18) Chresta CM and al. e, “AZD8055 is a potent, selective and orally bioavailable ATP-Competitive mTOR kinase inhibitor with in vitro and in vivo anti-tumor activity,” *In Press*, 2009.
  - 19) Garcia-Martinez JM, Moran J, Clarke RG, Gray A, Cosulich SC, Chresta CM, and Alessi DR, “Ku-0063794 is a specific inhibitor of the mammalian target of rapamycin (mTOR),” *Biochem J*, vol. 421, no. 1, pp. 29–42, 2009.
  - 20) Nowak P and al. e, “Discovery of potent and selective inhibitors of the mammalian target of rapamycin (mTOR) kinase,” *Journal of Medicinal Chemistry*, 2009.
  - 21) Yu K *et al.*, “Biochemical, cellular, and in vivo activity of novel ATP-competitive and selective inhibitors of the mammalian target of rapamycin,” *Cancer Res*, vol. 69, no. 15, pp. 6232–40, 2009.

- 22) Zask A *et al.*, “ATP-Competitive Inhibitors of the Mammalian Target of Rapamycin: Design and Synthesis of Highly Potent and Selective Pyrazolopyrimidines,” *J Med Chem*, 2009.
- 23) Thoreen CC, Kang SA, Chang JW, Liu Q, Zhang J, Gao Y, Reichling LJ, Sim T, Sabatini DM, and Gray NS, “An ATP-competitive mammalian target of rapamycin inhibitor reveals rapamycin-resistant functions of mTORC1,” *J Biol Chem*, vol. 284, no. 12, pp. 8023–32, 2009.
- 24) Brunn GJ, Williams J, Sabers C, Wiederrecht G, Lawrence J, and Abraham RT, “Direct inhibition of the signaling functions of the mammalian target of rapamycin by the phosphoinositide 3-kinase inhibitors, wortmannin and LY294002,” *Embo J*, vol. 15, no. 19, pp. 5256–67, 1996.
- 25) Vlahos CJ, Matter WF, Hui KY, and Brown RF, “A specific inhibitor of phosphatidylinositol 3-kinase, 2-(4-morpholinyl)-8-phenyl-4H-1-benzopyran-4-one (LY294002),” *J Biol Chem*, vol. 269, no. 7, pp. 5241–8, 1994.
- 26) Knight ZA *et al.*, “A pharmacological map of the PI3-K family defines a role for p110alpha in insulin signaling,” *Cell*, vol. 125, no. 4, pp. 733–47, 2006.
- 27) Maira SM *et al.*, “Identification and characterization of NVP-BEZ235, a new orally available dual phosphatidylinositol 3-kinase/mammalian target of rapamycin inhibitor with potent in vivo antitumor activity,” *Mol Cancer Ther*, vol. 7, no. 7, pp. 1851–63, 2008.
- 28) Folkes AJ *et al.*, “The identification of 2-(1H-indazol-4-yl)-6-(4-methanesulfonylpiperazin-1-ylmethyl)-4-morpholin-4-yl-thieno[3,2-d]pyrimidine (GDC-0941) as a potent, selective, orally bioavailable inhibitor of class I PI3 kinase for the treatment of cancer,” *J Med Chem*, vol. 51, no. 18, pp. 5522–32, 2008.

- 29) Raynaud FI *et al.*, “Biological properties of potent inhibitors of class I phosphatidylinositol 3-kinases: from PI-103 through PI-540, PI-620 to the oral agent GDC-0941,” *Mol Cancer Ther*, vol. 8, no. 7, pp. 1725–38, 2009.
- 30) Jacinto E and Lorberg A, “TOR regulation of AGC kinases in yeast and mammals,” *Biochem J*, vol. 410, no. 1, pp. 19–37, 2008.
- 31) Brunn GJ, Hudson CC, Sekulic A, Williams JM, Hosoi H, Houghton PJ, Lawrence J, and Abraham RT, “Phosphorylation of the translational repressor PHAS-I by the mammalian target of rapamycin,” *Science*, vol. 277, no. 5322, pp. 99–101, 1997.
- 32) Burnett PE, Barrow RK, Cohen NA, Snyder SH, and Sabatini DM, “RAFT1 phosphorylation of the translational regulators p70 S6 kinase and 4E-BP1,” *Proc Natl Acad Sci U S A*, vol. 95, no. 4, pp. 1432–7, 1998.
- 33) Guertin DA and Sabatini DM, “Defining the role of mTOR in cancer,” *Cancer Cell*, vol. 12, no. 1, pp. 9–22, 2007.
- 34) Pearson RB, Dennis PB, Han JW, Williamson NA, Kozma SC, Wettenhall RE, and Thomas G, “The principal target of rapamycin-induced p70s6k inactivation is a novel phosphorylation site within a conserved hydrophobic domain,” *Embo J*, vol. 14, no. 21, pp. 5279–87, 1995.
- 35) Chan TO and Tschlis PN, “PDK2: a complex tail in one Akt,” *Sci STKE*, vol. 2001, no. 66, p. PE1, 2001.
- 36) Sarbassov DD, Guertin DA, Ali SM, and Sabatini DM, “Phosphorylation and regulation of Akt/PKB by the rictor-mTOR complex,” *Science*, vol. 307, no. 5712, pp. 1098–101, 2005.

- 37) Guertin DA, Stevens DM, Thoreen CC, Burds AA, Kalaany NY, Moffat J, Brown M, Fitzgerald KJ, and Sabatini DM, "Ablation in mice of the mTORC components raptor, rictor, or mLST8 reveals that mTORC2 is required for signaling to Akt-FOXO and PKCalpha, but not S6K1," *Dev Cell*, vol. 11, no. 6, pp. 859–71, 2006.
- 38) Jacinto E, Facchinetti V, Liu D, Soto N, Wei S, Jung SY, Huang Q, Qin J, and Su B, "SIN1/MIP1 maintains rictor-mTOR complex integrity and regulates Akt phosphorylation and substrate specificity," *Cell*, vol. 127, no. 1, pp. 125–37, 2006.
- 39) Shiota C, Woo JT, Lindner J, Shelton KD, and Magnuson MA, "Multiallelic disruption of the rictor gene in mice reveals that mTOR complex 2 is essential for fetal growth and viability," *Dev Cell*, vol. 11, no. 4, pp. 583–9, 2006.
- 40) Garcia-Martinez JM and Alessi DR, "mTOR complex-2 (mTORC2) controls hydrophobic motif phosphorylation and activation of serum and glucocorticoid induced protein kinase-1 (SGK1)," *Biochem J*, 2008.
- 41) Yang J, Cron P, Good VM, Thompson V, Hemmings BA, and Barford D, "Crystal structure of an activated Akt/protein kinase B ternary complex with GSK3-peptide and AMP-PNP," *Nat Struct Biol*, vol. 9, no. 12, pp. 940–4, 2002.
- 42) Andjelkovic M, Alessi DR, Meier R, Fernandez A, Lamb NJ, Frech M, Cron P, Cohen P, Lucocq JM, and Hemmings BA, "Role of translocation in the activation and function of protein kinase B," *J Biol Chem*, vol. 272, no. 50, pp. 31 515–24, 1997.
- 43) Collins BJ, Deak M, Arthur JS, Armit LJ, and Alessi DR, "In vivo role of the PIF-binding docking site of PDK1 defined by knock-in mutation," *Embo J*, vol. 22, no. 16, pp. 4202–11, 2003.



- 44) Kannan N, Haste N, Taylor SS, and Neuwald AF, “The hallmark of AGC kinase functional divergence is its C-terminal tail, a cis-acting regulatory module,” *Proc Natl Acad Sci U S A*, vol. 104, no. 4, pp. 1272–7, 2007.
- 45) Facchinetti V *et al.*, “The mammalian target of rapamycin complex 2 controls folding and stability of Akt and protein kinase C,” *Embo J*, vol. 27, no. 14, pp. 1932–43, 2008.
- 46) Ikenoue T, Inoki K, Yang Q, Zhou X, and Guan KL, “Essential function of TORC2 in PKC and Akt turn motif phosphorylation, maturation and signalling,” *Embo J*, vol. 27, no. 14, pp. 1919–31, 2008.
- 47) Sonenberg N, Hershey JWB, and Mathews M, *Translational control of gene expression*, 2nd ed., ser. Cold Spring Harbor monograph series, 39. Cold Spring Harbor, NY: Cold Spring Harbor Laboratory Press, 2000.
- 48) Ruggero D, Montanaro L, Ma L, Xu W, Londei P, Cordon-Cardo C, and Pandolfi PP, “The translation factor eIF-4E promotes tumor formation and cooperates with c-Myc in lymphomagenesis,” *Nat Med*, vol. 10, no. 5, pp. 484–6, 2004.
- 49) Ruggero D and Pandolfi PP, “Does the ribosome translate cancer?” *Nat Rev Cancer*, vol. 3, no. 3, pp. 179–92, 2003.
- 50) Ruggero D and Sonenberg N, “The Akt of translational control,” *Oncogene*, vol. 24, no. 50, pp. 7426–34, 2005.
- 51) Richter JD and Sonenberg N, “Regulation of cap-dependent translation by eIF4E inhibitory proteins,” *Nature*, vol. 433, no. 7025, pp. 477–80, 2005.
- 52) Inoki K and Guan KL, “Tuberous sclerosis complex, implication from a rare genetic disease to common cancer treatment,” *Hum Mol Genet*, vol. 18, no. R1, pp. R94–100, 2009.

- 53) Manning BD, Logsdon MN, Lipovsky AI, Abbott D, Kwiatkowski DJ, and Cantley LC, "Feedback inhibition of Akt signaling limits the growth of tumors lacking Tsc2," *Genes Dev*, vol. 19, no. 15, pp. 1773–8, 2005.
- 54) Wan X, Harkavy B, Shen N, Grohar P, and Helman LJ, "Rapamycin induces feedback activation of Akt signaling through an IGF-1R-dependent mechanism," *Oncogene*, vol. 26, no. 13, pp. 1932–40, 2007.
- 55) Taniguchi CM, Emanuelli B, and Kahn CR, "Critical nodes in signalling pathways: insights into insulin action," *Nat Rev Mol Cell Biol*, vol. 7, no. 2, pp. 85–96, 2006.
- 56) Carracedo A *et al.*, "Inhibition of mTORC1 leads to MAPK pathway activation through a PI3K-dependent feedback loop in human cancer," *J Clin Invest*, vol. 118, no. 9, pp. 3065–74, 2008.
- 57) Kinkade CW *et al.*, "Targeting AKT/mTOR and ERK MAPK signaling inhibits hormone-refractory prostate cancer in a preclinical mouse model," *J Clin Invest*, vol. 118, no. 9, pp. 3051–64, 2008.
- 58) Li J *et al.*, "PTEN, a putative protein tyrosine phosphatase gene mutated in human brain, breast, and prostate cancer," *Science*, vol. 275, no. 5308, pp. 1943–7, 1997.
- 59) Samuels Y *et al.*, "High frequency of mutations of the PIK3CA gene in human cancers," *Science*, vol. 304, no. 5670, p. 554, 2004.
- 60) Abraham RT and Wiederrecht GJ, "Immunopharmacology of rapamycin," *Annu Rev Immunol*, vol. 14, pp. 483–510, 1996.
- 61) Fan QW, Knight ZA, Goldenberg DD, Yu W, Mostov KE, Stokoe D, Shokat KM, and Weiss WA, "A dual PI3 kinase/mTOR inhibitor reveals emergent efficacy in glioma," *Cancer Cell*, vol. 9, no. 5, pp. 341–9, 2006.

- 62) Walker EH, Pacold ME, Perisic O, Stephens L, Hawkins PT, Wymann MP, and Williams RL, "Structural determinants of phosphoinositide 3-kinase inhibition by wortmannin, LY294002, quercetin, myricetin, and staurosporine," *Mol Cell*, vol. 6, no. 4, pp. 909–19, 2000.
- 63) Apse B, Blair JA, Gonzalez B, Nazif TM, Feldman ME, Aizenstein B, Hoffman R, Williams RL, Shokat KM, and Knight ZA, "Targeted polypharmacology: discovery of dual inhibitors of tyrosine and phosphoinositide kinases," *Nat Chem Biol*, vol. 4, no. 11, pp. 691–9, 2008.
- 64) Kumar A, Harris TE, Keller SR, Choi KM, Magnuson MA, and Lawrence J, "Muscle-specific deletion of rictor impairs insulin-stimulated glucose transport and enhances Basal glycogen synthase activity," *Mol Cell Biol*, vol. 28, no. 1, pp. 61–70, 2008.
- 65) Hresko RC and Mueckler M, "mTOR.RICTOR is the Ser473 kinase for Akt/protein kinase B in 3T3-L1 adipocytes," *J Biol Chem*, vol. 280, no. 49, pp. 40 406–16, 2005.
- 66) Guertin DA, Stevens DM, Saitoh M, Kinkel S, Crosby K, Sheen JH, Mullholland DJ, Magnuson MA, Wu H, and Sabatini DM, "mTOR complex 2 is required for the development of prostate cancer induced by Pten loss in mice," *Cancer Cell*, vol. 15, no. 2, pp. 148–59, 2009.
- 67) Knight ZA and Shokat KM, "Features of selective kinase inhibitors," *Chem Biol*, vol. 12, no. 6, pp. 621–37, 2005.
- 68) Okuzumi T, Fiedler D, Zhang C, Gray DC, Aizenstein B, Hoffman R, and Shokat KM, "Inhibitor hijacking of Akt activation," *Nat Chem Biol*, vol. 5, no. 7, pp. 484–493, 2009.
- 69) Peterson TR, Laplante M, Thoreen CC, Sancak Y, Kang SA, Kuehl WM, Gray NS, and Sabatini DM, "DEPTOR is an mTOR inhibitor frequently overexpressed in multiple myeloma cells and required for their survival," *Cell*, vol. 137, no. 5, pp. 873–86, 2009.

- 70) Gingras AC, Raught B, Gygi SP, Niedzwiecka A, Miron M, Burley SK, Polakiewicz RD, Wyslouch-Cieszyńska A, Aebersold R, and Sonenberg N, “Hierarchical phosphorylation of the translation inhibitor 4E-BP1,” *Genes Dev*, vol. 15, no. 21, pp. 2852–64, 2001.
- 71) Wang X, Beugnet A, Murakami M, Yamanaka S, and Proud CG, “Distinct signaling events downstream of mTOR cooperate to mediate the effects of amino acids and insulin on initiation factor 4E-binding proteins,” *Mol Cell Biol*, vol. 25, no. 7, pp. 2558–72, 2005.
- 72) Gingras AC, Gygi SP, Raught B, Polakiewicz RD, Abraham RT, Hoekstra MF, Aebersold R, and Sonenberg N, “Regulation of 4E-BP1 phosphorylation: a novel two-step mechanism,” *Genes Dev*, vol. 13, no. 11, pp. 1422–37, 1999.
- 73) Shor B, Zhang WG, Toral-Barza L, Lucas J, Abraham RT, Gibbons JJ, and Yu K, “A new pharmacologic action of CCI-779 involves FKBP12-independent inhibition of mTOR kinase activity and profound repression of global protein synthesis,” *Cancer Res*, vol. 68, no. 8, pp. 2934–43, 2008.
- 74) Veverka V, Crabbe T, Bird I, Lennie G, Muskett FW, Taylor RJ, and Carr MD, “Structural characterization of the interaction of mTOR with phosphatidic acid and a novel class of inhibitor: compelling evidence for a central role of the FRB domain in small molecule-mediated regulation of mTOR,” *Oncogene*, vol. 27, no. 5, pp. 585–95, 2008.
- 75) Fang Y, Vilella-Bach M, Bachmann R, Flanigan A, and Chen J, “Phosphatidic acid-mediated mitogenic activation of mTOR signaling,” *Science*, vol. 294, no. 5548, pp. 1942–5, 2001.
- 76) Foster DA, “Regulation of mTOR by phosphatidic acid?” *Cancer Res*, vol. 67, no. 1, pp. 1–4, 2007.

77) Hanahan D and Weinberg RA, "The hallmarks of cancer," *Cell*, vol. 100, no. 1, pp. 57-70, 2000.

## Chapter 2

# Active-Site Inhibitors of mTOR Target Rapamycin-Resistant Outputs of mTORC1 and mTORC2



## Abstract

The mammalian target of rapamycin (mTOR) regulates cell growth and survival by integrating nutrient and hormonal signals. These signaling functions are distributed between at least two distinct mTOR protein complexes, mTORC1 and mTORC2. mTORC1 is sensitive to the selective inhibitor rapamycin and activated by growth factor stimulation via the canonical PI3-K $\Rightarrow$ Akt $\Rightarrow$ mTOR pathway. Activated mTORC1 kinase upregulates protein synthesis by phosphorylating key regulators of mRNA translation. By contrast, mTORC2 is resistant to rapamycin. Genetic studies have suggested that mTORC2 may phosphorylate Akt at S473, one of two phosphorylation sites required for Akt activation; this has been controversial, in part because RNAi and gene knockouts produce distinct Akt phospho-isoforms. The central role of mTOR in controlling key cellular growth and survival pathways has sparked interest in discovering mTOR inhibitors that bind to the ATP site and therefore target both mTORC2 and mTORC1. Here we investigate mTOR signaling in cells and animals with two novel and specific mTOR kinase domain inhibitors (TORKinibs). These TORKinibs (PP242 and PP30) are the first specific active-site inhibitors of mTOR and therefore the first specific inhibitors of mTORC2 and we use them to show that pharmacological inhibition of mTOR blocks the phosphorylation of Akt at S473 and prevents its full activation. Furthermore, we show that TORKinibs inhibit proliferation of primary cells more completely than rapamycin. Surprisingly, we find that mTORC2 is not the basis for this enhanced activity and show that the TORKinib PP242 is a more effective mTORC1 inhibitor than rapamycin. Importantly, at the molecular level PP242 inhibits cap-dependent translation under conditions in which rapamycin has no effect. Our findings identify new functional features of mTORC1 that are resistant to rapamycin but are effectively targeted by TORKinibs. These potent new pharmacological agents complement rapamycin in the study of mTOR and its role in normal physiology and human disease.

## 2.1 Introduction

The mammalian target of rapamycin (mTOR) is a serine-threonine kinase related to the lipid kinases of the phosphoinositide 3 kinase family (PI3-K). mTOR exists in two complexes, mTORC1 [1, 2] and mTORC2 [3, 4], which are differentially regulated, have distinct substrate specificities and are differentially sensitive to rapamycin. mTORC1 integrates signals from growth factor receptors with cellular nutritional status and controls the level of cap dependent mRNA translation by modulating the activity of key translational components such as the oncogene and cap binding protein eIF4E [5].

mTORC2 is insensitive to rapamycin and selective inhibitors of this complex have not been described. Partly because acute pharmacological inhibition of mTORC2 has not been possible, the functions of mTORC2 are less well understood than those of mTORC1. mTORC2 is thought to modulate growth factor signaling by phosphorylating the C terminal hydrophobic motif of some AGC kinases such as Akt [4, 6] and SGK [7] although other kinases including DNA PK and Ilk have also been implicated in Akt hydrophobic motif phosphorylation [8–11]. Growth factor stimulation of PI3-K causes activation of Akt by phosphorylation at two key sites: the activation loop (T308) and the C terminal hydrophobic motif (S473). Active Akt promotes cell survival in many ways including suppressing apoptosis, promoting glucose uptake, and modifying cellular metabolism [12]; consequently, there is significant interest in identifying the kinase(s) responsible for each activating phosphorylation, the relationship between these phosphorylation sites, and the role of differential Akt phosphorylation on Akt substrate phosphorylation. Of the two phosphorylation sites on Akt, activation loop phosphorylation at T308, mediated by PDK1, is indispensable for kinase activity, while hydrophobic motif phosphorylation at S473 enhances Akt kinase activity by approximately five-fold [13].



Disruption of mTORC2 by different genetic and pharmacological approaches has variable effects on Akt phosphorylation. Targeting mTORC2 by RNAi [6, 14], homologous recombination [15–17] or long-term rapamycin treatment [18], results in loss of Akt hydrophobic motif phosphorylation (S473), strongly implicating mTORC2 as the kinase responsible for phosphorylation of this site. RNAi targeting mTORC2 and long term rapamycin result in loss of Akt phosphorylation in activation loop (T308), but this phosphorylation remains intact in mouse embryonic fibroblasts (MEFs) lacking the critical mTORC2 component Sin1. It cannot be inferred from this genetic data whether acute pharmacological inhibition of mTORC2 would block the phosphorylation of Akt only at S473, resulting in partial Akt deactivation, or also disrupt phosphorylation at T308, resulting complete Akt inhibition. Several small molecules have been identified that directly inhibit mTOR by targeting the ATP binding site; these include LY294002, PI-103 and NVP-BEZ235 [19–22]. These molecules were originally discovered as inhibitors of PI3-Ks and later shown to also target mTOR. Because all of these molecules inhibit PI3-Ks and mTOR with similar potency, they cannot be used to selectively inhibit mTOR or PI3-Ks in cells. Indeed, because mTORC1 and mTORC2 function downstream of PI3-Ks in most settings, it is unclear to what extent the ability of these molecules to block the activation of signaling proteins such as Akt reflects PI3-K versus mTOR inhibition. It is possible that some of the functions attributed to PI3-Ks using the classical inhibitor LY294002 are a consequence of mTOR inhibition [22, 23], but it is has not been possible address this because small molecules that inhibit mTOR without inhibiting PI3-Ks have not been available.

We recently reported the synthesis of pyrazolopyrimidines that inhibit members of the PI3-K family including mTOR [24]. Two of these molecules, PP242 and PP30, are the first potent, selective, and ATP-competitive inhibitors of mTOR. Unlike rapamycin, these molecules inhibit both mTORC1 and mTORC2, and, unlike PI3-K family inhibitors such as LY294002, these molecules inhibit mTOR with a high degree of selectivity relative to PI3-Ks

and protein kinases. To distinguish these molecules from the allosteric mTORC1 inhibitor rapamycin, we are calling them TORKinibs for TOR Kinase domain inhibitors. The dual role of mTOR within the PI3-K $\Rightarrow$ Akt $\Rightarrow$ mTOR pathway as both an upstream activator of Akt and the downstream effector of pathway activity on cell growth and proliferation has excited interest in active-site inhibitors of mTOR [25–30]. We describe here the biological activity of these molecules.

## 2.2 Results

### 2.2.1 Specific Active-Site Inhibition of mTOR by the TORKinibs

#### PP242 and PP30

PP242 and PP30 inhibit mTOR *in vitro* with a half-maximal inhibitory concentration (IC<sub>50</sub>) of 8 nM and 80 nM, respectively (Table 2.1). As expected for active site inhibitors, PP242 and PP30 inhibit mTOR in both mTORC1 and mTORC2 (Table 2.2). Both compounds are selective within the PI3-K family, inhibiting other PI3-Ks only at substantially higher concentrations (Table 2.1). Testing of PP242 against 219 purified protein kinases at a concentration 100-fold higher than its mTOR IC<sub>50</sub> value revealed exceptional selectivity with respect to the protein kinome; most protein kinases were unaffected by this drug, and only four – PKC alpha, PKC beta, RET and JAK2 (V617F) – were inhibited more than 80 percent [24]. We determined IC<sub>50</sub> values for PP242 against these kinases *in vitro* using purified protein. In these assays, PP242 was relatively inactive against PKC beta, RET or JAK2 but inhibited PKC alpha with an *in vitro* IC<sub>50</sub> of 50 nM (Table 2.1). Importantly, PP30 showed no activity against PKC alpha or PKC beta in the same assay. These data indicate that PP242 is a highly selective inhibitor of mTOR and that PP30 can be used to confirm that the effects of PP242 are due to inhibition of mTOR and not PKC alpha. The availability

of a second structurally dissimilar mTOR inhibitor, PP30, provides additional control for an unanticipated off-target of PP242.

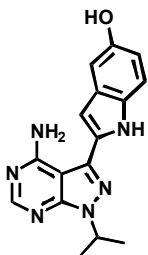
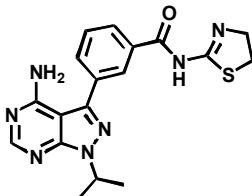
	PP242	PP30
		
mTOR	0.008	0.080
p110 $\alpha$	1.96	3
p110 $\beta$	2.2	5.8
p110 $\delta$	1.27	0.99
p110 $\gamma$	0.102	0.68
PI4K $\beta$	22	5.7
DNA-PK	0.408	0.339
PDK1	>10	>10
PKC $\alpha$	0.049	10
PKC $\beta$ I	0.198	>10
PKC $\beta$ II	0.185	>10
RET	0.224	ND
JAK2	0.11	ND

Table 2.1: *In vitro* IC<sub>50</sub> values in  $\mu$ M for PP242 and PP30 determined in the presence of 10  $\mu$ M ATP.

Compound	IC <sub>50</sub> $\mu$ M vs the Indicated Preparation of mTOR		
	mTOR (Invitrogen)	mTORC1	mTORC2
PP242	0.008	0.030	0.058
PP30	0.080	0.128	0.281
[ATP] $\mu$ M	10	100	100

Table 2.2: *In vitro* IC<sub>50</sub> determinations using three forms of mTOR.

## 2.2.2 Inhibition of mTORC2 and Akt Phosphorylation by TORKinibs

We characterized the effect of PP242 on the PI3-K $\Rightarrow$ Akt $\Rightarrow$ mTOR pathway. PP242 and PP30 both inhibited insulin stimulated phosphorylation of Akt at S473, confirming that mTOR kinase activity is required for hydrophobic motif phosphorylation (Fig 2.1A). Inhibition of mTOR by PP242 and PP30 also resulted in loss of Akt phosphorylation at T308, but

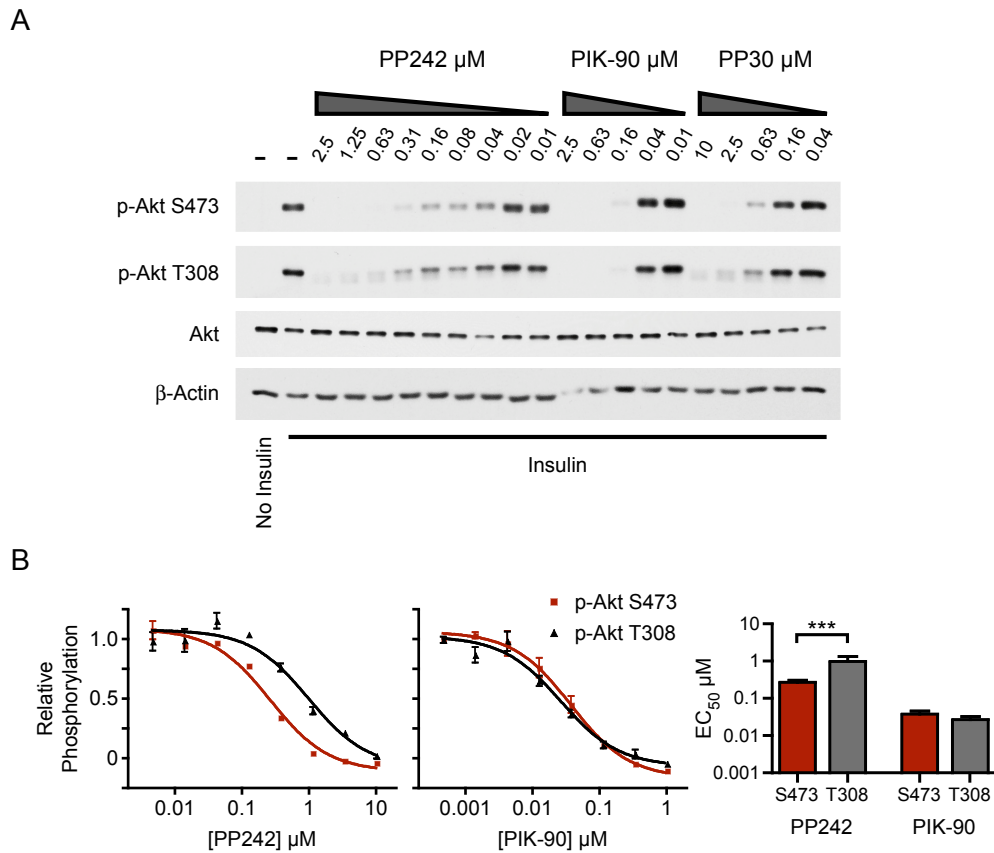


Figure 2.1: Inhibition of mTORC2 by TORKinibs affects pS473 and pT308 of Akt.

A) Serum-starved L6 myotubes were pre-treated with kinase inhibitors prior to stimulation with insulin for 3 minutes. Lysates were analyzed by western blotting.

B) PP242 inhibits pS473 of Akt more potently than pT308. Serum-starved L6 myotubes were treated with kinase inhibitors prior to stimulation with insulin for 10 minutes. Akt phosphorylation was measured by in-cell western and is shown relative to serum starvation and insulin stimulation (n = 3 for each inhibitor dose). EC<sub>50</sub> values from the best fit curves are plotted. \*\*\*p < 0.001, F test. EC<sub>50</sub> values for PIK-90 on pS473 and pT308 were not significantly different (p = 0.2, F test).

significantly higher doses of PP242 and PP30 were required to inhibit T308 as compared with S473 (Fig 2.1A and B). PP242 inhibited S473-P and T308 P at both early and late time points after insulin stimulation, indicating that the differential sensitivity of these sites to PP242 does not reflect differing kinetics of phosphorylation (Fig 2.2). By comparison, the PI3-K inhibitor PIK-90 which does not inhibit mTOR, inhibited the phosphorylation of both Akt sites equipotently (Fig 2.1B), as observed previously [20].

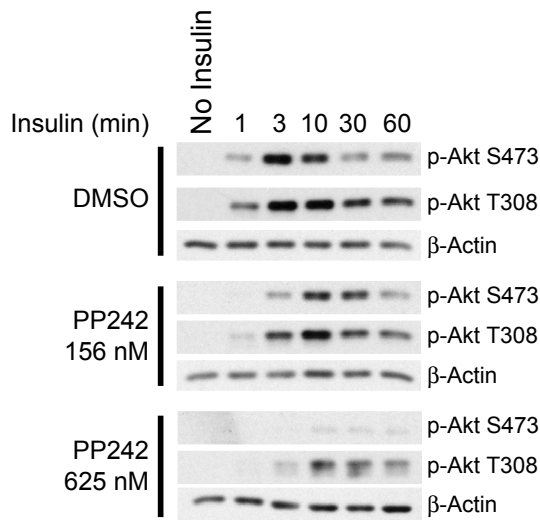


Figure 2.2: PP242 inhibits Akt phosphorylation over the course of one hour.

L6 myotubes were pre-treated with PP242 or DMSO for 30 minutes and stimulated with insulin for the indicated time prior to lysis and analysis by western blotting.

We sought to confirm that the loss of T308-P caused by PP242 and PP30 results from inhibition of mTOR mediated phosphorylation of S473, rather than inhibition of an off target kinase, or an effect of mTOR inhibition unrelated to S473-P. To do this we examined the effect of PP242 on T308 phosphorylation in two situations in which Akt could not be phosphorylated on S473. First we overexpressed S473A mutant Akt and stimulated these cells with insulin (Fig 2.3). S473A Akt was phosphorylated on T308 to a similar level as wild-type, yet in contrast to the wild-type, T308-P on S473A Akt was not inhibited by PP242. The lack of effect of PP242 on S473A Akt confirms that PP242 inhibition of pT308 requires S473 and also that PP242 does not inhibit PDK1 in cells as was suggested by direct testing of PDK1 *in vitro* (Table 2.1).

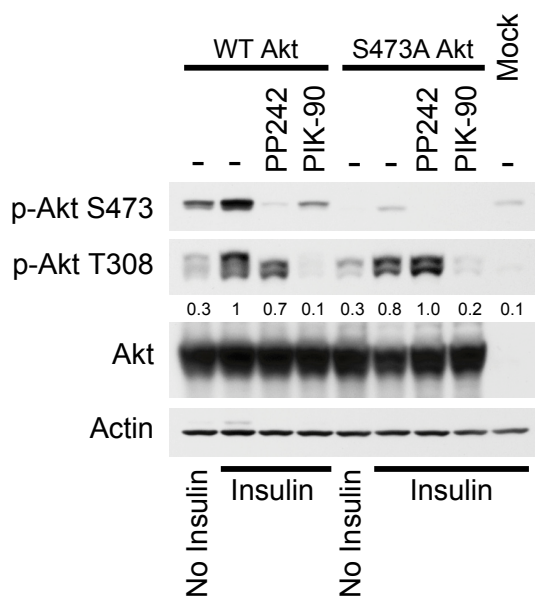


Figure 2.3: pT308 is not inhibited by PP242 in cells overexpressing S473A Akt. HEK293 cells were transfected with wild-type Akt, S473A Akt or not transfected (Mock) and were treated with 2.5  $\mu$ M PP242 or 625 nM PIK-90 as indicated prior to insulin stimulation. Lysates were analyzed by western blotting. Quantitation of pT308 relative to insulin treated cells overexpressing wild-type Akt (lane 2) is shown below that blot. Data are representative of two independent experiments.

As a further test of the specificity of PP242 and the requirement for functional S473 phosphorylation in order for PP242 to inhibit T308-P, we examined the effect of PP242 on the phosphorylation of Akt in primary MEFs from embryos that lack Sin1 [16] (Fig 2.4). Sin1 is a component of mTORC2, and knockout of Sin1 compromises the physical integrity of mTORC2 leading to a complete loss of Akt phosphorylation at S473 without affecting its phosphorylation at T308. Consistent with our results from L6 cells, PP242 inhibited the phosphorylation of Akt at both S473 and T308 in wild type MEFs. By contrast, PP242 had no effect on the phosphorylation of T308 in Sin1<sup>-/-</sup> MEFs that lack mTORC2. Furthermore, PP242 had no effect on the constitutive phosphorylation of the turn motif of Akt at T450 [16, 31]. As a further comparison we examined the effect of long term rapamycin which is known to block the assembly of mTORC2 in some cell lines [18]. Similar to PP242, long term rapamycin treatment inhibited S473-P and reduced the phosphorylation of T308-P as was seen previously [18]. Importantly, the PI3-K inhibitor PIK-90 and the PDK1 inhibitor BX-795 [32] blocked phosphorylation of T308 in Sin1<sup>-/-</sup> MEFs, indicating that the failure of PP242 to block T308 in Sin1<sup>-/-</sup> MEFs does not reflect a general resistance of

T308 to dephosphorylation in cells that lack mTORC2. From these data, we conclude that PP242's effect on T308-P is dependent on its inhibition of Akt phosphorylation by mTOR at S473. It remains unclear why mTORC2 knockout cells, but not cells treated with RNAi or pharmacological inhibitors of mTORC2, are able to retain T308 phosphorylation in the absence of phosphorylation at S473. However, there are a growing number of examples in which genetic deletion of a kinase results in compensatory changes that mask relevant phenotypes observed with the corresponding small molecule inhibitor [33].

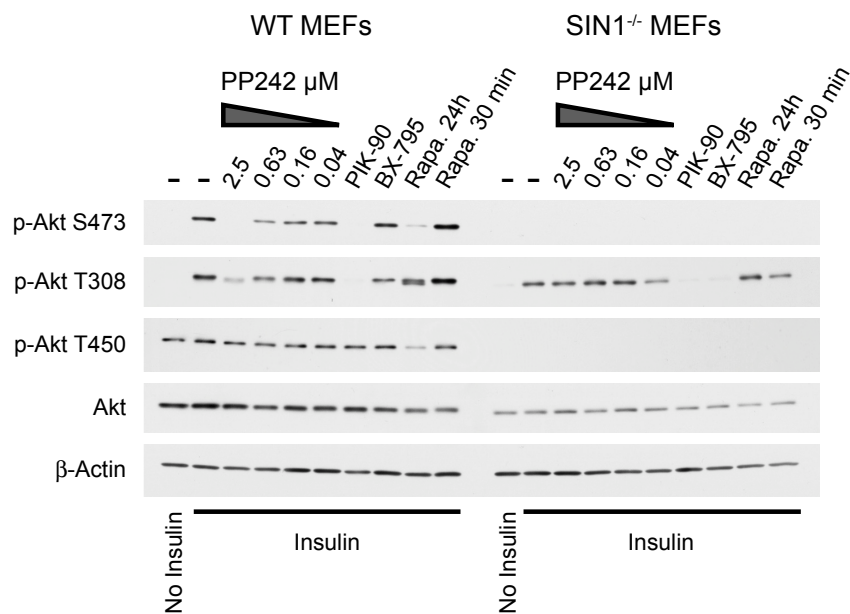


Figure 2.4: pT308 is not inhibited by PP242 in Sin1<sup>-/-</sup> MEFs which lack pS473. Primary wild-type (WT) and SIN1<sup>-/-</sup> mouse embryonic fibroblasts (MEFs) were pre-treated with 625 nM PIK-90, 10 μM BX-795, 100 nM rapa. for 24 hours, 100 nM rapa. for 30 minutes or the indicated concentrations of PP242 prior to stimulation with insulin. Lysates were analyzed by western blotting.

### 2.2.3 Akt Substrate Phosphorylation is Only Modestly Inhibited by PP242

Akt requires phosphorylation at both S473 and T308 for full biochemical activity *in vitro* [13] but it is unclear whether all of the cellular functions of Akt require it to be dually phosphorylated. Singly phosphorylated (T308-P) Akt from *Sin1*<sup>-/-</sup> MEFs is competent to phosphorylate the cytoplasmic Akt substrates GSK3 and TSC2, but not the nuclear target FoxO [16]. Because low concentrations of PP242 inhibit the phosphorylation of S473 and higher concentrations partially inhibit T308-P in addition to S473-P, we used PP242 to examine whether some substrates of Akt are especially sensitive to loss of S473-P (Fig 2.5). We compared PP242 to the PI3-K inhibitor PIK-90 and the allosteric Akt inhibitor Akti 1/2 [34], which inhibit

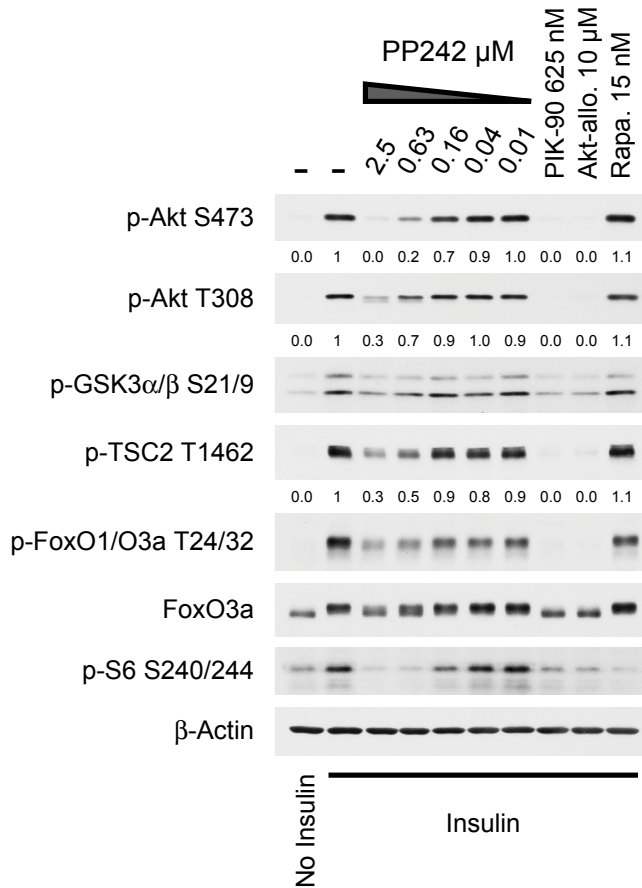


Figure 2.5: Phosphorylation of the Akt substrates GSK3 $\alpha/\beta$ , TSC2 and FoxO1/O3a is not potently inhibited by PP242.

Lysates from L6 myotubes treated with kinase inhibitors and stimulated with insulin were analyzed by western blotting. Quantitation of pAkt and pTSC2 relative to the insulin control (lane 2) is shown below these blots.



the phosphorylation of Akt at both sites. In contrast to PIK-90 and Akti-1/2 which completely inhibited the phosphorylation of Akt and its direct substrates, PP242 only partially inhibited the phosphorylation of cytoplasmic and nuclear substrates of Akt. This suggests that phosphorylation of the Akt substrates we examined is only modestly sensitive to loss of S473 P. A caveat of comparing Akt substrates in Sin1<sup>-/-</sup> MEFs with PP242 treated cells is the different turn motif (T450-P) status in these two conditions (Fig 2.4). In contrast to Akt which maintains T308-P, SGK activity is completely inhibited by genetic disruption of mTORC2 [7]. Because SGK can phosphorylate FoxO and its activity is completely inhibited by disruption of mTORC2, it was suggested that, while GSK and TSC2 are phosphorylated by Akt, FoxO is primarily phosphorylated by SGK [7]. Because Akti-1/2 does not inhibit SGK [34], but inhibits FoxO1/O3a phosphorylation at T24/T32 in L6 myotubes (Fig 2.5), Akt is likely the major kinase for T24/T32 of FoxO1/O3a in L6 myotubes.

#### **2.2.4 PKC-HM Phosphorylation**

Just as mTORC2 is the major hydrophobic motif kinase for Akt [6] (Fig 2.1), it has been suggested that mTORC2 also phosphorylates the hydrophobic motif (HM) of PKC (reviewed by Jacinto and Lornberg [35]). Initially a link between mTORC2 and PKC was found in yeast where overexpression of PKC1 suppresses the growth defect induced by loss of TORC2 [36]. In mammalian cells, reducing expression of mTORC2 by rictor RNAi decreases HM-P on PKC $\alpha$  [4], indicating the mTORC2 might phosphorylate the HM of PKC $\alpha$ . Full mouse knockout of mTORC2 also decreases the HM phosphorylation of PKC [15], in addition, to the complete dephosphorylation of the turn-motif (TM) of PKC [31, 37]. TM phosphorylation stabilizes PKC and, protein levels of PKC are generally lower, but highly variable, in cell lines derived from mice lacking mTORC2 [37]. Loss of TM phosphorylation and the consequent destabilization of PKC makes it difficult to interpret the loss of PKC-HM phosphorylation seen in cells lacking mTORC2.

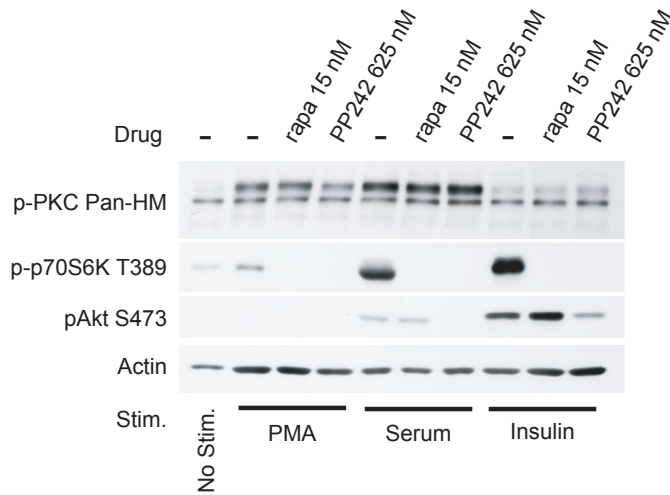


Figure 2.6: PKC-HM phosphorylation is not obviously impaired in cells treated with PP242. Western blot of lysates from L6 myotubes.

To examine the effect of acute mTOR inhibition on PKC-HM phosphorylation, we treated serum-starved L6 myotubes with PP242 prior to induction of PKC-HM phosphorylation by serum or phorbol-12-myristate-13-acetate (PMA) (Fig 2.6). PKC-HM phosphorylation was assessed by western blot using an antibody that recognizes the hydrophobic motif of all PKC isoforms. Upon treatment of L6 myotubes with serum or PMA, a robust increase in PKC-HM phosphorylation was seen. Longer exposures reveal several bands of slightly differing molecular weight becoming phosphorylated, probably due to the antibody recognizing multiple isoforms of PKC (data not shown). As expected, the increase in phosphorylation induced by serum and PMA was not blocked by rapamycin. More importantly, PP242 did not block PKC HM-P either, suggesting that mTOR is not the hydrophobic motif kinase for PKC. Previously it was seen that of the PKC isoforms examined, only PKC $\alpha$ 's HM was affected by rictor RNAi [4]. It is possible that the major stimulation induced phosphorylations seen with the pan-PKC-HM antibody in L6 myotubes do not include PKC $\alpha$ , although in HeLa cells this antibody specifically recognizes PKC $\alpha$  [4]. Further experiments, using pull-downs of PKC $\alpha$  will be required to definitively determine if acute inhibition of mTOR affects PKC $\alpha$ -HM phosphorylation. Nonetheless, the lack of effect of PP242 on PKC-HM phosphorylation seen in Figure 2.6, indicates that mTORC2 is not the hydrophobic motif kinase for every

isoform of PKC.

### 2.2.5 PP242 Does Not Have an Obvious Effect on Actin Stress Fibers

TORC2 is required for the generation of a polarized actin cytoskeleton in yeast [36]. Previous analysis of mTORC2 function using RNAi revealed a role for mTORC2 in the control of the actin cytoskeleton [3, 4], yet these findings were not confirmed in primary MEFs lacking mTORC2 [15, 17]. We examined actin stress fibers in NIH-3T3 cells treated with PP242 (Fig 2.7) and in primary MEFs (Data not shown). After 8 hours of treatment with PP242, we found no obvious effect on the morphology or abundance of actin stress fibers, suggesting that mTORC2 activity is not required for the maintenance of actin stress fibers in these cells. That PP242 didn't obviously affect the morphology or abundance of actin stress fibers, does not rule out a role for mTOR in the control of the actin cytoskeleton, but it does show pharmacological inhibition of mTORC2 does not affect the obvious changes in actin structure seen with RNAi.

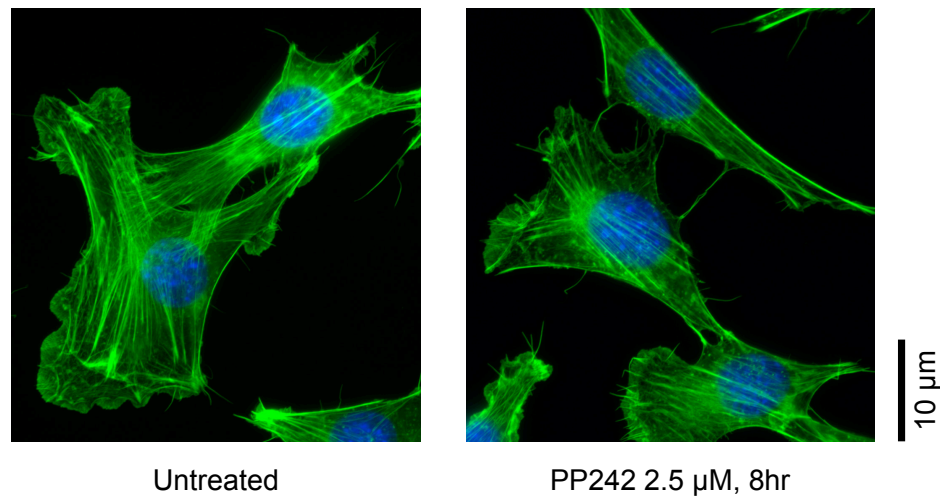


Figure 2.7: PP242 does not affect actin stress fibers. NIH-3T3 cells were stained for actin with Alexa 488-phalloidin (green) and for DNA with DAPI (blue). Images are representative of greater than 100 cells.

## 2.2.6 RSK Phosphorylation

p-90 ribosomal protein S6 kinase (RSK), like S6K, phosphorylates ribosomal protein S6 and may in addition phosphorylate other translational effectors such as eEF2 kinase and eIF4B [38]. RSK has two kinase domains, an N-terminal and a C-terminal kinase Domain (NTD and CTD). The CTD of RSK is a member of the calmodulin-dependent kinase or CamK kinase family, while the NTD is an AGC kinase. Full activation of RSK requires several steps involving phosphorylation of both kinase domains. Initially, RSK is phosphorylated on the activation loop of the CTD at T573 by ERK. ERK is a MAP Kinase downstream of Ras. Like other AGC kinases, the NTD has a hydrophobic motif c-terminal to the kinase domain, which in the case of RSK sits in a linker region between the NTD and the CTD. Once activated by ERK the CTD phosphorylates its only known substrate, the NTD-HM at S380 in the linker region between the two kinase domains. HM phosphorylation of the NTD recruits PDK1 which phosphorylates the activation loop of the NTD at S221, leading to full activity of the NTD. The NTD rather than the CTD is thought to phosphorylate RSK substrates.

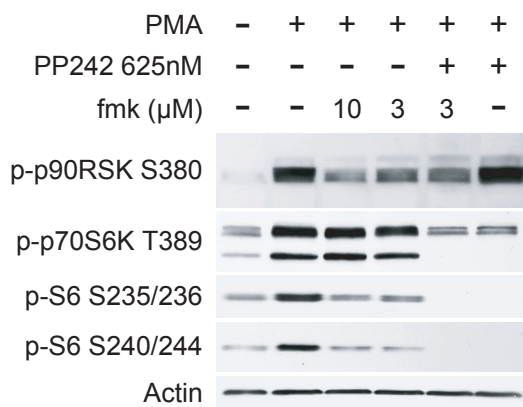


Figure 2.8: mTOR does not phosphorylate p90-RSK. Western blot of lysates from HEK-293 cells.

A specific and covalent inhibitor of the CTD of RSK was developed based on a bioinformatic analysis of the kinome [39]. The inhibitor, called fmk, exploits a fluoromethyl ketone group to react with a cysteine in the active site of RSK. fmk avoids inhibiting other kinases

with a similar cysteine in their active site because it requires the presence of a small residue at the gatekeeper position in the kinase active site. The identity of the amino acid at the gatekeeper position of a kinase active site plays a large role in determining the specificity of kinase inhibitors. fmk only binds and reacts with kinases that have a threonine or smaller residue at the gatekeeper position. Because the inhibitor is covalent it was possible to quantify the occupancy of the inhibition in the active site of the CTD or RSK [40]. Surprisingly, it was found that even when the CTD's active site was fully occupied with fmk, NTD-HM sometimes remained somewhat phosphorylated, suggesting that a kinase besides the CTD of RSK might be phosphorylated the HM or RSK. Because mTOR is the only kinase known to phosphorylate the HM of AGC kinases [35], we tested whether mTOR might participate in the phosphorylation of the HM of RSK (Fig 2.8). We stimulated HEK-293 cells with PMA, a stimulus known to induce HM phosphorylation of RSK which can be inhibited partially by fmk. fmk at 3 and 10  $\mu$ M reduced but did not eliminate RSK-HM phosphorylation at S380. PP242 on its own or in combination with 3  $\mu$ M of fmk also did not affect RSK-HM-P, but was sufficient to block the phosphorylation S6K and S6 at multiple sites. Interestingly, fmk reduced S6 phosphorylation without affecting S6K phosphorylation, suggesting that RSK phosphorylates S6. However PP242 completely inhibited S6 phosphorylation, without affecting HM-P of RSK. Therefore inhibition of mTOR prevents RSK from phosphorylating S6. These findings could be explained by S6 requiring a priming phosphorylation from mTOR or S6K before it can be phosphorylated by RSK, although more experiments will be required to confirm this mechanism.

### **2.2.7 PP242 Inhibits Proliferation More Completely than Rapamycin**

We next measured the effect of dual mTORC1/mTORC2 inhibition by PP242 on the proliferation of primary MEFs (Fig 2.9). For this analysis, we compared PP242 to selective mTORC1 inhibition by rapamycin. Rapamycin was tested at concentrations above its mTOR

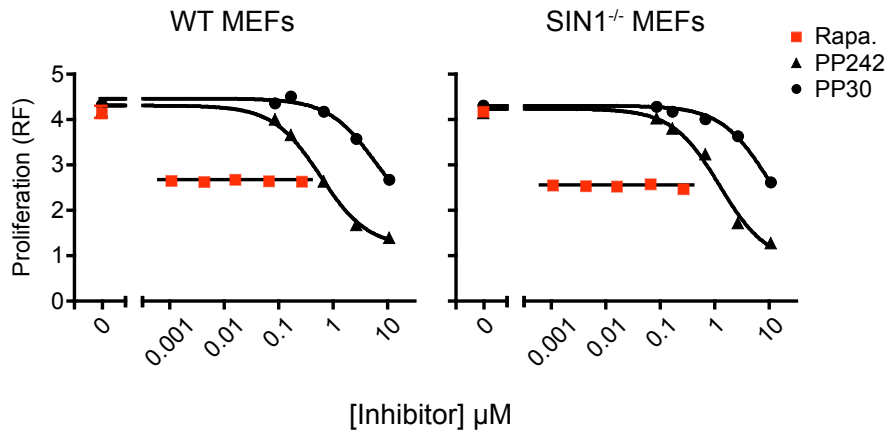


Figure 2.9: Differential inhibition of cell proliferation by PP242 and rapamycin does not require mTORC2.

Proliferation of primary MEFs cultured for three days in the presence of kinase inhibitors was assayed by resazurin fluorescence (RF) and is shown in arbitrary units.

IC<sub>50</sub> and at all concentrations tested it inhibited growth to the same extent. By contrast, PP242 had a dose dependent effect on proliferation and at higher doses was much more effective than rapamycin at blocking cell proliferation. The ability of PP242 to more efficiently block cell proliferation than rapamycin could be a result of its ability to inhibit mTORC2; rapamycin can only inhibit mTORC1. To test this possibility we measured the effects of both compounds on the proliferation of Sin1<sup>-/-</sup> MEFs which lack mTORC2. In Sin1<sup>-/-</sup> MEFs rapamycin was also less effective at blocking cell proliferation than PP242. That PP242 and rapamycin exhibit very different anti proliferative effects in Sin1<sup>-/-</sup> MEFs, suggests that the two compounds differentially affect mTORC1.

## 2.2.8 Rapamycin-Resistant mTORC1

mTORC1 regulates protein synthesis by phosphorylating the hydrophobic motif of p70S6 Kinase (S6K) at T389 and the eIF4E binding protein, 4EBP1, at multiple sites. Our proliferation experiments suggest that rapamycin and PP242 have distinct effects on mTORC1.

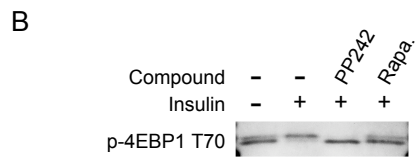
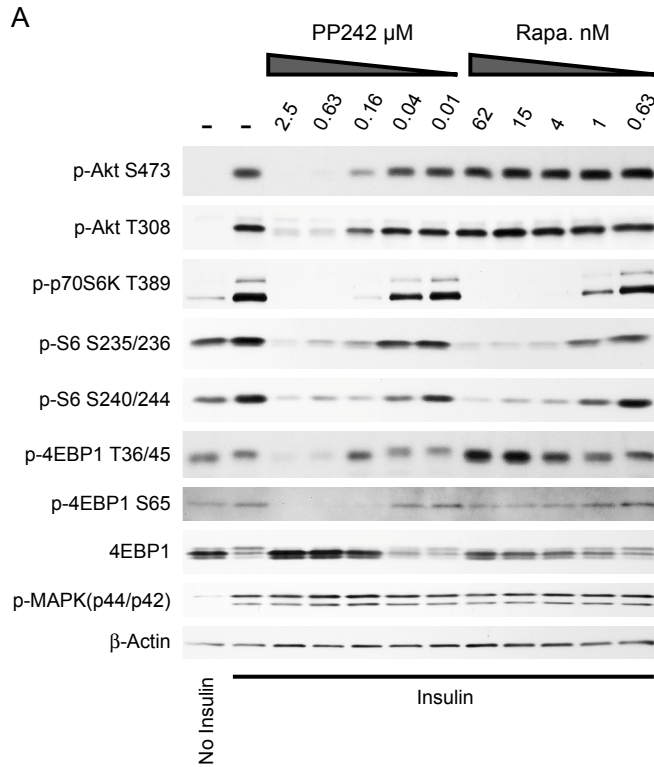


Figure 2.10: PP242 but not rapamycin inhibits 4EBP1 phosphorylation at T36/45.

Western blots of lysates from L6 myotubes treated with kinase inhibitors and stimulated with insulin for 10 minutes.

We compared the effects of acute treatment with rapamycin and PP242 on S6K, ribosomal protein S6 (S6) and 4EBP1 phosphorylation (Fig 2.10A), to see if these inhibitors differentially affect the phosphorylation of these canonical substrates of mTORC1. Both rapamycin and PP242 inhibited the phosphorylation of S6 Kinase and its substrate S6, and neither rapamycin nor PP242 affected the phosphorylation of 4EBP1 on T70 (Fig 2.10B). In contrast, PP242 fully inhibited the phosphorylation of 4EBP1 at T36/45 (same as T37/46 in human 4EBP1) and S65, while rapamycin only had a modest affect on these same phosphorylations. Treatment of cells with PP30 was also effective at reducing the phosphorylation of 4EBP1 at T36/45 (Fig 2.11) indicating that the block of T36/45 phosphorylation by PP242 is due to its inhibition of mTOR and not PKC alpha. PIK-90 did not reduce the phosphorylation of 4EBP1 at T36/45, demonstrating that inhibition of PI3-K and Akt activation alone is not sufficient to block the phosphorylation of 4EBP1 at T36/45 (Fig 2.11).

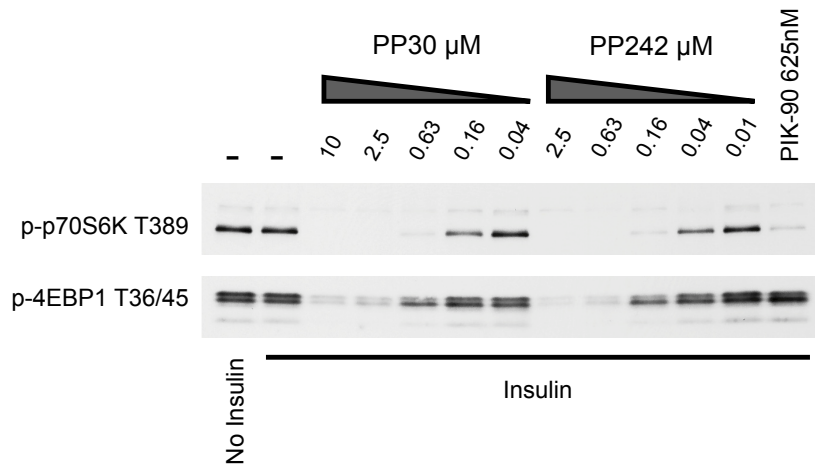


Figure 2.11: Rapamycin-resistant phosphorylation of 4EBP1 is sensitive to the TORKinibs PP30 and PP242 but not the PI3K inhibitor PIK-90. L6 myotube lysates from Figure 2.1 were analyzed by western blotting.

The enhanced dephosphorylation of 4EBP1 caused by PP242 as compared with rapamycin could be due to incomplete inhibition of mTORC1 by rapamycin or involvement of mTORC2 in the phosphorylation of 4EBP1. To examine these alternatives, we analyzed the effect of PP242 and rapamycin on the phosphorylation of 4EBP1 in *Sin1*<sup>-/-</sup> MEFs that lack mTORC2 (Fig 2.12). *Sin1*<sup>-/-</sup> MEFs showed higher levels of p4EBP1 suggesting that due to



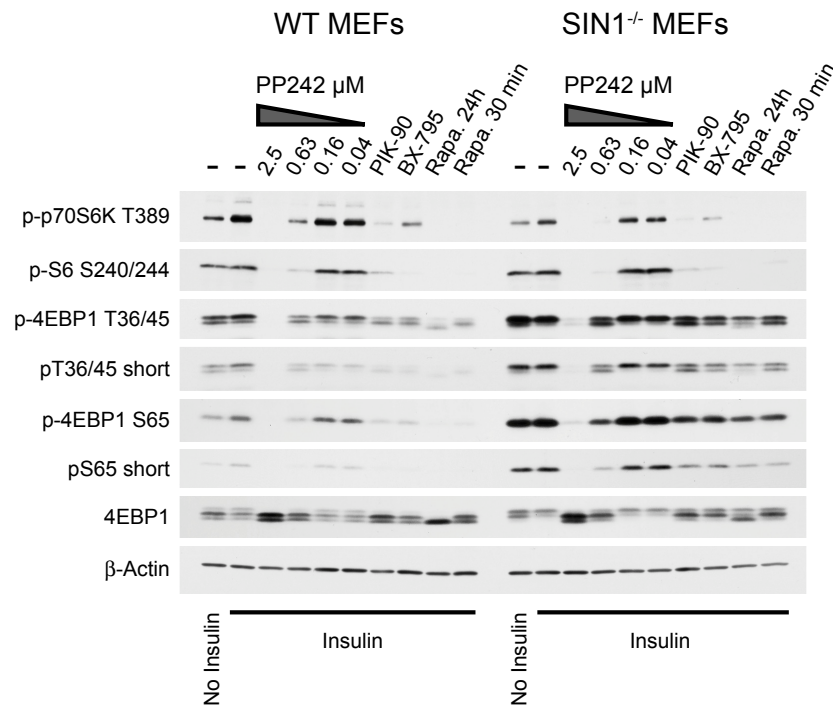


Figure 2.12: PP242 inhibits rapamycin-resistant mTORC1.

Western blots of lysates from Figure 2.4. Actin loading control is repeated here for clarity.

the lack of mTORC2, these cells have more mTORC1 activity, although stronger p70S6K phosphorylation in wild-type cells contradicts this simple interpretation. Despite an increase in p4EBP1 in Sin1<sup>-/-</sup> as compared with wild-type MEFs, shorter exposures of the p4EBP1 blots (Fig 2.12) show that PP242 inhibits p4EBP1 with the same potency in both cells. The fuller inhibition of p4EBP1 by PP242 than by rapamycin in wild-type and Sin1<sup>-/-</sup> MEFs, indicates that the presence of mTORC2 is not required for rapamycin and PP242 to have distinct effects on 4EBP1 phosphorylation, and suggests that PP242 is a more complete inhibitor of mTORC1 than rapamycin.

## 2.2.9 Inhibition of Translation by TORKinibs

While the precise role of S6K in translation control is still poorly understood, the hypophosphorylated 4EBP1 protein acts as negative regulator of the major cap binding protein eIF4E. We directly assessed the effect of PP242 on cap dependent translation downstream of mTOR activation. The phosphorylation of 4EBP1 by mTOR in response to growth factor and nutrient status causes it to dissociate from eIF4E allowing eIF4G and associated factors to bind to the 5' cap, recruit the 40S subunit of the ribosome and scan the mRNA for the start codon to initiate translation. The phosphorylation of 4EBP1 by mTOR is complicated in that it occurs at multiple sites and not all sites are equally effective at causing dissociation of 4EBP1 from eIF4E [41]. Furthermore, a hierarchy is thought to exist whereby the N terminal threonine phosphorylations at 37/46 precede and are required for the C terminal phosphorylations at S65 and T70 [42, 43]. Phosphorylation at S65 causes the greatest decrease in affinity of 4EBP1 for eIF4E [44, 45] and S65 is probably the most important site in cells for dissociation of 4EBP1 from eIF4E [46], but other sites are also important [41, 47].

We examined the effect of PP242 on the active eIF4E initiation complex of translation utilizing a cap binding assay. eIF4E binds tightly to beads coated with the cap analogue 7-methyl GTP ( $m^7GTP$ ) allowing proteins bound to eIF4E to be examined. Rapamycin caused partial inhibition of the insulin stimulated release of 4EBP1 from eIF4E (Fig 2.13)

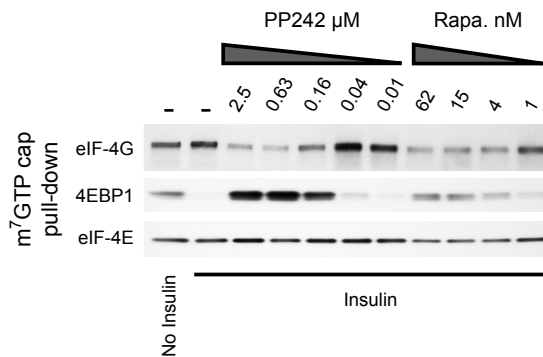


Figure 2.13: PP242 inhibits assembly of the active translation initiation complex. Cap-binding proteins in lysates from Figure 2.10 were purified by 7-methyl GTP ( $m^7GTP$ ) affinity and analyzed by western blotting.

consistent with its partial inhibition of S65 phosphorylation (Fig 2.10A). The rapamycin induced retention of 4EBP1 was accompanied by a loss of recovery of eIF4G because the binding of 4EBP1 and eIF4G to eIF4E are mutually exclusive. In contrast, treatment with PP242 caused a much larger retention of 4EBP1, raising the retention of 4EBP1 above the level seen in unstimulated serum-starved cells which are known to have low levels of protein translation [48].

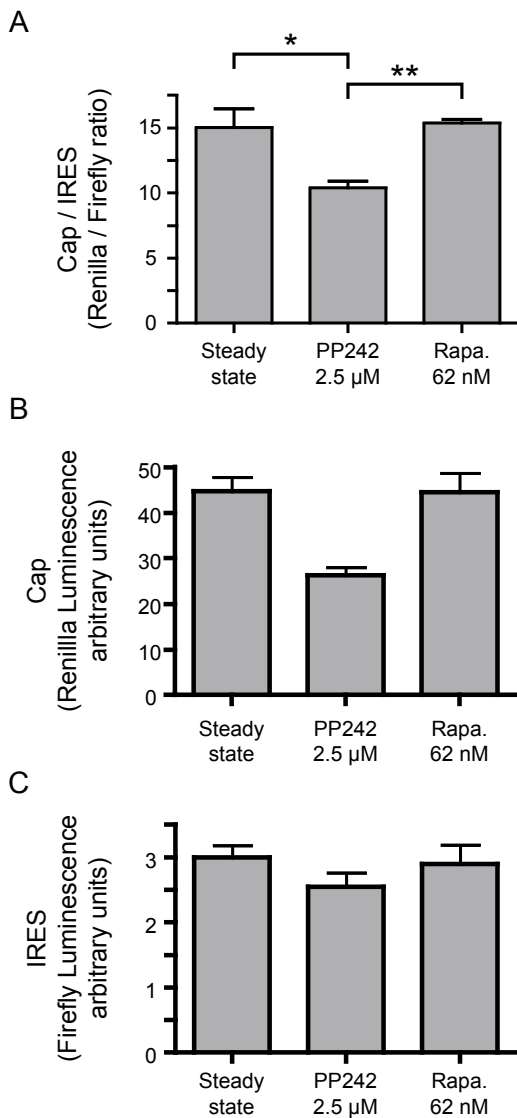


Figure 2.14: PP242 inhibits cap-dependent translation.

A) Primary MEFs were transfected with a bi-cistronic reporter vector. The ratio of renilla (Cap-dependent) to firefly (IRES-dependent) luciferase activity was measured after incubation overnight in either 10% serum (steady state) or with the indicated inhibitors in the presence of 10% serum (n = 3). \*p < 0.05, \*\*p < 0.01, ANOVA with Tukeys post test.

B) Renilla (Cap-dependent) luciferase activity.

C) Firefly (IRES-dependent) luciferase activity. Firefly luciferase activity of the PP242 treated sample is not significantly different from control (p = 0.4, ANOVA).

Translation initiation depending on eIF4E activity is the rate limiting step in cap-

dependent protein translation. PP242 caused a higher levels of binding between 4EBP1 and eIF4E than rapamycin (Fig 2.10A), suggesting that cap-dependent translation will be more highly suppressed by PP242 than by rapamycin. To quantify the efficiency of cap-dependent translation in the presence of PP242 and rapamycin, we used the well established bicistronic reporter assay where translation initiation of the first cistron is dependent on the 5' cap while initiation of the second cistron depends on a viral internal ribosome entry site (IRES) that bypasses the need for cap-binding proteins such as eIF4E [49]. PP242 caused a significant decrease in cap-dependent, but not IRES-dependent (Fig 2.14), translation while rapamycin did not have a statistically significant effect on cap dependent translation (Fig 2.14), consistent with the modest effect of rapamycin on 4EBP1 phosphorylation (Fig 2.10A). Based on this assay, inhibition of mTOR and p4EBP1 reduces cap-dependent translation by about 30%,

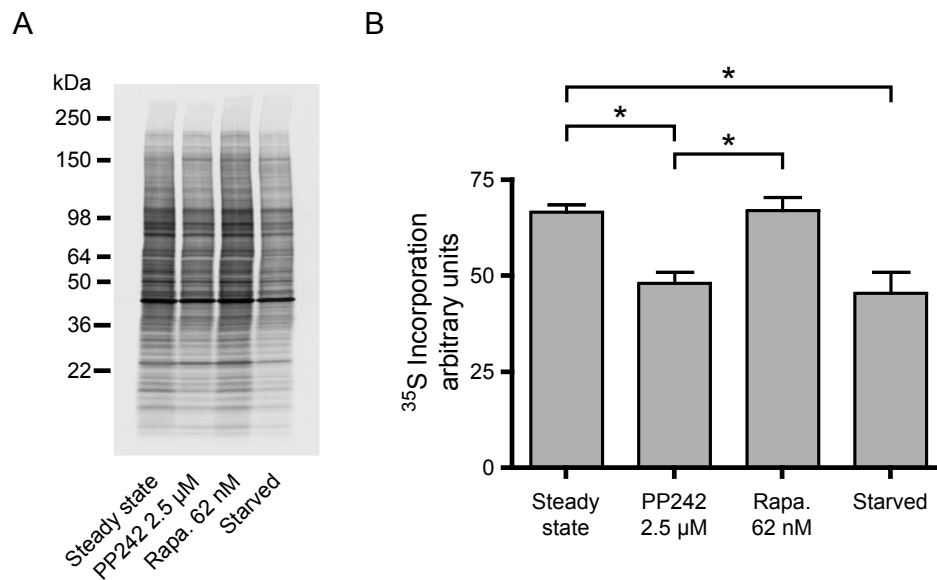


Figure 2.15: PP242 inhibits protein synthesis.

A) Primary MEFs were incubated overnight as in Figure 2.14 prior to labeling new protein synthesis with  $^{35}\text{S}$ . Newly synthesized proteins were separated by SDS-PAGE, transferred to nitrocellulose and visualized by autoradiography.

B) Newly synthesized protein from three experiments as in A was quantified. \* $p < 0.05$ , ANOVA with Tukeys post test.

suggesting that cap-dependent translation is only partially inhibited by hypophosphorylated 4EBP1. The majority of protein synthesis is thought to be cap-dependent, and consistent with this we find that PP242 also reduces total protein synthesis by about 30%, whereas rapamycin does not have a significant effect (Fig 2.15A and B).

### 2.2.10 Inhibition of mTORC1 and mTORC2 In Vivo

Mouse knock outs of mTORC1 or mTORC2 result in embryonic lethality and thus it has been difficult to examine the effects of loss of mTOR in animals. To begin to explore the tissue specific roles of mTORC1 and mTORC2 and confirm the pathway analysis from cell culture experiments, we treated mice with PP242 and rapamycin, and examined the acute effect of these drugs on insulin signaling in fat, skeletal muscle and liver tissue (Fig 2.16). In fat and liver, PP242 was able to completely inhibit the phosphorylation of Akt at S473 and T308, consistent with its effect on these phosphorylation sites observed in cell culture. Surprisingly, PP242 was only partially able to inhibit the phosphorylation of Akt in skeletal muscle and was more effective at inhibiting the phosphorylation of T308 than S473, despite its ability to fully inhibit the phosphorylation of 4EBP1 and S6. These results will

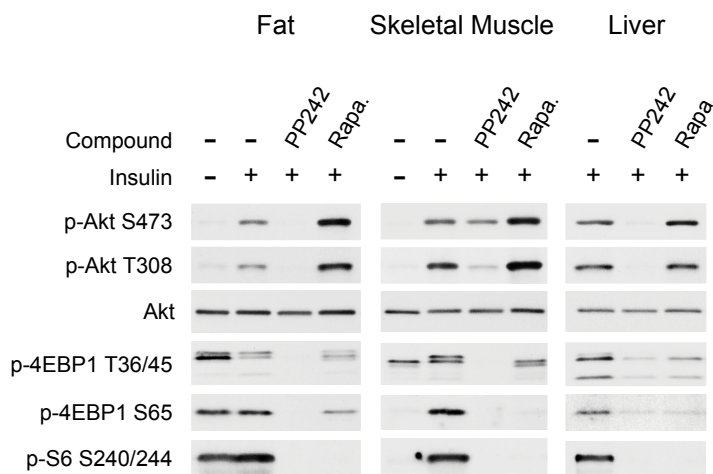


Figure 2.16: PP242 inhibits mTORC2 and rapamycin-resistant mTORC1 *in vivo*. Rapamycin (5 mg/kg), PP242 (20 mg/kg) or vehicle were injected into the intraperitoneal (IP) cavity of mice, followed by IP injection of 250mU insulin or saline. Lysates were prepared from perigenital fat, leg muscle and liver and analyzed by western blotting.

be confirmed by *in vivo* dose response experiments, but, consistent with the partial effect of PP242 on pAkt in skeletal muscle, a muscle specific knockout of the integral mTORC2 component rictor resulted in only a partial loss of Akt phosphorylation at S473 [50]. These results suggest that a kinase other than mTOR, such as DNA-PK [8, 9] may contribute to phosphorylation of Akt in muscle.

Rapamycin often stimulates the phosphorylation of Akt [51, 52], probably by relieving feedback inhibition from S6K to the insulin receptor substrate 1 (IRS1) [53], a key signaling molecule that links activation of the insulin receptor to PI3-K activation. In all tissues examined, and especially in fat and muscle, acute rapamycin treatment activated the phosphorylation of Akt at S473 and T308 (Fig 2.16). In contrast to rapamycin, by inhibiting both mTORC2 and mTORC1, PP242 suppresses rather than enhances Akt activation.

As was seen in cell culture, rapamycin and PP242 also differentially affect the mTORC1 substrates S6K and 4EBP1 *in vivo*. S6 phosphorylation was fully inhibited by rapamycin and PP242 in all tissues examined. While PP242 was effective at blocking the phosphorylation of 4EBP1 on both T36/45 and S65 in all tissues examined, rapamycin did not block 4EBP1 phosphorylation as completely as PP242. Further experiments will be required to identify the mechanism by which 4EBP1 phosphorylation is partially resistant to rapamycin.

## 2.3 Discussion

Rapamycin has been a powerful pharmacological tool allowing the discovery of mTOR's role in the control of protein synthesis. Since the discovery of a rapamycin-insensitive mTOR complex there has been a significant effort to develop pharmacological tools for studying this complex. Here we have used for the first time two structurally distinct compounds to pharmacologically dissect the effects of mTOR kinase inhibition toward mTORC1 and mTORC2 activity. We have shown through the use of these inhibitors that the inhibition of

mTOR kinase activity is sufficient to prevent the phosphorylation of Akt at S473, providing further evidence that mTORC2 is the kinase responsible for Akt hydrophobic motif phosphorylation upon insulin stimulation. We also find that phosphorylation at T308 is linked to phosphorylation at S473, as had been observed in experiments where mTORC2 was disabled by RNAi and long term rapamycin, but not homologous recombination. Surprisingly however, inhibition of mTORC2 does not result in a complete block of Akt signaling, as T308P is partially maintained and Akt substrate phosphorylation is only modestly affected when S473 is not phosphorylated.

Despite its modest effect on Akt substrate phosphorylation, PP242 was a strikingly more effective anti proliferative agent than rapamycin. These results were reproduced even in cells lacking mTORC2 (*Sin1<sup>-/-</sup>*), suggesting that downstream mTORC1 substrates might be responsible for PP242's strong anti-proliferative effects. Interestingly, we observe that phosphorylation of the mTORC1 substrate 4EBP1 is partially resistant to rapamycin treatment at concentrations that fully inhibit p70S6K while PP242 completely inhibits both p70S6K and 4EBP1. Because rapamycin can only partially inhibit the phosphorylation of 4EBP1, but it can fully inhibit the phosphorylation of p70S6K, rapamycin appears to be a substrate selective inhibitor of mTORC1. Consistent with this finding, experiments with purified proteins have shown that rapamycin/FKBP12 only partially inhibits the *in vitro* phosphorylation of 4EBP1 at Ser 65 by mTOR but can fully inhibit the *in vitro* phosphorylation of S6K [54]. By contrast, LY294002, a direct inhibitor of many PI3-K family members including mTOR, was equally effective at inhibiting the phosphorylation of S6K and 4EBP1 by mTOR *in vitro* [54] and in cells [23], though this finding is complicated by LY294002's inhibition of multiple lipid and protein kinases [55] including PIM, a kinase potentially upstream of 4EBP1 phosphorylation [56, 57]. These results argue that PP242, in addition to being useful for investigating mTORC2, can reveal rapamycin-resistant components of mTORC1 function. Indeed, proliferation of *Sin1<sup>-/-</sup>* MEFs is more sensitive to

PP242 than rapamycin (Fig 2.9), suggesting that rapamycin-resistant functions of mTORC1, including the aspects of translation initiation highlighted in Figures 2.13, 2.14 and 2.15 are key to the anti-proliferative effects of PP242. Furthermore, our findings suggest that the inhibition of translational control and the anti-proliferative effects of PP242 require inhibition of 4EBP1 phosphorylation and eIF4E activity.

Using TORKinibs to acutely inhibit mTOR has surprisingly led to the identification of outputs from mTORC1 that are rapamycin-resistant. These observations should motivate further studies aimed at understanding how rapamycin is able to selectively affect different outputs downstream of mTORC1. As active site inhibitors of mTOR join rapamycin and its analogs in the clinic [21, 26, 28], it will be important to understand the distinct effects of these pharmacological agents on cellular and organismal physiology and to evaluate their efficacy in the treatment of disease and cancer caused by hyperactivation of the PI3-K $\Rightarrow$ Akt $\Rightarrow$ mTOR pathway.

## **2.4 Materials and Methods**

### **Ethics Statement**

Mice were handled in accordance with protocols approved by the committee for animal research at the University of California, San Francisco.

### **Cell Culture**

Cells were grown in DMEM supplemented with 10% FBS, glutamine and penicillin/streptomycin. Confluent L6 myoblasts were differentiated into myotubes by culturing them for 5 days in media containing 2% FBS. L6 myotubes were maintained in media containing 2% FBS until use. Primary wild-type MEFs used in Figures 2.14 and 2.15 were isolated



at embryonic day 13.5 as previously described [58]. Primary Sin1<sup>-/-</sup> MEFs and matching wild-type controls were provided by B. Su and isolated as previously described [16].

## **Cell Lysis and Western Blotting**

Except where indicated otherwise, cells were serum starved overnight and incubated with inhibitors or 0.1% DMSO for 30 minutes prior to stimulation with 100 nM insulin for 10 minutes. All inhibitors were either synthesized as previously described [20, 24, 59] or were from Calbiochem (rapamycin and Akti-1/2). Cells were lysed by scraping into ice cold lysis buffer followed by brief sonication. Lysates were cleared by centrifugation, resolved by SDS-PAGE, transferred to nitrocellulose and immunoblotted with antibodies from Cell Signaling Technology. Unless otherwise indicated, cells were lysed in (300 mM NaCl, 50 mM Tris pH 7.5, 5 mM EDTA, 1% Triton X-100, 0.02% NaN<sub>3</sub>, 20nM microcystin (Calbiochem), Sigma phosphatase inhibitor cocktails 1 and 2, Roche protease inhibitor cocktail and 2 mM PMSF). For Fig 2.10, cells were lysed in cap lysis buffer (140 mM KCl, 10 mM Tris pH 7.5, 1 mM EDTA, 4 mM MgCl<sub>2</sub>, 1 mM DTT, 1% NP-40, 20 nM microcystin, Sigma phosphatase inhibitor cocktails 1 and 2, Roche protease inhibitor cocktail without EDTA and 2 mM PMSF).

## **Cap Pull-Down Assay**

L6 myotubes from one well of a six well plate were lysed in 300 µl of cap lysis buffer as described above. 50 µl of detergent free cap lysis buffer and 20 µl of pre-washed cap beads were added to 150 µl of cleared lysate and incubated at 4°C overnight with tumbling. The beads were washed twice with 400 µl of cap wash buffer (cap lysis buffer with 0.5% NP-40 instead of 1% NP-40) and twice with 500 µl PBS. The beads were boiled in SDS-PAGE sample buffer and the retained proteins analyzed by western blot. All antibodies were

from Cell Signaling Technologies except for the anti-eIF4E antibody which was from BD Biosciences.

### **PKC Kinase Assays**

Phosphorylation of histone H1 (4  $\mu$ M) by PKC was assayed in a buffer containing 200 ng/ml recombinant kinase (25 mM HEPES pH 7.5, 10 mM  $MgCl_2$ , 5 mM -glycerol phosphate, 0.05 mg/ml phosphatidylserine, 0.03% Triton X-100, 0.5 mg/ml BSA, 2.5 mM DTT, 100  $\mu$ M  $CaCl_2$ , 1  $\mu$ M PMA, 10  $\mu$ M ATP and 15  $\mu$ Ci/ml of  $\gamma$ - $^{32}P$ -ATP. Inhibitors were tested in a four-fold dilution series from 10  $\mu$ M to 600 pM and four measurements were made at each concentration. The kinase reaction was terminated by spotting onto nitrocellulose, which was washed 5 times with 1 M NaCl/1% phosphoric acid. The radioactivity remaining on the nitrocellulose sheet was quantified by phosphorimaging and  $IC_{50}$  values were determined by fitting the data to a sigmoidal dose-response curve using the Prism software package.

### **Other Kinase Assays**

PDK1, mTORC1 and mTORC2 were assayed as previously described [20].

### **In-Cell Western**

L6 myotubes were grown and differentiated in 96 well plates. The outside wells of the plate were not used for the experiment, but were kept filled with media. Following stimulation, cells were fixed for 15 minutes with 4% formaldehyde in PBS with  $Ca^{++}$  and  $Mg^{++}$ . The cells were washed 3 times with PBS and then blocked and permeabilized with 5% goat serum in PBS with 0.3% Triton X-100 (PBS-GS-TX). Primary antibodies to S473 (Cell Signaling #4060) and T308 (Cell Signaling #2965) were added at 1:1000 and 1:500 respectively in PBS-GS-TX and the plates were incubated at 4°C overnight. The plates were then washed 3

times with PBS and goat anti-rabbit secondary antibody (Pierce Biotechnology) was added at 0.01  $\mu\text{g/ml}$  in PBS-GS-TX. After 1 hour at room temperature, plates were washed 3 times more with PBS. ELISA chemiluminescent reagent (Femto, Pierce Biotechnology) was added to each well and after 1 minute the plate was read in a luminescence plate reader using a 100 ms integration time. The pAkt signal from pT308 and pS473 was normalized to control wells, so that 0 represents the level of pAkt in serum starved cells and 1 represents the level upon insulin stimulation.  $\text{EC}_{50}$  values were determined by fitting the data to a sigmoidal dose-response curve using the Prism software package. The significance of differences between  $\text{EC}_{50}$  values was evaluated using the F test.

### **Akt Transfection**

Akt was transfected into HEK293 cells using Lipofectamine 2000 according to the manufacturer's protocol. Two days after transfection, cells were serum starved overnight and the next day they were treated with inhibitors and processed for western blotting as described above.

### **Actin Cytoskeleton Staining**

NIH-3T3 cells were plated on poly-lysine coated coverslips at 30% confluence the day before the experiment. Following treatment with PP242 or 0.1% DMSO for 8 hours in 10% serum growth media, the actin cytoskeleton was stained as previously described [24].

## **Bicistronic Reporter Assay**

Primary MEFs were transfected with a bicistronic reporter [58] containing a viral IRES using Lipofectamine 2000 according to the manufacturers protocol. At two days post transfection, cells were treated overnight with compounds as indicated or starved of serum. The next day Renilla and Firefly luciferase activity were measured using the Dual-Luciferase kit (Promega). Differences in the ratio of Renilla to Firefly luciferase signals were analyzed for statistical significance by one-way ANOVA with Tukey's post test using the Prism software package.

## **<sup>35</sup>S Labeling of New Protein Synthesis**

Primary MEFs grown to 70% confluence in 6-well plates were incubated overnight in either 10% Serum (Steady State), kinase inhibitors in 10% serum, or 0.1% serum (starved). Cells were then washed once with DMEM lacking cysteine and methionine (DMEM-noS) and the media was replaced with DMEM-noS including dialyzed serum and kinase inhibitors as indicated. After incubation for 1 hour, 50  $\mu$ Ci of Expre<sup>35</sup>S<sup>35</sup>S (NEN) was added to each well and the cells were labeled for 4 hours. Cells were washed once with ice-cold PBS, and lysed as described above for western blotting. Following separation by SDS-PAGE, and transfer to nitrocellulose, <sup>35</sup>S labeled proteins were visualized by autoradiography with film. For quantitation, the membrane was exposed to a phosphorimager screen and the resulting image was quantified in ImageJ. Differences in <sup>35</sup>S incorporation were analyzed for statistical significance by one-way ANOVA with Tukey's post test using the Prism software package.

## ***In Vivo* Drug Treatment and Western Blotting**

Drugs were prepared in 100  $\mu$ l of vehicle containing 20% DMSO, 40% PEG-400 and 40% Saline. 6 week old male C57BL/6 mice were fasted overnight prior to drug treatment. PP242 (0.4 mg), rapamycin (0.1 mg) or vehicle alone was injected IP. After 30 minutes for the rapamycin-treated mouse or 10 min for the PP242 and vehicle treated mice, 250mU of insulin in 100  $\mu$ l of saline was injected IP. 15 minutes after the insulin injection, the mice were sacrificed by CO<sub>2</sub> asphyxiation followed by cervical dislocation. Tissues were harvested and frozen on liquid nitrogen in 200  $\mu$ l of cap lysis buffer. The frozen tissue was thawed on ice, manually disrupted with a mortar and pestle, and then further processed with a micro tissue-homogenizer (Fisher PowerGen 125 with Omni-Tip probe). Protein concentration of the cleared lysate was measured by Bradford assay and 5-10  $\mu$ g of protein was analyzed by western blot as described above.

## **Cell Proliferation Assay**

Wild-type and Sin1<sup>-/-</sup> MEFs were plated in 96 well plates at approximately 30% confluence and left overnight to adhere. The following day cells were treated with PP242, rapamycin or vehicle (0.1% DMSO). After 72 hours of treatment 10  $\mu$ l of 440  $\mu$ M resazurin sodium salt (Sigma) was added to each well, and after 18 hours the florescence intensity in each well was measured using a top-reading florescent plate reader with excitation at 530 nm and emission at 590 nm.

## References

- 1) Hara K, Maruki Y, Long X, Yoshino K, Oshiro N, Hidayat S, Tokunaga C, Avruch J, and Yonezawa K, “Raptor, a binding partner of target of rapamycin (TOR), mediates TOR action,” *Cell*, vol. 110, no. 2, pp. 177–89, 2002.
- 2) Kim DH, Sarbassov DD, Ali SM, King JE, Latek RR, Erdjument-Bromage H, Tempst P, and Sabatini DM, “mTOR interacts with raptor to form a nutrient-sensitive complex that signals to the cell growth machinery,” *Cell*, vol. 110, no. 2, pp. 163–75, 2002.
- 3) Jacinto E, Loewith R, Schmidt A, Lin S, Ruegg MA, Hall A, and Hall MN, “Mammalian TOR complex 2 controls the actin cytoskeleton and is rapamycin insensitive,” *Nat Cell Biol*, vol. 6, no. 11, pp. 1122–8, 2004.
- 4) Sarbassov DD, Ali SM, Kim DH, Guertin DA, Latek RR, Erdjument-Bromage H, Tempst P, and Sabatini DM, “Rictor, a novel binding partner of mTOR, defines a rapamycin-insensitive and raptor-independent pathway that regulates the cytoskeleton,” *Curr Biol*, vol. 14, no. 14, pp. 1296–302, 2004.
- 5) Ruggero D, Montanaro L, Ma L, Xu W, Londei P, Cordon-Cardo C, and Pandolfi PP, “The translation factor eIF-4E promotes tumor formation and cooperates with c-Myc in lymphomagenesis,” *Nat Med*, vol. 10, no. 5, pp. 484–6, 2004.
- 6) Sarbassov DD, Guertin DA, Ali SM, and Sabatini DM, “Phosphorylation and regulation of Akt/PKB by the rictor-mTOR complex,” *Science*, vol. 307, no. 5712, pp. 1098–101, 2005.
- 7) Garcia-Martinez JM and Alessi DR, “mTOR complex-2 (mTORC2) controls hydrophobic motif phosphorylation and activation of serum and glucocorticoid induced protein kinase-1 (SGK1),” *Biochem J*, 2008.

- 8) Bozulic L, Surucu B, Hynx D, and Hemmings BA, "PKBalpha/Akt1 acts downstream of DNA-PK in the DNA double-strand break response and promotes survival," *Mol Cell*, vol. 30, no. 2, pp. 203–13, 2008.
- 9) Feng J, Park J, Cron P, Hess D, and Hemmings BA, "Identification of a PKB/Akt hydrophobic motif Ser-473 kinase as DNA-dependent protein kinase," *J Biol Chem*, vol. 279, no. 39, pp. 41 189–96, 2004.
- 10) McDonald PC, Oloumi A, Mills J, Dobрева I, Maidan M, Gray V, Wederell ED, Bally MB, Foster LJ, and Dedhar S, "Rictor and integrin-linked kinase interact and regulate Akt phosphorylation and cancer cell survival," *Cancer Res*, vol. 68, no. 6, pp. 1618–24, 2008.
- 11) Persad S, Attwell S, Gray V, Mawji N, Deng JT, Leung D, Yan J, Sanghera J, Walsh MP, and Dedhar S, "Regulation of protein kinase B/Akt-serine 473 phosphorylation by integrin-linked kinase: critical roles for kinase activity and amino acids arginine 211 and serine 343," *J Biol Chem*, vol. 276, no. 29, pp. 27 462–9, 2001.
- 12) Manning BD and Cantley LC, "AKT/PKB signaling: navigating downstream," *Cell*, vol. 129, no. 7, pp. 1261–74, 2007.
- 13) Andjelkovic M, Alessi DR, Meier R, Fernandez A, Lamb NJ, Frech M, Cron P, Cohen P, Lucocq JM, and Hemmings BA, "Role of translocation in the activation and function of protein kinase B," *J Biol Chem*, vol. 272, no. 50, pp. 31 515–24, 1997.
- 14) Hresko RC and Mueckler M, "mTOR.RICTOR is the Ser473 kinase for Akt/protein kinase B in 3T3-L1 adipocytes," *J Biol Chem*, vol. 280, no. 49, pp. 40 406–16, 2005.
- 15) Guertin DA, Stevens DM, Thoreen CC, Burds AA, Kalaany NY, Moffat J, Brown M, Fitzgerald KJ, and Sabatini DM, "Ablation in mice of the mTORC components raptor,

- riCTOR, or mLST8 reveals that mTORC2 is required for signaling to Akt-FOXO and PKC $\alpha$ , but not S6K1,” *Dev Cell*, vol. 11, no. 6, pp. 859–71, 2006.
- 16) Jacinto E, Facchinetti V, Liu D, Soto N, Wei S, Jung SY, Huang Q, Qin J, and Su B, “SIN1/MIP1 maintains rictor-mTOR complex integrity and regulates Akt phosphorylation and substrate specificity,” *Cell*, vol. 127, no. 1, pp. 125–37, 2006.
  - 17) Shiota C, Woo JT, Lindner J, Shelton KD, and Magnuson MA, “Multiallelic disruption of the rictor gene in mice reveals that mTOR complex 2 is essential for fetal growth and viability,” *Dev Cell*, vol. 11, no. 4, pp. 583–9, 2006.
  - 18) Sarbassov DD, Ali SM, Sengupta S, Sheen JH, Hsu PP, Bagley AF, Markhard AL, and Sabatini DM, “Prolonged rapamycin treatment inhibits mTORC2 assembly and Akt/PKB,” *Mol Cell*, vol. 22, no. 2, pp. 159–68, 2006.
  - 19) Fruman DA, Meyers RE, and Cantley LC, “Phosphoinositide kinases,” *Annu Rev Biochem*, vol. 67, pp. 481–507, 1998.
  - 20) Knight ZA *et al.*, “A pharmacological map of the PI3-K family defines a role for p110 $\alpha$  in insulin signaling,” *Cell*, vol. 125, no. 4, pp. 733–47, 2006.
  - 21) Stauffer F, Maira SM, Furet P, and Garcia-Echeverria C, “Imidazo[4,5-c]quinolines as inhibitors of the PI3K/PKB-pathway,” *Bioorg Med Chem Lett*, vol. 18, no. 3, pp. 1027–30, 2008.
  - 22) Brunn GJ, Williams J, Sabers C, Wiederrecht G, Lawrence J, and Abraham RT, “Direct inhibition of the signaling functions of the mammalian target of rapamycin by the phosphoinositide 3-kinase inhibitors, wortmannin and LY294002,” *Embo J*, vol. 15, no. 19, pp. 5256–67, 1996.



- 23) Wang X, Beugnet A, Murakami M, Yamanaka S, and Proud CG, "Distinct signaling events downstream of mTOR cooperate to mediate the effects of amino acids and insulin on initiation factor 4E-binding proteins," *Mol Cell Biol*, vol. 25, no. 7, pp. 2558–72, 2005.
- 24) Apse B, Blair JA, Gonzalez B, Nazif TM, Feldman ME, Aizenstein B, Hoffman R, Williams RL, Shokat KM, and Knight ZA, "Targeted polypharmacology: discovery of dual inhibitors of tyrosine and phosphoinositide kinases," *Nat Chem Biol*, vol. 4, no. 11, pp. 691–9, 2008.
- 25) Averous J and Proud CG, "When translation meets transformation: the mTOR story," *Oncogene*, vol. 25, no. 48, pp. 6423–35, 2006.
- 26) Chiang GG and Abraham RT, "Targeting the mTOR signaling network in cancer," *Trends Mol Med*, vol. 13, no. 10, pp. 433–42, 2007.
- 27) Easton JB and Houghton PJ, "mTOR and cancer therapy," *Oncogene*, vol. 25, no. 48, pp. 6436–46, 2006.
- 28) Faivre S, Kroemer G, and Raymond E, "Current development of mTOR inhibitors as anticancer agents," *Nat Rev Drug Discov*, vol. 5, no. 8, pp. 671–88, 2006.
- 29) Guertin DA and Sabatini DM, "Defining the role of mTOR in cancer," *Cancer Cell*, vol. 12, no. 1, pp. 9–22, 2007.
- 30) Sabatini DM, "mTOR and cancer: insights into a complex relationship," *Nat Rev Cancer*, vol. 6, no. 9, pp. 729–34, 2006.
- 31) Ikenoue T, Inoki K, Yang Q, Zhou X, and Guan KL, "Essential function of TORC2 in PKC and Akt turn motif phosphorylation, maturation and signalling," *Embo J*, vol. 27, no. 14, pp. 1919–31, 2008.

- 32) Feldman RI *et al.*, “Novel small molecule inhibitors of 3-phosphoinositide-dependent kinase-1,” *J Biol Chem*, vol. 280, no. 20, pp. 19 867–74, 2005.
- 33) Knight ZA and Shokat KM, “Chemical genetics: where genetics and pharmacology meet,” *Cell*, vol. 128, no. 3, pp. 425–30, 2007.
- 34) Lindsley CW *et al.*, “Allosteric Akt (PKB) inhibitors: discovery and SAR of isozyme selective inhibitors,” *Bioorg Med Chem Lett*, vol. 15, no. 3, pp. 761–4, 2005.
- 35) Jacinto E and Lorberg A, “TOR regulation of AGC kinases in yeast and mammals,” *Biochem J*, vol. 410, no. 1, pp. 19–37, 2008.
- 36) Loewith R, Jacinto E, Wullschleger S, Lorberg A, Crespo JL, Bonenfant D, Oppliger W, Jenoe P, and Hall MN, “Two TOR complexes, only one of which is rapamycin sensitive, have distinct roles in cell growth control,” *Mol Cell*, vol. 10, no. 3, pp. 457–68, 2002.
- 37) Facchinetti V *et al.*, “The mammalian target of rapamycin complex 2 controls folding and stability of Akt and protein kinase C,” *Embo J*, vol. 27, no. 14, pp. 1932–43, 2008.
- 38) Hauge C and Frodin M, “RSK and MSK in MAP kinase signalling,” *J Cell Sci*, vol. 119, no. Pt 15, pp. 3021–3, 2006.
- 39) Cohen MS, Zhang C, Shokat KM, and Taunton J, “Structural bioinformatics-based design of selective, irreversible kinase inhibitors,” *Science*, vol. 308, no. 5726, pp. 1318–21, 2005.
- 40) Cohen MS, Hadjivassiliou H, and Taunton J, “A clickable inhibitor reveals context-dependent autoactivation of p90 RSK,” *Nat Chem Biol*, vol. 3, no. 3, pp. 156–60, 2007.

- 41) Fadden P, Haystead TA, and Lawrence J, "Identification of phosphorylation sites in the translational regulator, PHAS-I, that are controlled by insulin and rapamycin in rat adipocytes," *J Biol Chem*, vol. 272, no. 15, pp. 10 240–7, 1997.
- 42) Gingras AC, Gygi SP, Raught B, Polakiewicz RD, Abraham RT, Hoekstra MF, Aebersold R, and Sonenberg N, "Regulation of 4E-BP1 phosphorylation: a novel two-step mechanism," *Genes Dev*, vol. 13, no. 11, pp. 1422–37, 1999.
- 43) Gingras AC, Raught B, Gygi SP, Niedzwiecka A, Miron M, Burley SK, Polakiewicz RD, Wyslouch-Cieszynska A, Aebersold R, and Sonenberg N, "Hierarchical phosphorylation of the translation inhibitor 4E-BP1," *Genes Dev*, vol. 15, no. 21, pp. 2852–64, 2001.
- 44) Karim MM, Hughes JM, Warwicker J, Scheper GC, Proud CG, and McCarthy JE, "A quantitative molecular model for modulation of mammalian translation by the eIF4E-binding protein 1," *J Biol Chem*, vol. 276, no. 23, pp. 20 750–7, 2001.
- 45) Mothe-Satney I, Yang D, Fadden P, Haystead TA, and Lawrence J, "Multiple mechanisms control phosphorylation of PHAS-I in five (S/T)P sites that govern translational repression," *Mol Cell Biol*, vol. 20, no. 10, pp. 3558–67, 2000.
- 46) Mothe-Satney I, Brunn GJ, McMahon LP, Capaldo CT, Abraham RT, and Lawrence J, "Mammalian target of rapamycin-dependent phosphorylation of PHAS-I in four (S/T)P sites detected by phospho-specific antibodies," *J Biol Chem*, vol. 275, no. 43, pp. 33 836–43, 2000.
- 47) Ferguson G, Mothe-Satney I, and Lawrence J, "Ser-64 and Ser-111 in PHAS-I are dispensable for insulin-stimulated dissociation from eIF4E," *J Biol Chem*, vol. 278, no. 48, pp. 47 459–65, 2003.
- 48) Ruggero D and Sonenberg N, "The Akt of translational control," *Oncogene*, vol. 24, no. 50, pp. 7426–34, 2005.

- 49) Yoon A, Peng G, Brandenburger Y, Zollo O, Xu W, Rego E, and Ruggero D, "Impaired control of IRES-mediated translation in X-linked dyskeratosis congenita," *Science*, vol. 312, no. 5775, pp. 902–6, 2006.
- 50) Kumar A, Harris TE, Keller SR, Choi KM, Magnuson MA, and Lawrence J, "Muscle-specific deletion of rictor impairs insulin-stimulated glucose transport and enhances Basal glycogen synthase activity," *Mol Cell Biol*, vol. 28, no. 1, pp. 61–70, 2008.
- 51) O'Reilly KE *et al.*, "mTOR inhibition induces upstream receptor tyrosine kinase signaling and activates Akt," *Cancer Res*, vol. 66, no. 3, pp. 1500–8, 2006.
- 52) Wan X, Harkavy B, Shen N, Grohar P, and Helman LJ, "Rapamycin induces feedback activation of Akt signaling through an IGF-1R-dependent mechanism," *Oncogene*, vol. 26, no. 13, pp. 1932–40, 2007.
- 53) Um SH *et al.*, "Absence of S6K1 protects against age- and diet-induced obesity while enhancing insulin sensitivity," *Nature*, vol. 431, no. 7005, pp. 200–5, 2004.
- 54) McMahon LP, Choi KM, Lin TA, Abraham RT, and Lawrence J, "The rapamycin-binding domain governs substrate selectivity by the mammalian target of rapamycin," *Mol Cell Biol*, vol. 22, no. 21, pp. 7428–38, 2002.
- 55) Gharbi SI, Zvelebil MJ, Shuttleworth SJ, Hancox T, Saghir N, Timms JF, and Waterfield MD, "Exploring the specificity of the PI3K family inhibitor LY294002," *Biochem J*, vol. 404, no. 1, pp. 15–21, 2007.
- 56) Fox CJ, Hammerman PS, Cinalli RM, Master SR, Chodosh LA, and Thompson CB, "The serine/threonine kinase Pim-2 is a transcriptionally regulated apoptotic inhibitor," *Genes Dev*, vol. 17, no. 15, pp. 1841–54, 2003.

- 57) Jacobs MD, Black J, Futer O, Swenson L, Hare B, Fleming M, and Saxena K, “Pim-1 ligand-bound structures reveal the mechanism of serine/threonine kinase inhibition by LY294002,” *J Biol Chem*, vol. 280, no. 14, pp. 13 728–34, 2005.
- 58) Ruggero D, Grisendi S, Piazza F, Rego E, Mari F, Rao PH, Cordon-Cardo C, and Pandolfi PP, “Dyskeratosis congenita and cancer in mice deficient in ribosomal RNA modification,” *Science*, vol. 299, no. 5604, pp. 259–62, 2003.
- 59) Tamguney T, Zhang C, Fiedler D, Shokat K, and Stokoe D, “Analysis of 3-phosphoinositide-dependent kinase-1 signaling and function in ES cells,” *Exp Cell Res*, vol. 314, no. 11-12, pp. 2299–312, 2008.

## Chapter 3

# Molecular and Cellular Response to Isoform Specific PI3-K Inhibition

### Abstract

Growth factors and insulin activate receptor tyrosine kinases in the plasma membrane. Receptor tyrosine kinases, such as the insulin receptor, then activate the mytogen activated protein kinase (MAPK) pathway and the phosphoinositide 3-kinase (PI3-K) pathway. These two pathways are the most commonly mutated pathways driving cancer. PI3-K inhibitors are currently being developed and tested as anti-cancer therapeutics. PI3-K produces the lipid second messenger PIP<sub>3</sub> which recruits proteins with plextrin homology (PH) domains to the membrane. Akt is an important kinase which contains a PH domain and is activated by phosphorylation downstream of PI3-K; activation of Akt is responsible for many of the cellular effects of PI3-K activation. Two isoforms of PI3-K, p110 $\alpha$  and p110 $\beta$  are distributed throughout the body. Biochemically, p110 $\alpha$  and p110 $\beta$  appear to be quite similar, suggesting they might be redundant. We treated cells with specific inhibitors of p110 $\alpha$  and p110 $\beta$  to find that inhibitors of p110 $\alpha$  block insulin stimulation of Akt phosphorylation and

glucose uptake triggered by insulin. Inhibitors of p110 $\beta$  had no effect on Akt activation or glucose uptake in these assays, providing strong evidence that p110 $\alpha$  is the major isoform of PI3-K downstream of insulin receptor activation. Surprisingly, when we examined PIP<sub>3</sub> levels we saw that inhibition of either p110 $\alpha$  or p110 $\beta$  reduce PIP<sub>3</sub> levels to a similar extent. Consistent with the reduction in PIP<sub>3</sub> levels by inhibitors of p110 $\beta$ , pretreatment with the p110 $\beta$  inhibitor TGX-115, cooperated the p110 $\alpha$  inhibitor, PIK-75, to block the activation of Akt in muscle cells, but this synergy was not observed in Fat cells. These data are consistent with p110 $\beta$  generating basal levels of PIP<sub>3</sub> that cooperate, in some cell types, with agonist stimulated rises in PIP<sub>3</sub> generated by p110 $\alpha$ .

### 3.1 Introduction

Phosphoinositide 3-kinases (PI3-Ks) catalyze the synthesis of the phosphatidylinositol (PI) second messengers PI(3)P, PI(3,4)P<sub>2</sub>, and PI(3,4,5)P<sub>3</sub> (PIP<sub>3</sub> and see Fig 3.1) [1]. In the appropriate cellular context, these three lipids control diverse physiological processes including cell growth, survival, differentiation, and chemotaxis [2]. The PI3-K family comprises 15 kinases with distinct substrate specificities, expression patterns, and modes of regulation. The class I PI3-Ks (p110 $\alpha$ , p110 $\beta$ , p110 $\delta$ , and p110 $\gamma$ ) are activated by tyrosine kinases or G protein-coupled receptors to generate PIP<sub>3</sub>, which engages downstream effectors such as the Akt/PDK1 pathway, the Tec family kinases, and the Rho family GTPases. The class II and III PI3-Ks play a key role in intracellular trafficking through the synthesis of PI(3)P and PI(3,4)P<sub>2</sub>. The PIKKs are protein kinases that control cell growth (mTORC1) or monitor genomic integrity (ATM, ATR, DNA-PK, and hSmg-1).

The importance of these enzymes in diverse pathophysiology has made the PI3-K family the focus of intense interest as a new class of drug targets [3]. This interest has been fueled by the recent discovery that p110 $\alpha$  is frequently mutated in primary tumors [4] and evidence

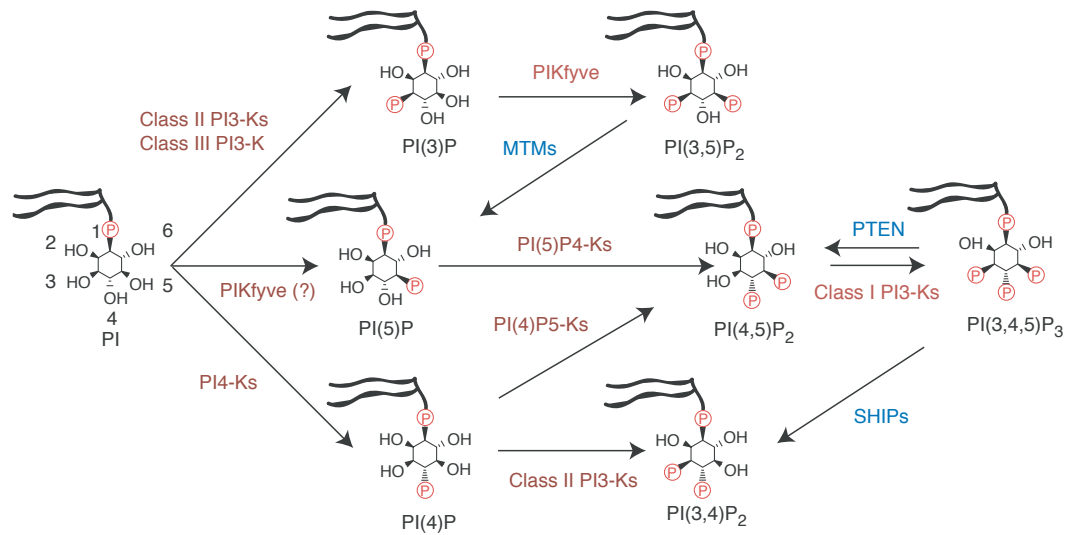


Figure 3.1: Routes for the synthesis of phosphoinositides in mammalian cells. Lipid kinases are shown in red and lipid phosphatases are shown in blue.

that the lipid phosphatase PTEN, an inhibitor of PI3-K signaling, is a commonly inactivated tumor suppressor [5]. Efforts are underway to develop small molecule PI3-K inhibitors for the treatment of inflammation and autoimmune disease (p110 $\delta$ , p110 $\gamma$ , and mTOR), thrombosis (p110 $\beta$ ), viral infection (the PIKKs), and cancer (p110 $\alpha$ , mTOR, and others). Recently, the first selective inhibitors of these enzymes have been reported [6–11].

A key challenge in targeting the PI3-K family with drugs is to understand how individual PI3-K isoforms control normal physiology, as this defines the therapeutic window for targeting a specific isoform. Genetic approaches to uncouple the action of PI3-K isoforms have been frustrated by the complex coordinate regulation of these enzymes. Homozygous deletion of either p110 $\alpha$  or p110 $\beta$  (the two most widely expressed PI3-Ks) leads to embryonic lethality in mice [12, 13]. Heterozygous deletion of these isoforms is complicated by a compensatory downregulation of the p85 regulatory subunit [14]. Knockout of p85 isoforms induces a paradoxical increase in PI3-K signaling [15, 16], reflecting the fact that p85 both promotes PI3-K activity (by stabilizing the p110 catalytic subunit) and inhibits it (by reduc-



ing basal activity and sequestering essential signaling complexes [17, 18]. A similar effect has been observed among the PIKKs, where a deficiency in DNA-PK alters the expression of ATM and hSmg-1 [19]. In addition to these compensatory mechanisms, PI3-Ks possess kinase-independent signaling activities that can cause inhibitors and knockouts to induce different phenotypes [20, 21]. For example, p110 $\gamma$  knockout mice develop cardiac damage in response to chronic pressure overload, whereas mice bearing a p110 $\gamma$  kinase-dead allele do not [22]. In this case, the difference was traced to an allosteric activation of PDE3B by p110 $\gamma$  that is disrupted in the knockout but unaffected by the kinase-dead allele or an inhibitor.

Cell-permeable small molecule inhibitors make it possible to directly assess the phenotypic consequences of inhibiting a kinase with a drug in a physiologically relevant model system. The challenge for pharmacological target validation is that few well-characterized, selective kinase inhibitors are known. This has been particularly true for the PI3-Ks, as the two primary pharmacological tools available, wortmannin and LY294002, are broadly active within the family. We report here a set of potent, chemotypically diverse small molecule inhibitors that span the PI3-K family. Critically, this panel includes representatives from a large number of PI3-K inhibitor chemotypes currently in preclinical drug development and therefore anticipates the biological activities likely to be found in eventual clinical candidates. Using this chemical array, we identify p110 $\alpha$  as the key PI3-K activity downstream of the insulin receptor.

## 3.2 PI3-K Inhibitors

Representatives from nine chemical classes of PI3-K inhibitors were selected from compounds under development by the pharmaceutical industry. Compounds from each class were synthesized and their activity against the class I PI3-Ks measured in vitro. The extended specificity profile of these compounds was determined by measuring IC<sub>50</sub> values in vitro against 15 purified PI3-K family members (Fig 3.1). As this panel includes almost all proteins with sequence homology to p110 $\alpha$ , it is highly enriched for the likely targets of these inhibitors. These compounds were also tested against 40 additional purified kinases from three families: the PIPKs, the class II PI4-Ks, and the protein kinases (data not shown).

	PIK23	TGX115	AMA37	PIK39	IC87114	TGX286	PIK75	PIK90	PIK93	PIK108	PI-103	PIK124	KU-55399
<b><i>PI3Ks</i></b>													
p110 $\alpha$	>200	61	32	>200	>200	4.5	0.0058	0.011	0.039	2.6	0.008	0.023	3.3
p110 $\beta$	42	0.13	3.7	11	16	0.12	1.3	0.35	0.59	0.057	0.088	1.1	1.2
p110 $\delta$	0.097	0.63	22	0.18	0.13	1	0.51	0.058	0.12	0.26	0.048	0.34	0.72
p110 $\gamma$	50	100	100	17	61	10	0.076	0.018	0.016	4.1	0.15	0.054	9.9
PI3KC2 $\alpha$	>100	>100	>100	>100	>100	>100	~10	0.047	~16	~100	~1	0.14	ND
PI3KC2 $\beta$	100	50	>100	100	>100	~100	~1	0.064	0.14	~20	0.026	0.37	ND
PI3KC2 $\gamma$	>100	100	50	100	>100	ND	ND	ND	ND	ND	ND	ND	ND
hsVPS34	~50	5.2	>100	>100	>100	3.1	2.6	0.83	0.32	~5	2.3	10	~10
<b><i>PI4Ks</i></b>													
PI4KII $\alpha$	>100	>100	>100	>100	>100	>100	>100	>100	>100	>100	>100	>100	>100
PI4KIII $\alpha$	>100	>100	>100	>100	>100	>100	>100	0.83	1.1	~50	>100	>100	>100
PI4KIII $\beta$	>100	>100	>100	>100	>100	>100	~50	3.1	0.019	>100	~50	>100	>100
<b><i>PIKKs</i></b>													
ATR	>100	>100	>100	>100	>100	>100	21	15	17	>100	0.85	2	20
ATM	>100	20	ND	>100	>100	>100	2.3	0.61	0.49	35	0.92	3.9	0.005
DNA-PK	>100	1.2	0.27	>100	>100	~50	0.002	0.013	0.064	0.12	0.002	1.5	~10
mTORC1	>100	>100	>100	>100	>100	>100	~1	1.05	1.38	~10	0.02	9	~20
mTORC2	>101	>100	>100	>100	>100	ND	~10	ND	ND	ND	0.083	ND	>100
<b><i>PIPKs</i></b>													
PI4P5KI $\alpha$	>100	>100	>100	>100	>100	>100	>100	>100	>100	>100	>100	>100	>100
PI4P5KI $\beta$	>100	>100	>100	>100	>100	>100	>100	>100	>100	>100	>100	>100	>100
PI5P4KI $\beta$	>100	>100	>100	>100	>100	>100	>100	>100	>100	>100	>100	>100	ND

Table 3.1: IC<sub>50</sub> value in  $\mu$ M for selected PI3-K inhibitors against lipid kinases. All IC<sub>50</sub> values were determined in the presence of 10  $\mu$ M ATP except IC<sub>50</sub> values in italics, which were determined at 100  $\mu$ M ATP.

### **3.3 The Role of PI3-K Isoforms in Insulin Signaling**

Class I PI3-Ks are activated by the insulin receptor [23], and PI3-K activity is required for the metabolic effects of insulin [2]. The central role of PI3-K in insulin signaling raises the possibility that therapeutic use of PI3-K inhibitors may cause insulin resistance and associated morbidity. Broad spectrum pharmacological inhibition of all PI3-Ks would be predicted to block the metabolic effects of insulin, although this has not been demonstrated in vivo. While it may be possible to selectively inhibit individual PI3-K isoforms without impairing glucose homeostasis, the sensitivity of this process to pharmacological inhibition of each class I PI3-K remains to be defined. Asano and coworkers have argued that p110 $\beta$  is the primary insulin-responsive PI3-K in adipocytes, relying largely on adenoviral overexpression of p110 isoforms and microinjection of isoform-specific inhibitory antibodies [24]. These pioneering studies were among the first to explore signaling by PI3-K isoforms, but it is unclear to what extent these approaches can anticipate the effects of small molecule inhibitors. The use of knockout animals to study the role of p110 isoforms in insulin signaling has been complicated by the inability to generate viable homozygotes and a compensatory downregulation of the p85 subunit that is observed in heterozygous animals [14]. For these reasons, the key translational question with respect to insulin signaling by PI3-K—the sensitivity of this process to pharmacological inhibition of each isoform—remains unresolved. We therefore chose to examine this question using isoform-selective PI3-K inhibitors.

### **3.4 p110 $\alpha$ Is the Primary Insulin Responsive PI3-K in Adipocytes and Myotubes**

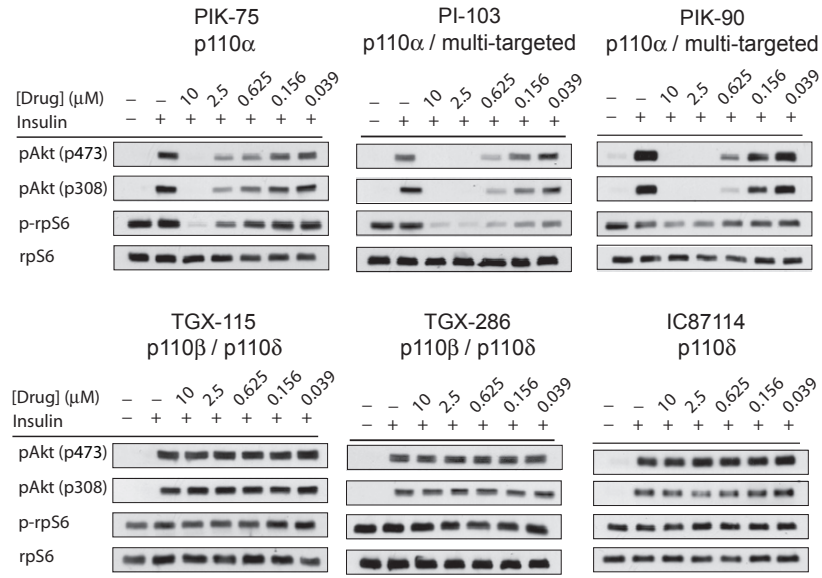
We initially explored the effects of PI3-K inhibitors in 3T3-L1 adipocytes and L6 myotubes, two widely used model systems for studying insulin action in fat and muscle, respectively.

Activation of the PI3-K pathway was monitored by Western blotting for phosphorylation of known PI3-K effectors (Fig 3.2) and cellular inositol lipids were quantified by  $^{32}\text{P}$ -orthophosphate metabolic labeling (Fig 3.5). To measure inositol lipid levels from cells labeled with  $^{32}\text{P}$ , lipids are first deacylated (Fig 3.3), followed by HPLC analysis of the lipid headgroups (Fig 3.4).

All p110 $\alpha$  inhibitors potently blocked insulin-stimulated phosphorylation of Akt in adipocytes (data not shown) and myotubes (Fig 3.2A). This was observed for multitargeted inhibitors such as PIK-90 and PI-103 (which inhibit p110 $\alpha$  most potently but also target p110 $\beta$  at concentrations 10 to 30-fold higher) as well as PIK-75, which inhibits p110 $\alpha$  > 200-fold more potently than p110 $\beta$ . Consistent with their effect on pathway effectors, PIK-75 and PI-103 also potently blocked production of PI(3,4)P<sub>2</sub> and PIP<sub>3</sub> in adipocytes and PIP<sub>3</sub> in myotubes (PI(3,4)P<sub>2</sub> was not detected in myotubes).

By contrast, inhibitors of p110 $\beta$  (TGX-115 and TGX-286) and p110 $\delta$  (IC87114 and PIK-23) had no effect on the insulin-stimulated phosphorylation of Akt (Fig 3.2A). Strikingly, the p110 $\beta$  inhibitor TGX-115 reduced insulin-stimulated PI(3,4)P<sub>2</sub> and PIP<sub>3</sub> levels in adipocytes by 50%, yet failed to block Akt or mTORC1 activation in these cells (Fig 3.5). However, TGX-115 and TGX-286 did potently inhibit Akt phosphorylation induced by lysophosphatidic acid (Fig 3.2B), a stimulus that activates p110 $\beta$  [25], confirming that these inhibitors can functionally block p110 $\beta$  activity in these cells. These data argue that p110 $\beta$  and p110 $\delta$  play a less-significant role in insulin signaling in adipocytes and myotubes.

**A**



**B**

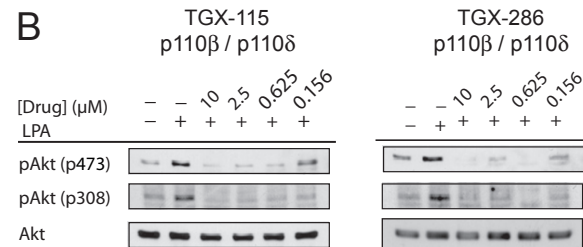


Figure 3.2: Inhibitors of p110 $\alpha$  block activation of Akt

A) Western blots of lysates from L6 myotubes stimulated with insulin (100 nM) in the presence of PI3-K inhibitors. Phosphorylation site of rpS6 is S235/S236.

B) Western blots of lysates from L6 myotubes stimulated with LPA (10  $\mu$ M) in the presence of PI3-K inhibitors.

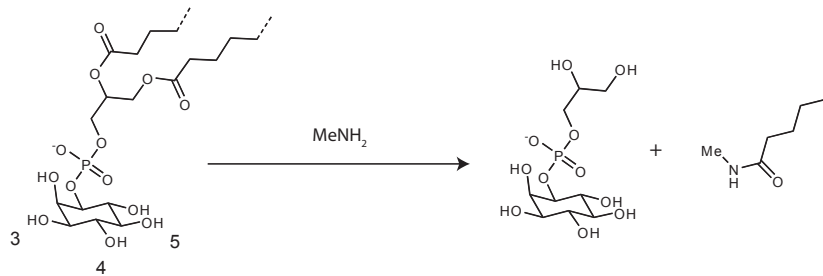


Figure 3.3: Deacylation of phosphoinositides.

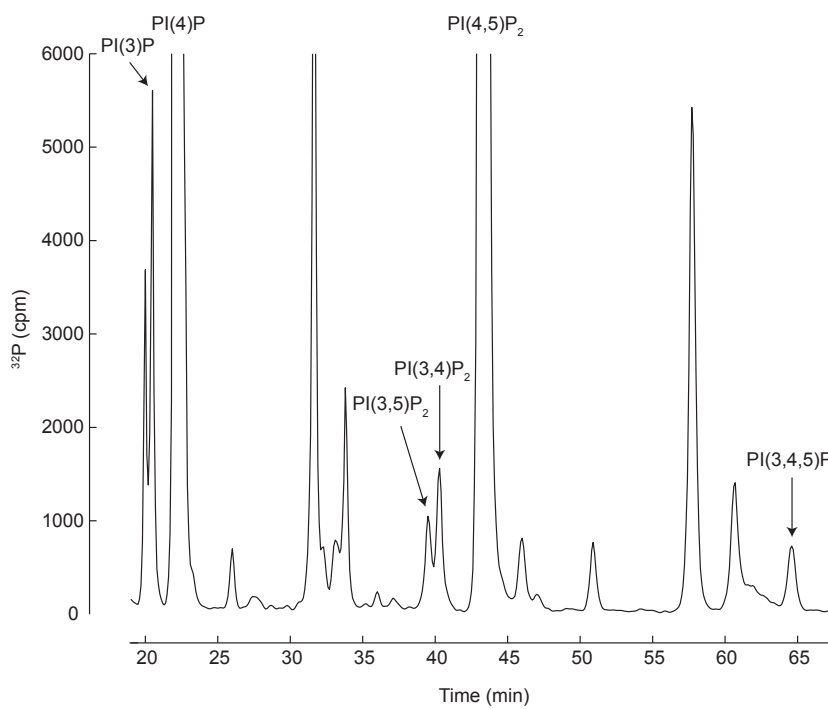


Figure 3.4: HPLC analysis of deacylated lipids.

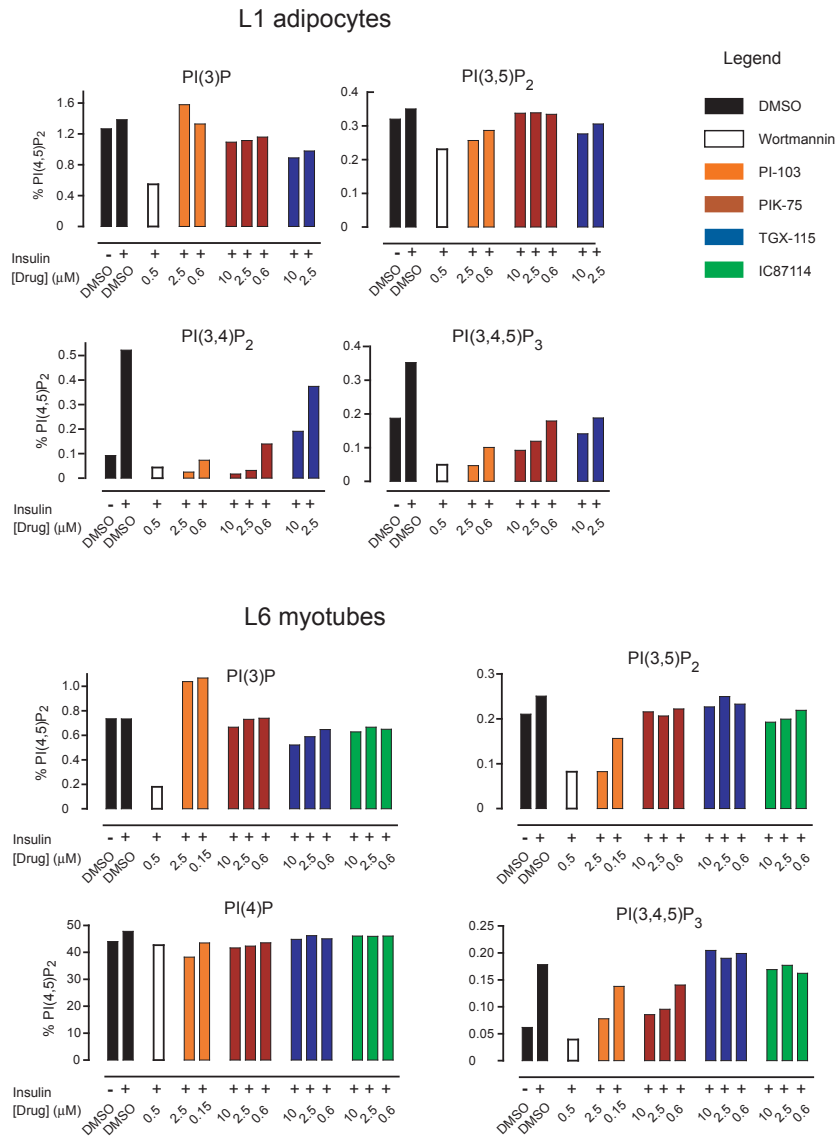


Figure 3.5: Phosphoinositides levels following insulin stimulation (100 nM) in the presence of PI3-K inhibitors.

### 3.5 Functional Inhibition of Glucose Transport

We next investigated whether biochemical inhibition of the PI3-K pathway by these inhibitors induces functional inhibition of glucose transport in cells. We find that p110 $\alpha$  inhibitors blocked insulin-stimulated glucose uptake in adipocytes with a dose response that closely mirrors their ability to block Akt phosphorylation (Fig 3.6). By contrast, the p110 $\beta$  inhibitor TGX-115 had no effect on glucose transport, whereas TGX-286 had a small effect at the highest dose; we attribute this weak activity of TGX-286 to p110 $\alpha$  inhibition at high concentrations, as this compound is less selective than TGX-115 (Table 3.1).

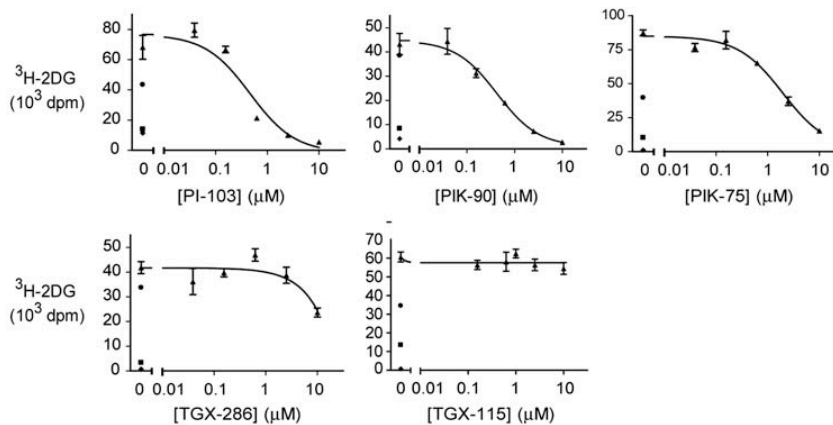


Figure 3.6: Insulin (100 nM) stimulated glucose uptake in L1 adipocytes is blocked by inhibitors of p110 $\alpha$  but not p110 $\beta$ .

### 3.6 p110 $\alpha$ /p110 $\delta$ Set a Phenotypic Threshold in Myotubes, but not Adipocytes

It is possible that p110 $\beta$  or p110 $\delta$  contributes a pool of PIP<sub>3</sub> that is not independently required for Akt phosphorylation but which defines a threshold for the amount of p110 $\alpha$  activity necessary to activate the pathway. A prediction of this model is that inhibition of



p110 $\beta$  or p110 $\delta$  should shift the amount of p110 $\alpha$  activity required to activate Akt and other downstream effectors.

We tested this hypothesis by measuring the effect of the p110 $\beta$ /p110 $\delta$  inhibitor TGX-115 on the ability of the p110 $\alpha$  inhibitor PIK-75 to block Akt phosphorylation at Thr 308. TGX-115 alone at concentrations up to 10  $\mu$ M had no effect on insulin-stimulated Thr 308 phosphorylation in either adipocytes (data not shown) or myotubes (Fig 3.7A, black). PIK-75 alone blocked Thr 308 phosphorylation in these two cell types with IC<sub>50</sub> values of 1.2 and 1.3  $\mu$ M, respectively (data not shown for adipocytes and Fig 3.7A, blue). When PIK-75 was retested in the presence of 10  $\mu$ M TGX-115, the dose response in myotubes shifted to 8-fold lower concentrations (IC<sub>50</sub> = 0.17  $\mu$ M); an identical dose shift was observed for phosphorylation of Akt Ser 473 (data not shown). By contrast, no significant shift was observed in adipocytes (data not shown).

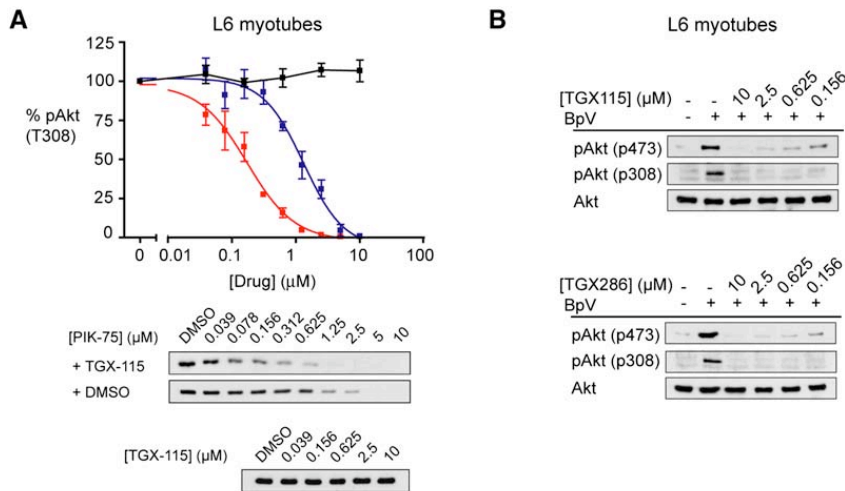


Figure 3.7: Inhibition of p110 $\beta$  cooperates with inhibition of p110 $\alpha$  to block pAkt in L6 myotubes.

These results support a model in which p110 $\beta$ /p110 $\delta$  synthesize a basal pool of PIP<sub>3</sub> in myotubes that lowers the amount of p110 $\alpha$  activity required for Akt phosphorylation; the change in this phenotypic threshold is detected as a shift in the dose-response curve for

the p110 $\alpha$  inhibitor PIK-75. Nonetheless, we did not observe a significant decrease in bulk PIP<sub>3</sub> levels in myotubes in response to TGX-115 treatment (Fig 3.5). This may reflect the difficulty in quantifying small changes in PIP<sub>3</sub> levels by metabolic labeling or the fact that only certain pools of PIP<sub>3</sub> are functionally coupled to Akt phosphorylation.

We reasoned that one way to provide support for this model would be to use an inhibitor of PTEN to acutely unmask basal PIP<sub>3</sub> synthesis. Treatment with the PTEN inhibitor bpV(pic) [26] induced rapid Akt phosphorylation in both myotubes and adipocytes, and the inhibitor sensitivity of this Akt phosphorylation was measured (Fig 3.7B). p110 $\beta$  inhibitors potently blocked this Akt phosphorylation in myotubes but had no effect in adipocytes (data not shown). This is consistent with our findings from dose-shift experiments and supports a model in which p110 $\beta$  generates a basal pool of PIP<sub>3</sub> that is coupled to Akt phosphorylation in myotubes.

## **3.7 Materials and Methods**

### **Cell Culture**

3T3-L1 fibroblasts were differentiated to adipocytes essentially as described [27]. Adipocytes were used between 5 and 25 days post-differentiation and in all cases > 95% differentiated. L6 myoblasts were differentiated to myotubes by growing cells to confluence and then culturing in low serum (2% FBS) containing media for 5 days.

## **<sup>32</sup>P-orthophosphate Lipid Profiling**

Metabolic labelling was performed essentially as described [28]. Adipocytes or myotubes were differentiated in 10 cm dishes. Prior to labelling, cells were serum starved overnight in DMEM + 0.1% BSA. The following morning, the cells were washed once with phosphate-free DMEM + 0.1% BSA, and then incubated for two hours in 10 mL of the same. After this incubation, <sup>32</sup>P-orthophosphate was added to each dish (1.5 mCi per dish for myotubes, 2 mCi per dish for adipocytes), and the cells were incubated an additional 2 hours. After this 2 hour incubation, inhibitors were added at the indicated concentrations and incubated for 10 minutes. Insulin was then added (final concentration, 100 nM) and the cells were incubated for an additional 10 minutes. The media was then removed, cells were washed once with ice-cold PBS (Ca<sup>++</sup> and Mg<sup>++</sup> free), and then dissolved in 1 mL of MeOH:HCl (10:1). Cells were scraped off plates, transferred to eppendorf tubes, and CHCl<sub>3</sub> (1 mL) was added. Cells were vortexed, water (1 mL) was added, cells were vortexed again, centrifuged (14,000 rpm for 1 minute), and the organic layer (bottom) was transferred to a new tube. One mL of MeOH:HCl (10:1) was added, followed by 0.1 M EDTA (1 mL), the solution was vortexed, centrifuged (14,000 rpm for 1 minute), and the organic phase was transferred to a new tube.

Lipids were deacylated as follows. The organic phase was concentrated to dryness (SpeedVac). 0.75 mL of the following solution was then added: 13.4 parts of a 40% MeNH<sub>2</sub> solution in water; 8 parts water; 22.9 parts methanol; and 5.7 parts n-butanol by volume. This solution was incubated for 50 minutes at 53°C in a heat block. This solution was then concentrated to dryness (SpeedVac) resuspended in water (0.5 mL), sonicated (bath sonicator, 1 minute), and then 0.5 mL of the following solution as added: 20 parts n- butanol, 4 parts petroleum ether, and 1 part ethyl formate. The solution was vortexed, and the aqueous phase (bottom) was extracted. For adipocytes, this extraction was repeated twice. The aqueous phase was then concentrated to dryness (SpeedVac) and redissolved in 10 mM (NH<sub>4</sub>H<sub>2</sub>PO<sub>4</sub>

(0.5 mL). A fraction of this sample (typically 0.25 mL) was then analyzed by HPLC using a Partisphere-5 SAX column (25 cm) with the following program at 1 mL/min.: 5 minutes at 10 mM  $\text{NH}_4\text{H}_2\text{PO}_4$ , followed by a gradient from 10 mM to 800 mM  $\text{NH}_4\text{H}_2\text{PO}_4$  over one hour.  $^{32}\text{P}$  was measured by automated mixing of effluent with scintillant (Monoflow 4) at a ratio of 3:1 and scintillation counting by a Packard Radiomatic detector. Retention times of inositol lipids were assigned using  $^{32}\text{P}$ -labelled standards. The following retention times were observed: PI(3)P, 20.5 min.; PI(4)P, 22.1 min.; PI(3,5)P<sub>2</sub>, 39.5 min.; PI(3,4)P<sub>2</sub>, 40.3 min.; PI(4,5)P<sub>2</sub>, 43.3 min.; PI(3,4,5)P<sub>3</sub>, 64.7 min.

### **PI3-K Pathway Western Blotting**

Fully differentiated adipocytes or myotubes were serum starved overnight, and pre-incubated with inhibitor at the indicated concentration for 30 minutes. Cells were then stimulated with insulin (100 nM) for 5 minutes and lysed in RIPA buffer. These lysates were resolved by SDS-PAGE, transferred to nitrocellulose, and analyzed by western blotting. Antibody dilutions were 1/1000 for all primary antibodies except those for rpS6 (1/3000), and 1/1000 for secondary antibodies (Pierce).

### **Glucose Uptake**

Glucose uptake in adipocytes was measured essentially as described [27]. Adipocytes in 12-well plates were serum-starved (3 hr) and then incubated in PBS with compound (30 min), at which point cells were stimulated with insulin (100 nM).  $^3\text{H}$ -2-deoxyglucose (100  $\mu\text{M}$ , 1  $\mu\text{Ci/ml}$ ) was added 15 min after insulin stimulation and uptake was allowed to proceed for an additional 15 min. Adipocytes were washed three times with PBS, dissolved in 0.1% SDS, and the internalized radioactivity was measured by scintillation counting.

## References

- 1) Fruman DA, Meyers RE, and Cantley LC, "Phosphoinositide kinases," *Annu Rev Biochem*, vol. 67, pp. 481–507, 1998.
- 2) Katso R, Okkenhaug K, Ahmadi K, White S, Timms J, and Waterfield MD, "Cellular function of phosphoinositide 3-kinases: implications for development, homeostasis, and cancer," *Annu Rev Cell Dev Biol*, vol. 17, pp. 615–75, 2001.
- 3) Ward S, Sotsios Y, Dowden J, Bruce I, and Finan P, "Therapeutic potential of phosphoinositide 3-kinase inhibitors," *Chem Biol*, vol. 10, no. 3, pp. 207–13, 2003.
- 4) Samuels Y *et al.*, "High frequency of mutations of the PIK3CA gene in human cancers," *Science*, vol. 304, no. 5670, p. 554, 2004.
- 5) Cantley LC and Neel BG, "New insights into tumor suppression: PTEN suppresses tumor formation by restraining the phosphoinositide 3-kinase/AKT pathway," *Proc Natl Acad Sci U S A*, vol. 96, no. 8, pp. 4240–5, 1999.
- 6) Camps M *et al.*, "Blockade of PI3Kgamma suppresses joint inflammation and damage in mouse models of rheumatoid arthritis," *Nat Med*, vol. 11, no. 9, pp. 936–43, 2005.
- 7) Condliffe AM *et al.*, "Sequential activation of class IB and class IA PI3K is important for the primed respiratory burst of human but not murine neutrophils," *Blood*, vol. 106, no. 4, pp. 1432–40, 2005.
- 8) Jackson SP *et al.*, "PI 3-kinase p110beta: a new target for antithrombotic therapy," *Nat Med*, vol. 11, no. 5, pp. 507–14, 2005.
- 9) Knight ZA, Chiang GG, Alaimo PJ, Kenski DM, Ho CB, Coan K, Abraham RT, and Shokat KM, "Isoform-specific phosphoinositide 3-kinase inhibitors from an arylmorpholine scaffold," *Bioorg Med Chem*, vol. 12, no. 17, pp. 4749–59, 2004.

- 10) Lau A, Swinbank KM, Ahmed PS, Taylor DL, Jackson SP, Smith GC, and O'Connor MJ, "Suppression of HIV-1 infection by a small molecule inhibitor of the ATM kinase," *Nat Cell Biol*, vol. 7, no. 5, pp. 493–500, 2005.
- 11) Sadhu C, Masinovsky B, Dick K, Sowell CG, and Staunton DE, "Essential role of phosphoinositide 3-kinase delta in neutrophil directional movement," *J Immunol*, vol. 170, no. 5, pp. 2647–54, 2003.
- 12) Bi L, Okabe I, Bernard DJ, Wynshaw-Boris A, and Nussbaum RL, "Proliferative defect and embryonic lethality in mice homozygous for a deletion in the p110alpha subunit of phosphoinositide 3-kinase," *J Biol Chem*, vol. 274, no. 16, pp. 10963–8, 1999.
- 13) Bi L, Okabe I, Bernard DJ, and Nussbaum RL, "Early embryonic lethality in mice deficient in the p110beta catalytic subunit of PI 3-kinase," *Mamm Genome*, vol. 13, no. 3, pp. 169–72, 2002.
- 14) Brachmann SM, Ueki K, Engelman JA, Kahn RC, and Cantley LC, "Phosphoinositide 3-kinase catalytic subunit deletion and regulatory subunit deletion have opposite effects on insulin sensitivity in mice," *Mol Cell Biol*, vol. 25, no. 5, pp. 1596–607, 2005.
- 15) Ueki K, Yballe CM, Brachmann SM, Vicent D, Watt JM, Kahn CR, and Cantley LC, "Increased insulin sensitivity in mice lacking p85beta subunit of phosphoinositide 3-kinase," *Proc Natl Acad Sci U S A*, vol. 99, no. 1, pp. 419–24, 2002.
- 16) Ueki K, Fruman DA, Yballe CM, Fasshauer M, Klein J, Asano T, Cantley LC, and Kahn CR, "Positive and negative roles of p85 alpha and p85 beta regulatory subunits of phosphoinositide 3-kinase in insulin signaling," *J Biol Chem*, vol. 278, no. 48, pp. 48453–66, 2003.

- 17) Luo J, Field SJ, Lee JY, Engelman JA, and Cantley LC, "The p85 regulatory subunit of phosphoinositide 3-kinase down-regulates IRS-1 signaling via the formation of a sequestration complex," *J Cell Biol*, vol. 170, no. 3, pp. 455–64, 2005.
- 18) Yu J, Zhang Y, McIlroy J, Rordorf-Nikolic T, Orr GA, and Backer JM, "Regulation of the p85/p110 phosphatidylinositol 3'-kinase: stabilization and inhibition of the p110alpha catalytic subunit by the p85 regulatory subunit," *Mol Cell Biol*, vol. 18, no. 3, pp. 1379–87, 1998.
- 19) Peng Y, Woods RG, Beamish H, Ye R, Lees-Miller SP, Lavin MF, and Bedford JS, "Deficiency in the catalytic subunit of DNA-dependent protein kinase causes down-regulation of ATM," *Cancer Res*, vol. 65, no. 5, pp. 1670–7, 2005.
- 20) Knight ZA and Shokat KM, "Features of selective kinase inhibitors," *Chem Biol*, vol. 12, no. 6, pp. 621–37, 2005.
- 21) Vanhaesebroeck B, Ali K, Bilancio A, Geering B, and Foukas LC, "Signalling by PI3K isoforms: insights from gene-targeted mice," *Trends Biochem Sci*, vol. 30, no. 4, pp. 194–204, 2005.
- 22) Patrucco E *et al.*, "PI3Kgamma modulates the cardiac response to chronic pressure overload by distinct kinase-dependent and -independent effects," *Cell*, vol. 118, no. 3, pp. 375–87, 2004.
- 23) Ruderman NB, Kapeller R, White MF, and Cantley LC, "Activation of phosphatidylinositol 3-kinase by insulin," *Proc Natl Acad Sci U S A*, vol. 87, no. 4, pp. 1411–5, 1990.
- 24) Asano T *et al.*, "p110beta is up-regulated during differentiation of 3T3-L1 cells and contributes to the highly insulin-responsive glucose transport activity," *J Biol Chem*, vol. 275, no. 23, pp. 17671–6, 2000.

- 25) Yart A, Roche S, Wetzker R, Laffargue M, Tonks N, Mayeux P, Chap H, and Raynal P, “A function for phosphoinositide 3-kinase beta lipid products in coupling beta gamma to Ras activation in response to lysophosphatidic acid,” *J Biol Chem*, vol. 277, no. 24, pp. 21 167–78, 2002.
- 26) Schmid AC, Byrne RD, Vilar R, and Woscholski R, “Bisperoxovanadium compounds are potent PTEN inhibitors,” *FEBS Lett*, vol. 566, no. 1-3, pp. 35–8, 2004.
- 27) Lakshmanan J, Elmendorf JS, and Ozcan S, “Analysis of insulin-stimulated glucose uptake in differentiated 3T3-L1 adipocytes,” *Methods Mol Med*, vol. 83, pp. 97–103, 2003.
- 28) Serunian LA, Auger KR, and Cantley LC, “Identification and quantification of polyphosphoinositides produced in response to platelet-derived growth factor stimulation,” *Methods Enzymol*, vol. 198, pp. 78–87, 1991.



## Chapter 4

# *Spot*: Software for the Analysis of Kinase Assays

### Abstract

Kinases are involved in the regulation of every cellular process. Kinases can be inhibited by small molecules binding their catalytic active sites, and partly for this reason, kinases have emerged as major drug targets for the treatment of disease and cancer. There are 518 protein kinases in the human kinome and many more lipid and small molecule kinases. Kinase inhibitors often inhibit multiple kinases. To discover selective kinase inhibitors, multiple inhibitors must be tested against multiple kinases. We employ a simple and robust format for the manual assay of protein and lipid kinases. Here we present a computer program called *Spot* that greatly aids in the analysis of these kinase assays.

## 4.1 Kinases and Kinase Inhibitors

By transferring a phosphate from ATP onto a protein or other substrate such as a lipid or metabolite, kinases change the charge and shape of the substrate often drastically altering the substrate's cellular function. The cellular activity of many proteins is regulated by phosphorylation. For some proteins the presence or absence of a phosphate will determine whether the protein is targeted for degradation. For other proteins, their enzymatic activity is regulated by phosphorylation. For instance, many protein kinases are themselves regulated by phosphorylation. Kinases possess a solvent exposed loop near their active sites called the activation loop. Kinases are often active only when phosphorylated on their activation loop. Some kinases, such as Glycogen Synthase Kinase, are inhibited by phosphorylation.

Lipids are phosphorylated by a dedicated set of kinases distinct from the protein kinases. Many bulk membrane lipids have phosphorylated headgroups because the integrity of the lipid bilayer requires polar headgroups combined with hydrophobic lipid tails. In addition to their structural role, membranes are also an important platform for the communication of signals from the outside of the cell to the interior. One way that extracellular signals are transmitted to the inside of the cell is by triggering the phosphorylation of membrane lipids to serve as second messengers. The phosphoinositides are an important class of cellular lipids that often serve as second messengers (Fig 3.1). In particular, PIP<sub>3</sub> production by PI3-K has emerged as an important oncogenic signal driving cancer and for this reason, inhibitors of PI3-K and PI3-K effectors are being developed to treat cancer (Chapters 1 and 2).

The best way to validate a kinase as a drug target is to generate a specific inhibitor of the kinase and test it *in vitro* and *in vivo* against models of cancer and disease. Knockout and RNAi strategies to study kinase function often yield phenotypes that are due to the loss of a scaffolding function of the kinase rather than loss of kinase activity. Because kinases are

related through an evolutionary common ancestor and their active sites are constrained to all bind ATP, kinase active sites are all quite similar from a pharmacological point of view. To discover a selective inhibitor of a kinase requires testing many inhibitors against many kinases, to find those that inhibit one or perhaps a few kinases. Structural variants of the most promising compounds are then generated, followed by more testing. This procedure is repeated until an inhibitor with the desired potency and selectivity is generated.

## 4.2 Potency and Selectivity of Kinase Inhibitors

The potency of a kinase inhibitor for an individual target is usually measured by finding the concentration of compound required to inhibit 50% of the activity of a kinase in an *in vitro* assay; this concentration is the  $IC_{50}$  of a compound for an individual kinase. Kinase assays are often performed in the presence of 10–100  $\mu\text{M}$  ATP, while the cellular concentration of ATP is 1–5 mM. Active-site kinase inhibitors are less potent in cells than *in vitro* because the inhibitor has to compete with cellular levels of 1–5 mM ATP for binding to the active site of a kinase. The precise shift in potency depends on the affinity of the kinase for ATP according to the Cheng-Prusoff relationship [1], but typically the cellular potency of a kinase inhibitor will be about 50 fold weaker than its *in vitro* potency [2]. We prefer to use

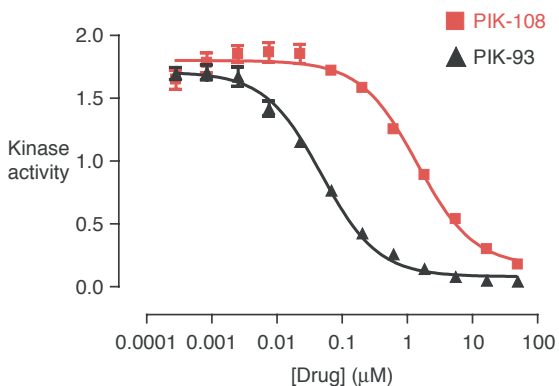


Figure 4.1: Determination of  $IC_{50}$  values for p110 $\alpha$  with the PI3-kinase inhibitors PIK-108 and PIK-93 using the membrane capture assay.

Quantitated dose-response data for each compound. Y axis represents PI3-K activity in arbitrary units.  $IC_{50}$  (PIK-108) = 1.4  $\mu\text{M}$ ,  $IC_{50}$  (PIK-93) = 0.048  $\mu\text{M}$ . Raw data for this kinase assay is shown in Figure 4.2 and analysis of this assay by *Spot* is shown in Figure 4.4

kinase inhibitors at  $< 10 \mu\text{M}$  because, in general, the specificity of small molecule inhibitors decreases dramatically when they are used above  $10 \mu\text{M}$ . Active-site kinase inhibitors, should therefore have an *in vitro*  $\text{IC}_{50}$  of  $< 10\text{--}20 \text{ nM}$ . Finding a kinase inhibitor with an *in vitro*  $\text{IC}_{50}$  of  $5 \text{ nM}$  and using it at  $< 10 \mu\text{M}$  does not guarantee selectivity for a single kinase. Kinase inhibitor selectivity is evaluated by measuring the  $\text{IC}_{50}$  of an inhibitor for multiple kinases. Ideally every kinase would be tested, but even the most comprehensive commercial kinase screens only cover about half of the protein kinases.

### 4.3 Low Throughput Kinase Assays

There are many ways to assay a kinase including detection of the phosphorylated product by an antibody and measurement of ATP consumption [3] or ADP release [4], but the most direct and reliable way to assay a kinase is by measuring transfer of radioactive phosphate from  $\gamma\text{-}^{32}\text{P}\text{-ATP}$  onto the kinase substrate. Because of the wide dynamic range inherent to the detection of radioactivity, this assay format can effectively assay kinases with vastly different levels of *in vitro* kinase activity.

A radioactive kinase assay is prepared by mixing a kinase and its substrate with a suitable buffer. A low but defined concentration of cold ATP such as  $10 \mu\text{M}$  is then added in addition to a few  $\text{nM}$  of  $\gamma\text{-}^{32}\text{P}\text{-ATP}$  which serves as a tracer for the reaction. After the kinase reaction is complete, the key step is to remove the unused radioactive ATP and measure how much radioactive phosphate was transferred onto the substrate by the kinase. In the case of protein kinases, separating the kinase from the substrate can be accomplished by running a gel. The ATP is highly charged and runs to the bottom of the gel, while the protein is retained. For lipid kinase assays, the lipid substrate can be separated from the unused ATP by thin layer chromatography (TLC) on silica. The non-polar lipid tails pull the lipid substrate up the

plate, while the more polar ATP is retained at the baseline. Both gel and TLC assays are laborious for more than about 10 samples.

## 4.4 Kinase Assays by Substrate Capture on Nitrocellulose

The assay format we use avoids running a gel or a TLC plate and relies on the fact that proteins and lipids stick essentially irreversibly to nitrocellulose, while ATP can be washed away. A small portion of a kinase assay, typically 1–3  $\mu\text{l}$ , is spotted down onto nitrocellulose. The unused ATP is then washed away with a high salt buffer containing phosphoric acid. The substrate remains bound to the nitrocellulose. Radioactivity transferred by the kinase from  $\gamma\text{-}^{32}\text{P}\text{-ATP}$  to the substrate is then quantified by exposing the nitrocellulose sheet to a phosphorimager plate and reading the plate to create an image. An example image of a kinase assay is shown in Figure 4.2. Each spot on the image represents an individual assay. Darker spots reflect higher kinase activity. Kinase activity is measured by integrating the intensity of the spots in the image. This assay format is applicable to a wide variety of purified lipid kinases (Fig 4.3). Without any fundamental changes, protein kinases can be assayed using the same assay format. The  $\text{IC}_{50}$  values for PKC, PDK1, and mTOR in Table 2.1 were determined using this membrane capture assay.

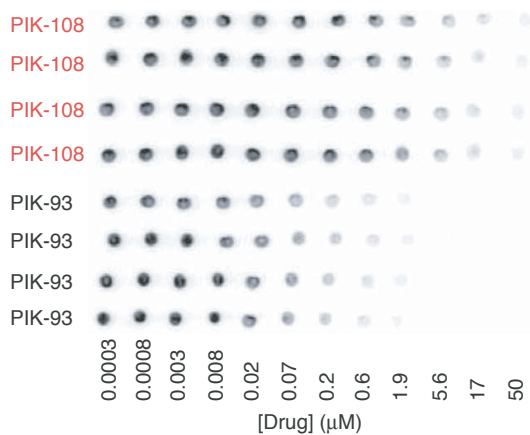


Figure 4.2: Lipid kinase assay for p110 $\alpha$  manually spotted onto nitrocellulose. Raw dose–response data for each compound. Compounds were assayed in quadruplicate at threefold dilutions across the range 50–0.0003  $\mu\text{M}$ .

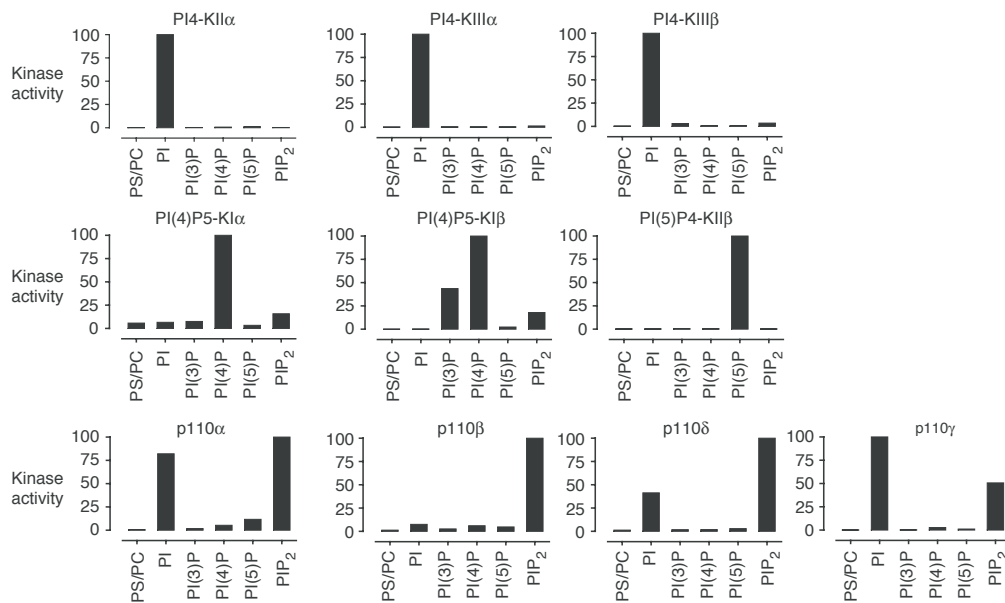


Figure 4.3: Substrate specificity of lipid kinases.

Kinases were incubated in the appropriate reaction buffer with  $\gamma$ -<sup>32</sup>P-ATP (5  $\mu$ Ci per each 50  $\mu$ l reaction), nonradioactive ATP (10  $\mu$ M), BSA (0.5 mg/ml) and each phosphoinositide (0.1 mg/ml) in the presence of the carrier lipids PS/PC (0.1 mg/ml). Reactions were spotted on nitrocellulose, washed and assayed by phosphorimaging. Kinase activity was normalized to 100% for the preferred lipid substrate. PIP<sub>2</sub> denotes PI(4,5)P<sub>2</sub>.

## 4.5 Image Processing Approaches used by *Spot*

Because the kinase assay is spotted down manually with a multichannel pipette, the exact location of the assay spots will vary from one assay to another. If the spots were always in the same place it would be trivial to measure their intensity. Historically, we manually placed a region of interest (ROI) over each spot using an image analysis program such as ImageJ or ImageQuant. The integrated intensity in each ROI was then measured by the program and returned as a list of values. Placing the ROIs requires 10–15 minutes and is very tedious, so it is desirable to use a computer program to automatically find the spots in the kinase assay, integrate their intensities and format the data into a convenient array for subsequent analysis. *Spot* performs all these tasks with minimal manual intervention.

Before we describe how to use of *Spot* to analyze a kinase assay we will explain the image analysis techniques it employs.

### **4.5.1 Finding the Spots**

The intensity of the spots varies greatly across the kinase assay, so the spots must be located in a manner that is independent of their intensity. This requirement excludes a common image processing technique where the image is thresholded to create a binary version of the image and then the binary operations are used to erode each spot to a single pixel. Instead, finding the spots in the kinase assay image relies on the fact that a spot must be brighter than its neighboring pixels. Unfortunately, some pixels are brighter than their neighbors because of noise introduced in the process of recording an image and due to random chance in the process of radioactive decay. To exclude noise and only find the locations where a kinase assay was spotted down, the image is first smoothed, to create a blurred version of the image. Smoothing or blurring an image makes each pixel dependent its neighbors, so only robust groups of bright pixels will survive the blurring. After blurring the image, legitimate spots from the kinase assay will appear as a smooth hills on a flat background. At the top of each hill is a pixel whose intensity is brighter than all of its neighbors. To mark the location of each assay, *Spot* places an ROI centered on the top of each hill in the smoothed image.

### **4.5.2 Refining the Spot Locations**

Smoothing the image is a great way to find the general location of the spots, but sometimes the exact ROI locations chosen during the smoothing procedure fail to completely cover the radioactive spots in the original image. To make sure that all the ROIs are well centered over their respective kinase assays, *Spot* refines the ROI positions. To refine the spot positions,

*Spot* tests multiple locations for each ROI and chooses the position that maximizes the intensity captured by the ROI.

### **4.5.3 Arraying the Spots**

Kinase assays are often performed in 96 well plates. Rather than a list of intensities and spot locations, the intensities should be reported in a grid format having the same dimensions as the original kinase assay. The assay format need not be a 96 well plate, but the analysis will be explained assuming a 96 well plate oriented as usual with 8 rows and 12 columns. *Spot* must discover the row and column position of each spot. This is achieved by first clustering the y coordinates into 8 groups where each group represents all the spots in a single row from the 96 well plate. Clustering works because the y coordinates of the spots within a single row should be more similar to each other than to any other row. If the assay is not oriented horizontally, but instead the rows are angled so that their y coordinates overlap, clustering into rows will fail. Once the spots within each row have been identified, the column positions are identified by sorting each row of spots by their x coordinates. *Spot* then organizes the data into an array format for output.



## 4.6 Using *Spot* to Analyze a Kinase Assay

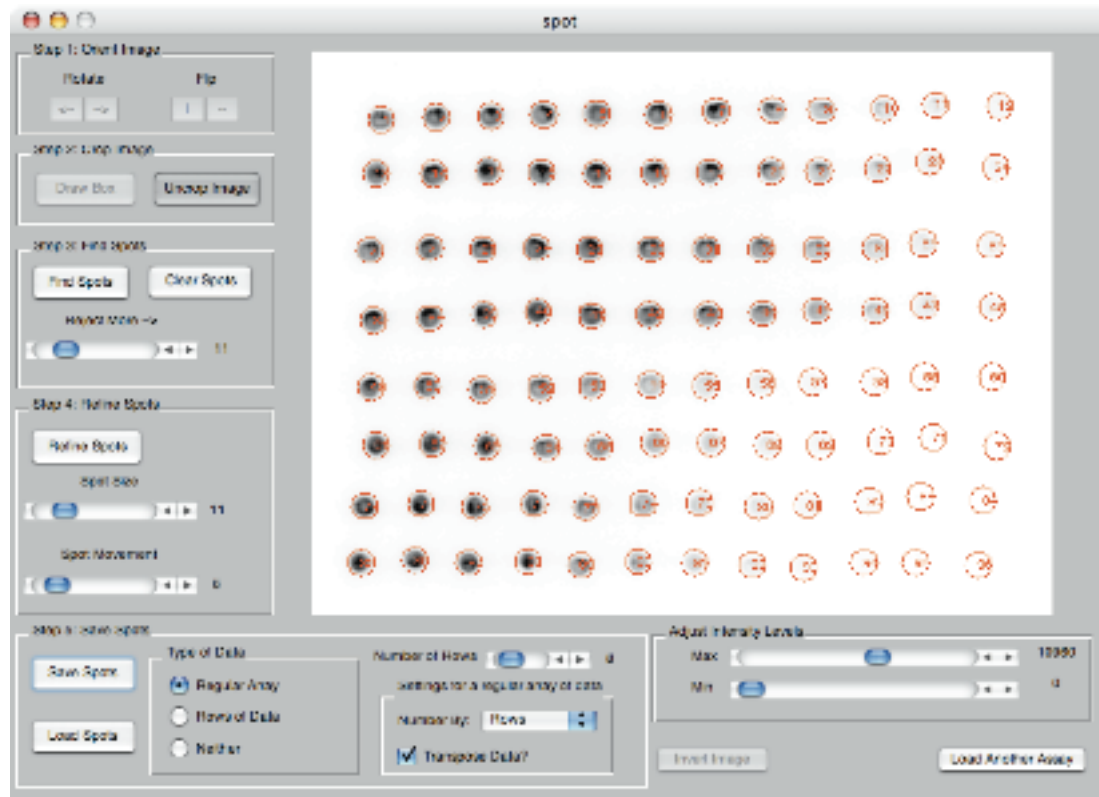


Figure 4.4: Screenshot depicting the analysis of dose–response data from Figures 4.1 and 4.2 using the MATLAB image analysis script *Spot*. Automatic location, refinement and integration of radioactive spots were accomplished by following the five steps indicated on the left panel of the graphical interface.

### 1) Starting *Spot*

At the MATLAB command prompt type 'spot' to start the software. Use the dialog box to choose an image file for analysis. Typhoon Gel files as well as Tiffs are accepted.

The graphical interface is organized by steps to help guide the user. Each step is a set of software buttons and options grouped together within a box. Use the 'Rotate' and 'Flip' button within 'Step 1' to adjust the image orientation.

## **2) Crop the Image**

Click on 'Draw Box' within 'Step 2' and draw a box on the image that only contains the spots to be analyzed. Click on 'Crop Image' to focus on the spots to be analyzed.

## **3) Find the Spots**

Click on 'Find Spots' within 'Step 3'. If too few spots are found, adjust the rejection slider to a lower value, and if too many are found, move the slider to a higher value. Left click on the image to manually identify a spot. Right click on the edge of an already identified spot to delete it. Left click and hold on a spot identifier to move it.

## **4) Refine the Spots**

Use the 'Spot Size' slider in 'Step 4' to adjust the spot size so that the darkest spots are just contained within the spot indicators. Adjust the intensity level of the image to confirm that low-intensity pixels are contained within the spot indicators. Click 'Refine Spots' to optimize the location of each spot. If the spots move too far, adjust the 'Spot Movement' slider to a lower value and return to Step 3).

## **5) Array and Save the Spots**

Before saving the spots, click on the button that best indicates the type of data (Regular Array, Rows of Data or Neither). For data in rows or in a regular array, specify the number of rows. For data in a regular array, also specify whether to number the data by rows or columns and whether to transpose the data before writing it to file. Click 'Save Spots' and assign a file name in the dialog box. A tab-delimited text file will be written. If the spots are misnumbered, see below for troubleshooting advice. After saving the file, the data will also be available on the clipboard.

## Viewing Saved Data

To view previously saved spots, first perform Step 1) and then press 'Load Spots'. At the file selection dialog, choose a file created previously at Step 5).

## Troubleshooting

Sometimes spots will be misnumbered if the rows overlap. In this case, the spots must be manually chosen. First clear the current spot identifiers by clicking 'Clear Spots'. Manually add new spot identifiers by left clicking on the image. Add the spot identifiers in the order they should be numbered. Click 'Refine Spots' to refine their positions. Before saving, specify 'Neither' as the data type. The spots will be numbered in the order in which they were selected.

## 4.7 Obtaining *Spot*

Matlab source code for *Spot* is freely available under the GPL license from:

<http://shokatlab.ucsf.edu/SPOT.htm>.

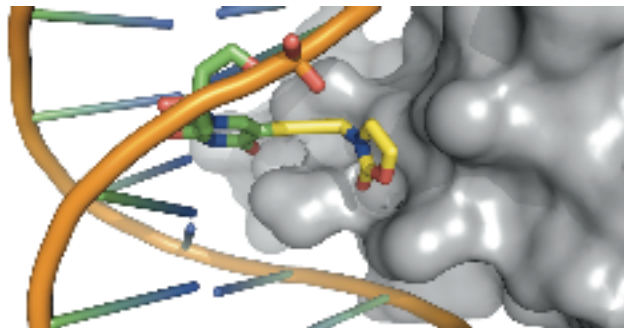
## References

- 1) Cheng Y and Prusoff WH, "Relationship between the inhibition constant (K<sub>1</sub>) and the concentration of inhibitor which causes 50 per cent inhibition (I<sub>50</sub>) of an enzymatic reaction," *Biochem Pharmacol*, vol. 22, no. 23, pp. 3099–108, 1973.
- 2) Knight ZA and Shokat KM, "Features of selective kinase inhibitors," *Chem Biol*, vol. 12, no. 6, pp. 621–37, 2005.

- 3) Koresawa M and Okabe T, “High-throughput screening with quantitation of ATP consumption: a universal non-radioisotope, homogeneous assay for protein kinase,” *Assay Drug Dev Technol*, vol. 2, no. 2, pp. 153–60, 2004.
- 4) Srinivasan J *et al.*, “ADP-specific sensors enable universal assay of protein kinase activity,” *Chem Biol*, vol. 11, no. 4, pp. 499–508, 2004.

## Chapter 5

# The Structure and Properties of a Re-Engineered Homeodomain Protein–DNA Interface



### Abstract

The homeodomain–DNA interface has been conserved over 500 million years of evolution. Despite this conservation, we have successfully re-engineered the engrailed homeodomain to specifically recognize an unnatural nucleotide using a phage display selection. Here we

report the synthesis of novel nucleosides and the selection of mutant homeodomains that bind these nucleotides using phage display. The high resolution crystal structure of one mutant in complex with modified and unmodified DNA demonstrates that, even with the substantial perturbation to the interface, this selected mutant retains a canonical homeodomain structure. Dissection of the contributions due to each of the selected mutations reveals that the majority of the modification-specific binding is accomplished by a single mutation (I47G) but that the remaining mutations re-tune the stability of the homeodomain. These results afford a detailed look at a re-engineered protein–DNA interaction and provide insight into the opportunities for re-engineering highly conserved interfaces.

## 5.1 Introduction

The re-design of one member of a highly conserved and large protein family has been useful for the generation of tools to dissect individual protein function in complex biological systems. Protein kinases, for example, contain highly conserved ATP binding pockets and can be studied by introducing a large-to-small mutation at a conserved position in the active site, thereby creating an engineered kinase that uniquely inhibitable using an enlarged inhibitor that is too bulky to fit into the active site of wild-type kinases [1–3]. Similarly, an Asp-to-Asn mutation in the active site of a GTPase can switch the nucleotide specificity from GTP to another nucleotide, XTP, allowing the activity of an engineered GTPase to be tracked in the presence of other GTPases [4–7]. In these cases, the high sequence conservation of the engineered protein’s family allowed extension of an engineering solution from one protein to other members within the family. While these examples illustrate the utility of engineering protein-small molecule interactions, many proteins exert their regulatory roles in the cell through protein–protein or protein–DNA interactions. Therefore we wondered

whether highly conserved, extended interfaces can be re-engineered to incorporate new functionality.

Several extended interfaces have been engineered including the interacting surfaces between human growth hormone with its receptor [8], zinc fingers with diverse DNA sequences [9–11] and the protein heterodimerization interface of an endonuclease [12]. Perhaps the most dramatic example of an adaptive protein surface is the variable region of an antibody, which can recognize chemically diverse haptens including those derived from the synthetic elaboration of biomolecules [13]. Although these examples highlight the adaptability of protein interfaces, they also demonstrate that protein engineers have focused on interfaces that have a high degree of natural functional variability and generally the amino acids at these interfaces are poorly conserved. In contrast, to take advantage of the frequent occurrence of highly conserved domains and their interacting surfaces, we are interested in how much adaptability—and corresponding potential for re-engineering—exists within highly conserved biomolecular interfaces. To address this question, we chose to focus on the homeodomain–DNA interaction.

The homeodomain (HD) is a DNA-binding domain that has been conserved over 500-million years of evolution in both structure and function [14]. The 60 amino acid HD is composed of three alpha helices (Fig 5.1A), the C-terminal of which is referred to as the recognition helix due to base-specific contacts it makes in the major groove of DNA with the sequence TAATXX (Fig 5.1A and 5.1B in green) [15–18]. These conserved contacts include: a hydrophobic interaction of either Ile or Val at position 47 with the C5-methyl group of thymidine 4, two invariant hydrogen bonds from Asn51 to adenosine 3, and contacts between either a Gln or a Lys at position 50 that specify the last two base pairs in the recognition sequence (TAATTA or TAATCC, respectively) [19]. While these residues are nearly invariant in naturally occurring homeodomains, we recently reported the re-engineering of this interface using a phage display selection with a synthetic DNA

oligomer bearing an unnatural nucleotide [20]. This selected homeodomain ( $\text{HD}_\Phi$ ) binds with specificity for DNA bearing an oxazolidinone appendage projecting into the major groove of the DNA on an alkynyl linker.

Here we report mutations recovered from phage display selections against DNA strands bearing other modified nucleotides. We also report extensive characterization of one mutant,  $\text{HD}_\Phi$ , including biochemical dissection of the roles for each mutation in binding studies and we analyze the stability of these mutants using CD spectroscopy. Finally, we report the high-resolution crystal structure of  $\text{HD}_\Phi$  bound to modified and unmodified DNA. Together, these results provide insight into the engineering of highly conserved interfaces.

## 5.2 Design and Synthesis of Derivatized Nucleosides

Our work re-engineering homeodomain–DNA interactions, has focused on the well characterized Q50K mutant of the engrailed homeodomain ( $\text{HD}_i$ ). The Q50K variant is naturally occurring in some HDs (*e.g.*, Bicoid) and alters the binding specificity from the palindromic consensus sequence of the wild-type HD, TAATTA, to the nonpalindromic sequence TAATCC, therefore simplifying biochemical analysis. To engineer HD–DNA interactions, we have focused on regions of the  $\text{HD}_i$ –DNA interface [21] where the homeodomain makes highly conserved contacts to the DNA (Fig 5.1A). The hydrophobic contact between Ile47 and the C5-methyl group of thymidine 4 in the recognition motif (TAATTA) was attractive because a large-to-small mutation at Ile47 might create sufficient space to accommodate prosthetic groups appended to the C5 position of T4. Furthermore, the Ile47 contact contributes substantially to DNA binding but, unlike Asn51 (another conserved residue that contacts the DNA), Ile47 is not completely essential ( $K_{d,147A}/K_{d,WT} \sim 20$ ,  $K_{d,N51A}/K_{d,WT} > 1000$  [22]).



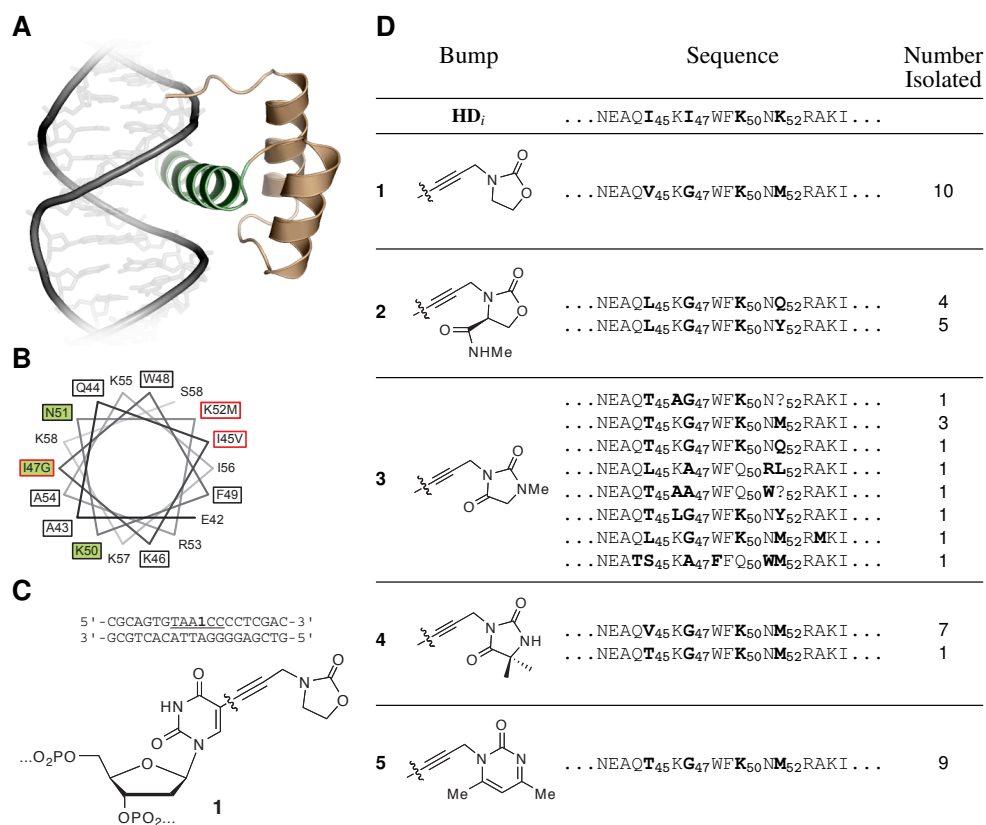


Figure 5.1: Sequences and schematic representation of the homeodomain mutants recovered from phage selections.

A) HD<sub>i</sub> is shown bound to TAATCC with its recognition helix ( $\alpha$ 3) shown in green.

B) Helical wheel representation of the HD recognition helix with the three canonical base-specific contacts (Ile47, Lys50 and Asn51) shown in green, residues that were varied in the library presented in boxes and mutations that comprise HD <sub>$\phi$</sub>  indicated in the sequence and shown in red.

C) Example DNA sequence used in the phage selections with oxazolidinone-modified nucleoside **1** incorporated into the HD<sub>i</sub> binding site.

D) The clones recovered from selections for binding to the modified DNA strands, TAA1CC (**1**), TAA2CC (**2**), TAA3CC (**3**), TAA4CC (**4**) and TAA5CC (**5**). In two cases (indicated with a question mark) the sequencing led to ambiguous results at position 52.

With this region of the protein-DNA interface in mind, we have designed synthetic appendages to the DNA that introduce diverse chemical functionality and steric demands into the interface, yet are unlikely to compromise the basic structure of the B-form DNA or clash with the backbone of the helix-turn-helix motif, which is fundamental to the HD fold [20]. The use of allyl or propargyl linkers appended to the C5 of thymidine bases allows the incorporation of diverse chemical functionality and the impact of these modifications has been systematically explored elsewhere [23]. In these cases, the extended  $\pi$ -system can contribute to the base-base stacking within the DNA helix thereby stabilizing the desired B-form DNA-structure.

Due to the limited space between the major groove of the DNA and the protein backbone of the recognition helix, we chose to focus on flat, five and six-membered heterocycles connected to the base through a propargyl linker at C5 of thymidine (**1–5**). These alkynyl heterocycles were synthesized as shown in Supplementary Scheme 1. To install these appendages onto the nucleoside base, Sonogashira conditions were used to couple these terminal alkynes to 5'-dimethoxytrityl (DMT) protected 2'-deoxy-5-iodouridine (Supplementary Scheme 2) as we have reported previously [20]. Installing the DMT-protecting group prior to the Sonogashira coupling proved advantageous both because this route allowed the use of a common starting material, and also because this protection scheme allowed the reaction to be performed in THF. Using THF as solvent accelerated the reaction dramatically relative to DMF and simplified the work up of the desired nucleosides. These modified nucleosides were then incorporated into DNA oligomers (Fig 5.1C) using solid phase DNA synthesis as previously described [20].

### 5.3 Phage-Display Selections

Models and biochemical data [20] demonstrate that a steric clash between Ile47 and alkynyl substituents prevents HD<sub>i</sub> from binding to the modified DNA. Therefore, we have sought mutant HDs that bind specifically to the modified DNA strands, presumably including a large-to-small mutation at Ile47. To select for such mutants, we employed a phage selection with a HD displayed on the major coat protein (P8) of M13 phage. The phage display system has been used previously to select for mutants of engrailed HD that bind to unmodified [24, 25] and oxazolidinone **1** modified DNA [20]. The selections using unmodified DNA have validated this approach; the amino acids enriched in the selections largely recapitulated those found in naturally occurring HDs.

To generate the library of mutant HDs, we used a variant of Kunkel mutagenesis to introduce mutations focused around Ile47 (Fig 5.1B, boxed residues) and, to increase the proportion of functional HDs, the library was biased towards approximately 4 mutations per clone using split-and-pool DNA synthesis to construct the degenerate oligonucleotide used for mutagenesis [20]. With this approach, we were able to obtain high coverage of the library using only modest numbers of unique transformants ( $1.8 \times 10^7$  Amp<sup>r</sup> colonies).

Using this library and previously established selection conditions, we enriched for DNA-binding phage within 3–4 rounds of selection. To identify mutations enriched by these selections, we sequenced several clones from each enriched pool (Fig 5.1D). The sequenced clones demonstrated common mutations derived from independent library members and for TAA**1**CC a single clone dominated the selection.

As we expected, the sequences largely contained Lys50, consistent with the known role for this residue specifying the last two base pairs of the DNA binding site used in the selection (*i.e.*, TAAX**X**CC). While it was encouraging that most of the clones contained a small residue at position 47, this bias was programmed into the original library (50% Ala;

50% Gly). Nonetheless, the bias toward Gly47 (see Figure 5.1D) was expected from previous data demonstrating that I47A has low binding affinity and specificity. From the selected clones, we found a preponderance of mutations at two other positions: Ile45 and Lys52. These mutations are on the back side of the recognition helix from Ile47. Closer examination of the sequences from the selected clones demonstrates that these clones clustered into two groups: those with consensus mutations (Lys50, Gly47, I45V/T/L and K52M) and clones that did not have these mutations but are also missing residues identified as particularly important for homeodomain function (*e.g.*, Trp48 and Asn51) suggesting that this second population is composed of residual clones that do not bind the desired DNA.

Having identified consensus mutations in selection against various modified DNA strands, we chose to focus on one mutant in particular, HD<sub>Φ</sub> (I45V, I47G, Q50K and K52M) because it completely dominated the pool enriched using oxazolidinone **1** and furthermore it was the only clone to give a strongly positive result in a phage ELISA [20]. Replacement of Ile45 by Val is not entirely surprising given that Ile and Val are equally likely to occur in natural homeodomains at position 45 and this substitution is quite conservative. The replacement of Lys52 with Met however is quite surprising; out of 129 human homeodomains, 103 have Arg at position 52, 10 have Lys, 7 have Ala, but none have Met [26].

## 5.4 Biochemical Analysis of a Selected Mutant

When given the choice in a competition EMSA assay, HD<sub>Φ</sub> binds 5 fold more tightly to TAA1CC<sub>20</sub> than unmodified DNA, while HD<sub>i</sub> binds specifically to unmodified DNA (Fig 5.21A). The preference of HD<sub>Φ</sub> for TAA1CC<sub>20</sub> was seen previously using HD<sub>Φ</sub> fused to maltose binding protein [20]. Untagged HD<sub>Φ</sub> also prefers binding to TAA1CC<sub>20</sub> over TAA2CC<sub>20</sub>, another oxazolidinone-bearing strand(Fig 5.21B).

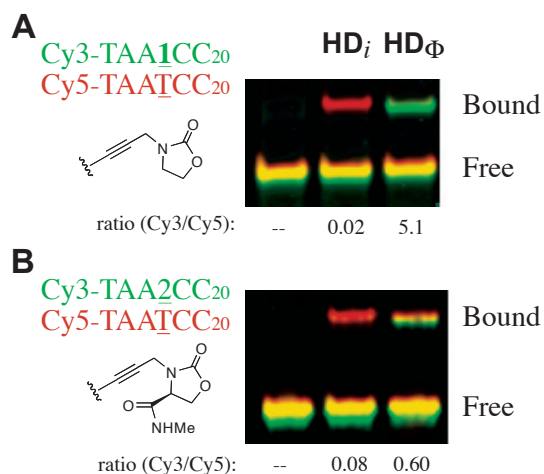


Figure 5.2: Selectivity of HD<sub>i</sub> and HD<sub>Φ</sub> for modified and unmodified DNA.

A) A competition Cy3/Cy5 EMSA, where the ratio of binding each DNA strand is assayed by comparing the ratio Cy3 to Cy5 fluorescence in the shifted band, demonstrates that untagged HD<sub>i</sub> binds specifically to unmodified DNA (TAA1CC<sub>20</sub>, lane 2) and that HD<sub>Φ</sub> binds specifically to TAA1CC<sub>20</sub> (lane 3).

B) HD<sub>Φ</sub> does not prefer another oxazolidinone modification, TAA2CC<sub>20</sub> (lane 3). In the absence of HD, no shifted band is observed (lane 1).

Next we investigated the role of the two mutations in the hydrophobic core of the homeodomain by mutating these residues back to the wild-type sequence, either individually (HD<sub>i</sub> I47G, I45V and HD<sub>i</sub> I47G, K52M) or together (HD<sub>i</sub> I47G). In electrophoretic mobility shift assays (EMSAs) using either modified or unmodified DNA strands, we were surprised to find that HD<sub>i</sub> I47G functioned with specificity and affinity comparable with HD<sub>Φ</sub> (Table 5.1 and Fig 5.3). While the conditions presented also suggest the selectivity of HDs lacking the hydrophobic mutations is somewhat depressed, the importance of this result is mitigated by modest variability of the selectivities observed under different conditions. Nonetheless, under all conditions tested, HD<sub>Φ</sub> is the tightest and most selective HD, demonstrating that HD<sub>Φ</sub> binds with the desired specificity for TAA1CC<sub>20</sub>.

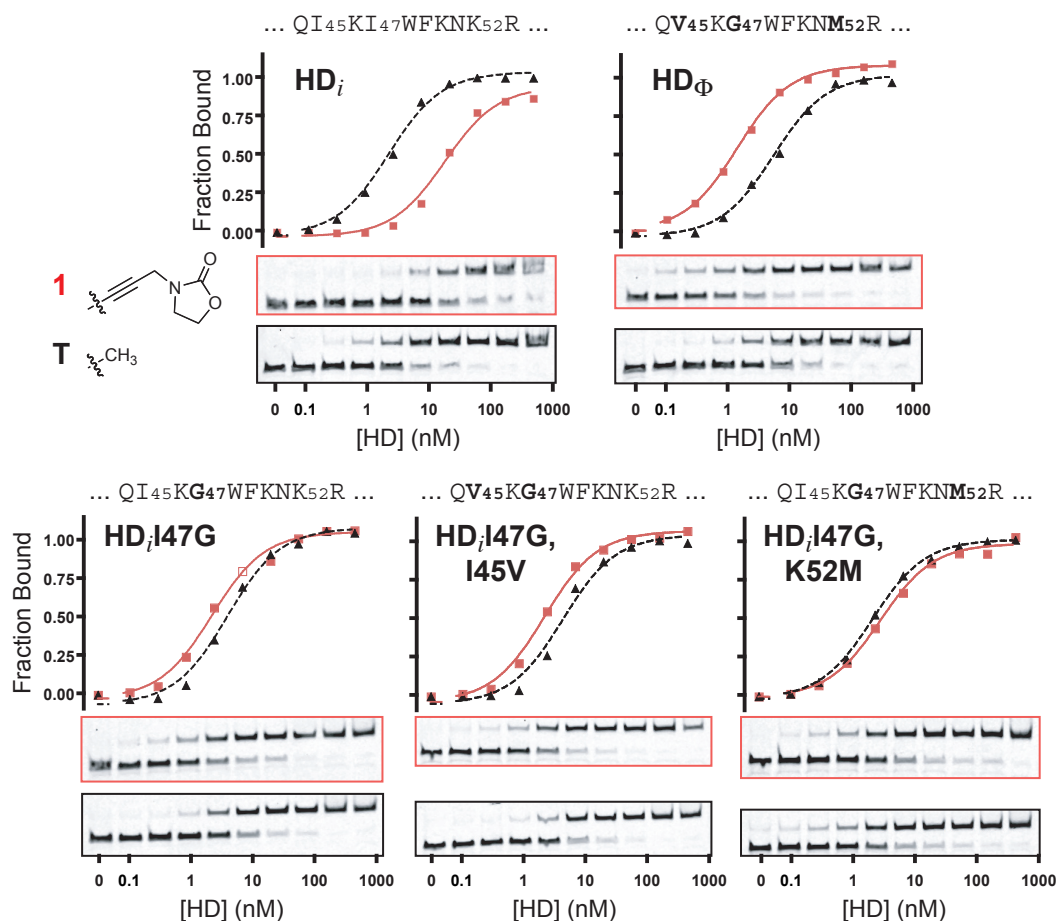


Figure 5.3: Biochemical dissection of the mutations that comprise  $HD_{\Phi}$ . EMSA were performed with  $TAATCC_{20}$  ( $\blacktriangle$ , dashed) and  $TAA1CC_{20}$  (red  $\blacksquare$ , red solid) to determine the relative binding affinities of HDs harboring one ( $HD_i$  I47G) or two ( $HD_i$  I47G, I45V and  $HD_i$  I47G, K52M) mutations.

Mutant	$K_d$ (nM)				$T_m$ ( $^{\circ}C$ )	$\Delta H$ (kcal/mol)
	$TAATCC_{20}$	$TAA1CC_{20}$	$TAATGC_{20}$	$TAATCG_{20}$		
$HD_i$	$2.1 \pm 0.3$	$17.8 \pm 3.5$	$8.8 \pm 0.2$	$6.0 \pm 1.0$	$52.6 \pm 0.7$	$-30 \pm 2$
$HD_{\Phi}$	$5.8 \pm 0.6$	$1.5 \pm 0.1$	$4.5 \pm 0.6$	$18.0 \pm 1.5$	$53.9 \pm 0.5$	$-36 \pm 2$
$HD_i$ I47G	$4.2 \pm 0.6$	$2.3 \pm 0.3$			$47.3 \pm 0.5$	$-29 \pm 1$
$HD_i$ I47G, I45V	$2.3 \pm 0.1$	$3.1 \pm 0.3$			$59.4 \pm 0.4$	$-36 \pm 2$
$HD_i$ I47G, K52M	$4.6 \pm 1.0$	$2.3 \pm 0.3$			$43.1 \pm 0.5$	$-26 \pm 1$

Table 5.1: Binding affinities and thermal stabilities for HD mutants.

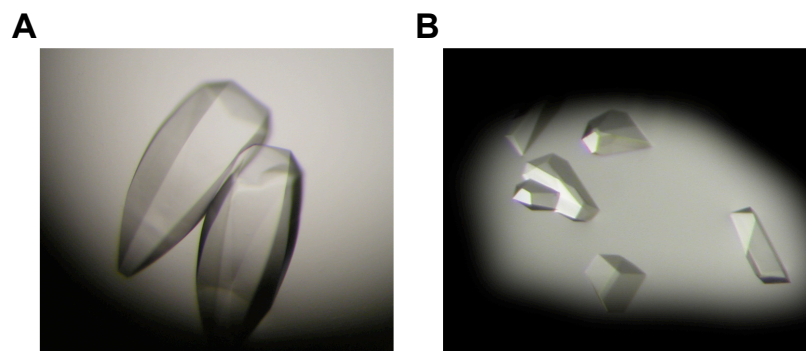


Figure 5.4: HD<sub>Φ</sub> requires high PEG-400 to crystallize.

A) Crystals grown in low (1%) PEG-400.

B) Crystals grown in high (20%) PEG-400 are isomorphous to those previously grown of HD<sub>i</sub>-TAATCC [15].

## 5.5 Structural Analysis of the Selected Mutant in Complex with DNA

To understand the structural basis for this re-engineered HD–DNA interaction, we solved x-ray crystal structures HD<sub>Φ</sub> in complex with both modified and unmodified DNA to 2.2 Å and 1.9 Å respectively (Fig 5.4 and Table 5.2). Analysis of the structures reveals that, despite the perturbation of the mutations in the HD and the modification to the DNA, HD<sub>Φ</sub> still adopts a canonical HD structure as judged by the nearly identical ribbon representations of C $\alpha$ -positions for the HD<sub>i</sub>-TAATCC, HD<sub>Φ</sub>-TAATCC and HD<sub>Φ</sub>-TAA1CC structures (Fig 5.5A). The oxazolidinone modification is clearly visible in the electron density (Fig 5.5B) and projects into the cavity created by the I47G mutation (Fig 5.5E). The average B factor of the oxazolidinone modification (34 Å<sup>2</sup>) is similar to the base to which it is connected (33 Å<sup>2</sup>) and is also similar to the average B factor of sidechains Lys50 (35 Å<sup>2</sup>) and Asn51 (37 Å<sup>2</sup>), suggesting that the oxazolidinone is well ordered within the context of the re-engineered interface. In the complex of HD<sub>Φ</sub> with unmodified DNA, the cavity created by the I47G mutation (compare Figure 5.5C and 5.5D) is occupied by three ordered water molecules (Fig

<b>Data Collection</b>			
DNA	TAA1CC	TAATCC	
PDB code	2HOT	2HOS	
Space group	C2	C2	
Unit cell parameters			
a (Å)	127.86	127.10	
b (Å)	45.05	45.03	
c (Å)	73.57	73.08	
$\beta$ (°)	118.65	118.41	
Wavelength (Å)	1.11588	1.11588	
Resolution (Å)	2.19 (2.27-2.19)	1.90 (1.97-1.90)	
Number of Observations			
Total	54,224	101,609	
Unique	19,157	29,027	
Completeness (%)	95.3 (76.7)	92.4 (62.6)	
Mosaicity (°)	0.68	0.61	
$R_{\text{sym}}^a$	0.040 (0.310)	0.033 (0.399)	
$\langle I/\sigma \rangle$	13.8 (2.6)	15.3 (2.1)	
<b>Refinement</b>			
Resolution range (Å)	65-2.19 (2.25-2.19)	35-1.90 (1.95-1.90)	
Number of observations used	15,928	23,285	
R value <sup>b</sup>	0.22	0.22	
$R_{\text{free}}^c$	0.26 (0.40)	0.26 (0.42)	
Free R fraction (%)	6.9	6.8	
Number of atoms			
Protein	938	976	
DNA	863	855	
Solvent	92	159	
Average B-factors			
Protein (Å <sup>2</sup> )	39	42	
DNA (Å <sup>2</sup> )	39	42	
Solvent (Å <sup>2</sup> )	40	48	
RMS differences in B-factor			
Between bonded main chain atoms (Å <sup>2</sup> )	0.6	0.7	
Between bonded side chain atoms (Å <sup>2</sup> )	1.5	1.7	
RMS deviations from ideality <sup>d</sup>			
Bond lengths (Å)	0.010	0.010	
Bond angles (°)	1.7	1.7	
Residues in core $\phi$ - $\psi$ regions (%)	99	100	
Residues in disallowed regions (%)	0	0	

Values in parentheses are for the highest resolution shell. <sup>a</sup> $R_{\text{sym}} = \sum_h \sum_i |I_i(h) - \langle I(h) \rangle| / \sum_h \sum_i I_i(h)$ , where  $I_i(h)$  is the  $i^{\text{th}}$  measurement and  $\langle I(h) \rangle$  is the mean intensity of symmetry-equivalent observations. <sup>b</sup> $R = \sum |F_{\text{obs}} - F_{\text{calc}}| / \sum F_{\text{obs}}$ , where  $F_{\text{obs}}$  and  $F_{\text{calc}}$  are the observed and calculated structure factors. <sup>c</sup> $R_{\text{free}}$  is the R value obtained from a set of diffraction data not used for refinement. <sup>d</sup>Root mean squared deviations are with respect to the Eng and Huber parameters.

Table 5.2: Crystallographic data and refinement.



5.5D). In both structures of HD<sub>Φ</sub>, with the exception of the waters immediately surrounding the modification and cavity, the waters at the protein DNA interface are similar to those found in the unengineered HD<sub>i</sub>-TAATCC interface.

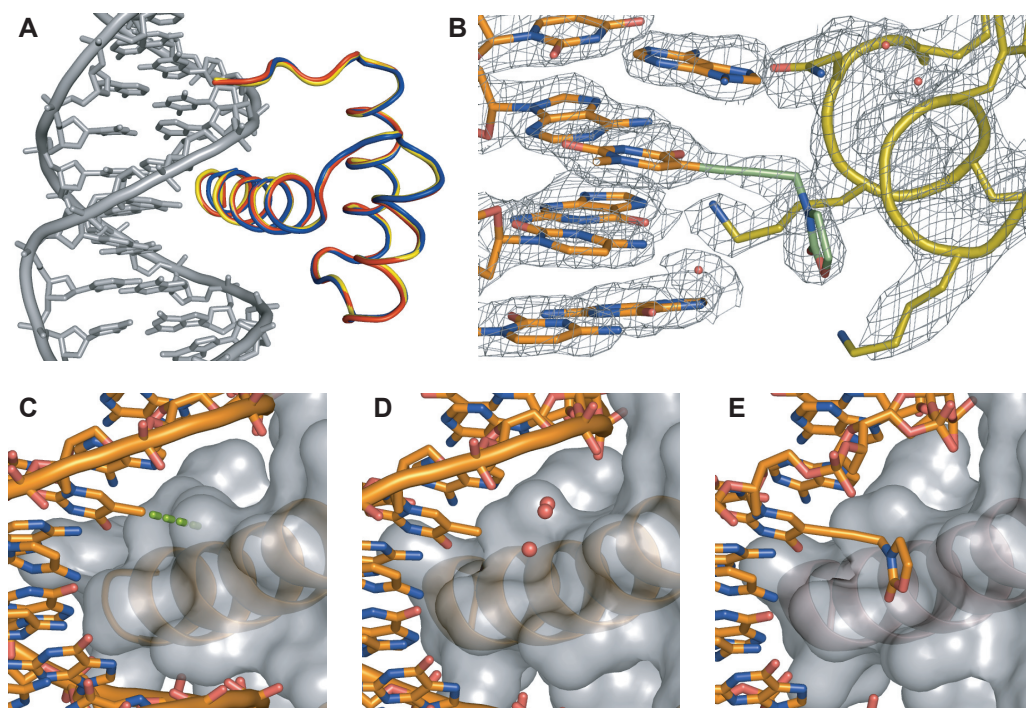


Figure 5.5: The structure of HD<sub>Φ</sub> bound to TAATCC and TAA1CC.

A) Ribbon overlay of HD-DNA complexes (HD<sub>i</sub>-TAATCC [15] in blue, HD<sub>Φ</sub>-TAA1CC in red and HD<sub>Φ</sub>-TAATCC in yellow).

B) Electron density in the vicinity of the alkynyl nucleoside.  $2F_o - F_c$  electron density from a simulated-annealing composite omit map is contoured at  $1\sigma$ .

C) HD<sub>i</sub>-TAATCC. The hydrophobic contact between Ile47 and the C5-methyl of thymidine in the recognition sequence TAATTCC is indicated by green dashes.

D) HD<sub>Φ</sub>-TAATCC. Three waters shown in red occupy the cavity created by the I47G mutation in HD<sub>Φ</sub>. For clarity, only these three waters are displayed.

E) HD<sub>Φ</sub>-TAA1CC. The oxazolidinone substituent packs against the cavity created by I47G and displaces the three waters seen in D).

In the structure of HD<sub>i</sub> bound to TAATCC, residue Lys50 contacts the last two bases through two alternate conformations allowing it to bind specifically to both base pairs [15]. However, in the electron density for HD<sub>Φ</sub> bound to either TAA1CC (Fig 5.6) or

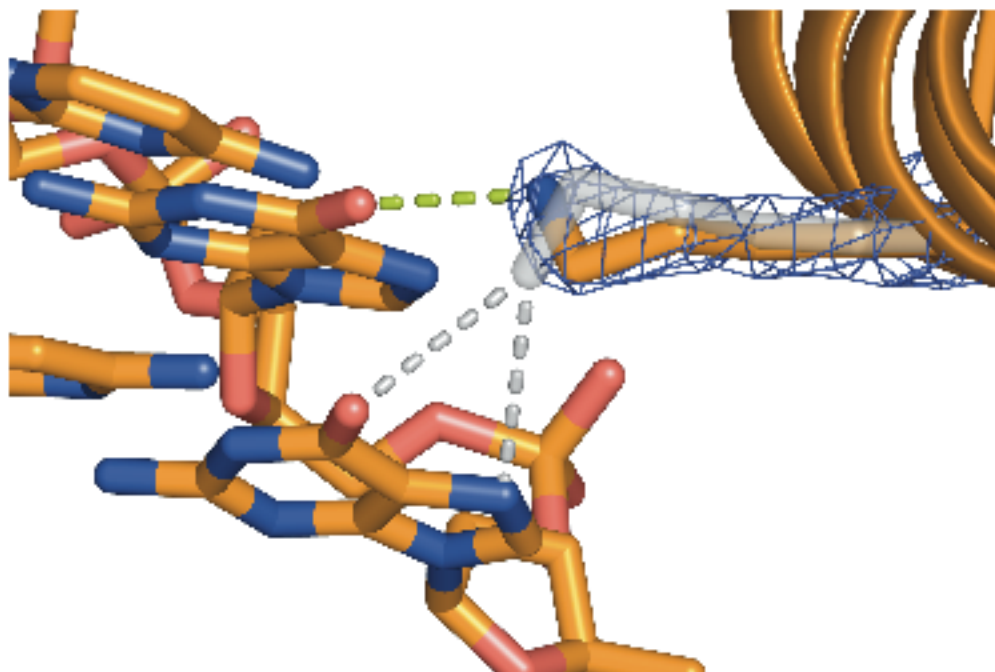


Figure 5.6: Conformation of Lys50.

The  $2F_o - F_c$  electron density from  $HD_\Phi$ -TAATCC contoured at  $2\sigma$  in the vicinity of Lys50. Lys50 makes a hydrogen bond (green dashes) to guanosine opposite C5 in the recognition sequence TAATCC. In the structure of  $HD_i$ -TAATCC [15] Lys50 adopts an alternate conformation (gray) that makes hydrogen bonds (gray dashes) to guanosine opposite C6 in the recognition sequence TAATCC. Consistent with the electron density, Lys50 in  $HD_\Phi$ -TAATCC (shown here) and  $HD_\Phi$ -TAA1CC (not shown) has been modeled in a single conformation (shown here in orange).

TAATCC, K50 only occupies one of these conformations, with no apparent structural basis for specifying the final base TAATCC. To test if  $HD_\Phi$  has decreased specificity for the last C-G base pair (TAATCC) compared to the previous C-G base-pair (TAATCC),  $HD_\Phi$  and  $HD_i$  binding to TAATCG and TAATGC were assayed by EMSA (Fig 5.7). We found that  $HD_\Phi$  retains specificity for the final basepair despite the single orientation of Lys50 observed in the crystal structure. Furthermore, we found that  $HD_\Phi$  binding to its preferred DNA target is competed at approximately the same concentration of salmon sperm DNA as was found for  $HD_i$  (Fig 5.7C).

We next turned our attention to the two hydrophobic mutations, I45V and K52M found

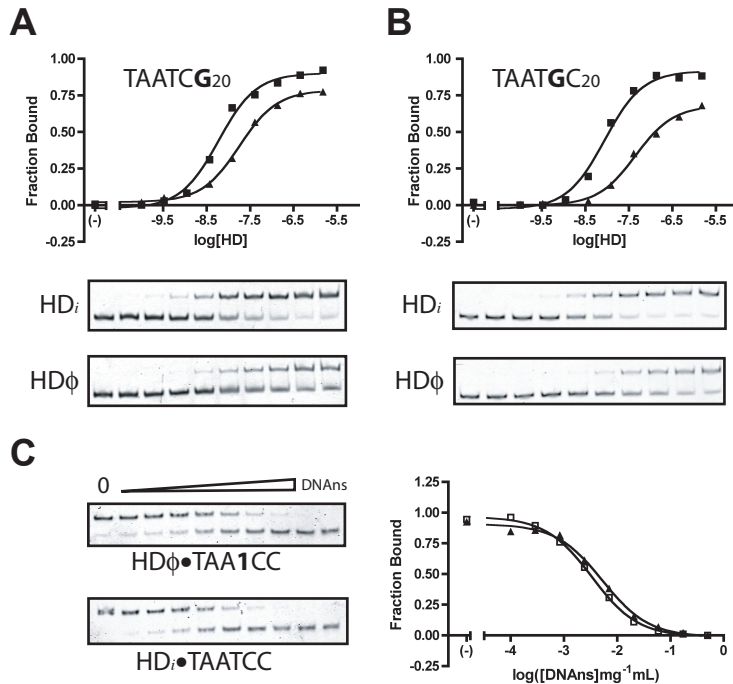


Figure 5.7: The specificity of HD<sub>i</sub> and HD<sub>Φ</sub> for the final two basepairs of TAATCC. A) The affinity of HD<sub>i</sub> (■) and HD<sub>Φ</sub> (▲) for TAATCG. B) The affinity of HDs for TAATGC. C) Binding of HD<sub>Φ</sub> to TAA1CC (▲) and HD<sub>i</sub> to TAATCC (□) in the presence of competing salmon sperm DNA. The associated gels are shown below each curve.

in HD<sub>Φ</sub>. Examining the region of HD<sub>Φ</sub> around Val45 revealed only minor changes relative to HD<sub>i</sub> such electron density best explained by Ser35 adopting a second conformation. It is possible that this second conformation requires the slightly reduced steric volume of the I45V mutation, but the importance of this second conformation is unclear. Examination of the environment surrounding the K52M mutation reveals that this mutation could relieve electrostatic repulsion caused by three lysine residues (K17, K52 and K55) in close proximity to one another. Engrailed is a member of a small subset of homeodomains that have basic amino acids at both position 17 and position 52. Most homeodomains possess a salt bridge between Glu17 and Arg52 in the homeodomain consensus sequence [27]. The high density of positive charge caused by the presence of K17, K52 and K55 is destabilizing and can be relieved by K52A and K52E mutations, which stabilize engrailed HD as previously demonstrated [28]. This result suggests that K52M may impact protein stability and led us to wonder more generally about the effects of the HD<sub>Φ</sub> mutations on HD stability.

## 5.6 Analysis of the Stability of the Selected Mutant

To examine the stability of the HDs used in this study, we monitored their thermal denaturation by CD spectroscopy (Fig 5.8). Starting with HD<sub>i</sub>, introducing the I47G mutation is destabilizing to the protein ( $\Delta T_m -5.3$  °C). In general, the replacement of an amino acid with glycine is destabilizing because the unfolded state of the protein is entropically stabilized by extra conformations available to glycine [29] especially in an alpha helix [30]. As predicted from the relief of repulsive charge-charge interactions, the K52M mutation is stabilizing, not only recovering the stability lost by I47G, but further stabilizing HD<sub>Φ</sub> V45I to a net 6.8 °C above HD<sub>i</sub>. The dramatic stabilizing effect of the K52M mutation is consistent with the notion that selection favored HDs with stabilizing mutations, but more surprising, the other mutation, I45V, destabilizes the HD by 4–6 °C, depending on the sequence context,

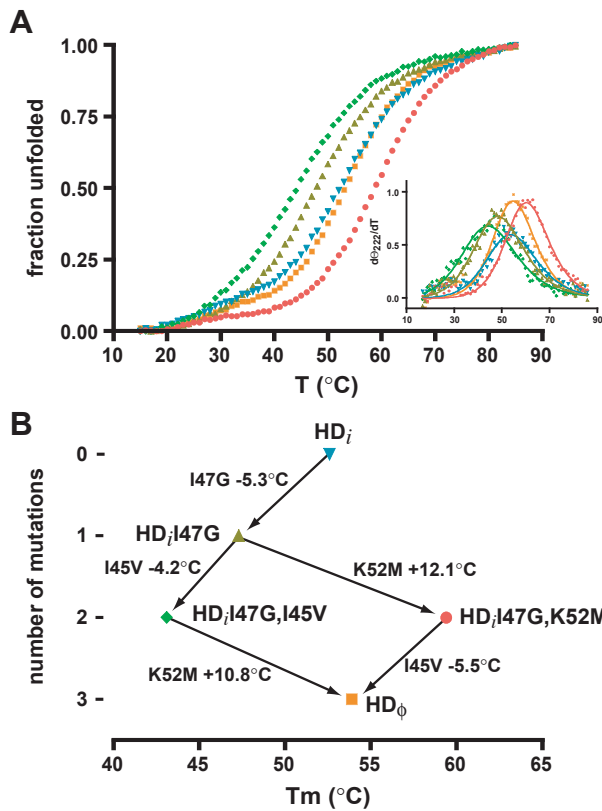


Figure 5.8: Analysis of the effect of HD<sub>Φ</sub> mutations on HD stability.

A) CD spectroscopy was used to monitor the thermal denaturation of HDs. The derivative of the CD curve was used to determine the melting temperature (inset) [31]. The colors and symbols for each mutant are shown in B) along with the effects of mutations on the thermal stability of the mutant HDs.

bringing the net thermal stability of HD $_{\Phi}$  close to that of HD $_i$  (Fig 5.8B and Table 5.1). The phage selected mutations re-tuned the stability of the HD, leading to similar stabilities of HD $_{\Phi}$  with HD $_i$ .

## 5.7 Conclusions

Despite the high conservation of HD–DNA contacts, particularly Gln/Lys50, Asn51 and Ile/Val47, using phage display and nucleoside chemistry we were able to re-engineer the HD–DNA interface, completely disrupting one of the conserved contacts (Ile47–T4) and replacing it with an elaborated nucleoside that packs against the cavity created by an I47G mutation. Although these modification represent a dramatic perturbation, the high resolution structure of this interface reveals that the selected mutant functions without affecting the HD fold. Furthermore we found that the selected mutations tuned the stability of the selected HD to be similar to the starting HD. Analysis of the HD $_{\Phi}$ –TAA1CC interaction reported here demonstrates that even highly conserved interfaces, such as the homeodomain–DNA interface, contain sufficient adaptability to allow the installation of novel function—in this case specific binding to modified DNA. This latent adaptability is of importance to protein engineers who wish to make tractable the enormity of the proteome by exploiting its conserved motifs and domains, including the homeodomain.

## 5.8 Materials and Methods

### Synthesis

The synthesis of alkynes **1** and **3**, and their corresponding nucleosides have been reported previously [20].

## **Phage Library Construction and Selection**

The phage library used for these selections and the conditions for the selections have been published elsewhere [20].

## **Expression and Purification of Mutant HDs**

Mutations were introduced using QuikChange mutagenesis. Expression and purification of the HDs were carried out using maltose binding fusions and subsequent Factor Xa cleavage according to the manufacturers instructions (NEB) with the following exceptions. After loading, the MBP column was rinsed with 10 column volumes of a high salt buffer (1M NaCl, 20 mM HEPES pH 7.6, 1 mM EDTA, 0.001% (w/v) NaN<sub>3</sub>) to remove DNA contaminants. The bound material was eluted into ammonium acetate (50 mM) with maltose (10 mM) and the eluent was lyophilized. The resulting white powder was resuspended to 3.3 mM in 100 mM ammonium acetate and treated with Factor Xa (0.05 mg/mL) for 1 h at room temp.. Overcleavage of the N-terminal sequence GSDEKRPR was evident upon extended treatment, so the reaction conditions were carefully optimized and the desired protein purified using gel filtration over a superdex 75 prep grade column in 100 mM ammonium acetate. The HDs were further purified by reverse phase HPLC as necessary. Concentrations of the purified HDs were determined using the calculated extinction coefficient at 280 nM ( $6970 \text{ M}^{-1} \text{ cm}^{-1}$ ). The purity of the proteins was analyzed by denaturing PAGE (10–20% polyacrylamide, SDS/Tris-Glycine, Biorad) and the identity was established by MALDI-TOF on a Voyager-DE STR.

## **Conventional Electrophoretic Mobility Shift Assays**

Binding of the protein to DNA was determined essentially as described [20, 24] except using HDs cleaved from the maltose binding protein tag (see above), and the following conditions. DNA probes (0.5 nM) were combined with increasing concentrations of protein in assay buffer (100 mM KCl, 20 mM HEPES pH 7.6, 2 mM MgCl<sub>2</sub>, 1 mM EDTA, 5% glycerol, 0.02% NP-40, 0.1 μg/mL BSA). The binding reactions were incubated for at least 30 min. at room temp. and were then run on 15% 0.5 X TBE polyacrylamide gels (pre-run for at least 30 min. at 200 V) for approx. 35 min. at 200 V. The fluorescence was recorded on a Typhoon scanner, integrating the bound and free bands to determine the fraction bound. Apparent equilibrium dissociation constants were determined by fitting the fraction bound as a function of the Log [HD] to the sigmoidal dose-response model using GraphPad Prism [32].

## **Cy3/Cy5 Competition EMSA Analysis of HDs**

Competition EMSA experiments were performed essentially as described [20], except using the untagged homeodomain and a modified assay buffer (100 mM KCl, 20 mM HEPES pH 7.6, 2 mM MgCl<sub>2</sub>, 1 mM EDTA, 5% glycerol, 0.02% NP-40, 0.1 μg/mL BSA). Briefly, the HD (40 nM) was incubated with two competing probes (200 nM ea.), one Cy3-labeled, the other Cy5-labeled. Similar binding reactions were performed without competition to serve as Cy3 and Cy5 standards to facilitate quantification of the ratio bound (each channel was normalized to its respective standard).

## Circular Dichroism

Ellipticity at 222 nm ( $\Theta_{222}$ ) was followed as a function of temperature essentially as described [19, 22]. Pure lyophilized homeodomain was resuspended to 20  $\mu\text{M}$  in a buffer containing 20 mM potassium phosphate (pH 7.4) and 100 mM potassium chloride.  $\Theta_{222}$  of each sample in a 0.2 cm quartz cuvette was monitored at 1  $^{\circ}\text{C}$  intervals from 15 to 85  $^{\circ}\text{C}$  with one minute of equilibration at each temperature. A Jasco J-710 spectropolarimeter equipped with peltier temperature control acquired samples with a 10 second update interval, a 16 second response time and a 2 nm spectral bandwidth. After being heated to 85  $^{\circ}\text{C}$  the sample was returned to 15  $^{\circ}\text{C}$  and  $\Theta_{222}$  was re-measured to confirm that the denaturation was reversible. Initial and final measurements of  $\Theta_{222}$  at 15  $^{\circ}\text{C}$  differed by less than 10%. Melting temperature and enthalpy of denaturation were determined by fitting the derivative of the denaturation curves to the van't Hoff difference equation [31]. Fitting the difference data obviates the need to fit baselines to the data thus reducing the number of free parameters available to the fit. Thermal denaturation curves were numerically differentiated, smoothed over a 3  $^{\circ}\text{C}$  window and fit to the van't Hoff difference equation using Levenberg-Marquardt least squares minimization (Fig 5.8A inset) using scripts written in Matlab [33].

## Crystallization and Cryo-Protection

Crystals grew in hanging drop essentially as described [21] except that a higher concentration of PEG-400 was used in the well solution. DNA strands were resuspended to 1 mM in 3 M ammonium acetate and annealed by repeated cycles of heating and cooling in a thermal cycler. HD $\Phi$  was also resuspended to 1 mM in 10 mM bis-tris propane (pH 7.0). HD $\Phi$ -DNA complex was formed by mixing 2 parts DNA duplex with 1 part HD $\Phi$ . Hanging drops were formed by combining 1  $\mu\text{l}$  HD $\Phi$ -DNA with 1  $\mu\text{l}$  of a well solution containing PEG-400 and a lower (100–250 mM) concentration of ammonium acetate. Initially we prepared



hanging drops using a well solution containing 250 mM ammonium acetate and 1% (v/v) PEG-400. These drops yielded crystals shaped like partial footballs that diffracted poorly and had unit cell parameters of  $a = 68 \text{ \AA}$ ,  $b = 68 \text{ \AA}$ ,  $c = 211 \text{ \AA}$ ,  $\alpha = 90^\circ$ ,  $\beta = 89^\circ$  and  $\gamma = 60^\circ$  when indexed in P1 (Supplementary Figure 3, panel a). Raising the concentration of PEG-400 yielded a different crystal form (Supplementary Figure 3, panel b) that diffracted better and indexed in C2 with unit cell parameters  $a = 127 \text{ \AA}$ ,  $b = 45 \text{ \AA}$ ,  $c = 73 \text{ \AA}$  and  $\beta = 118^\circ$  (isomorphous to published crystals of HD<sub>i</sub>-TAATCC [15]). 20% (v/v) PEG-400 and 100 mM ammonium acetate is an optimal well solution for growing this crystal form. Crystals were cryo-protected by the slow (over several minutes) addition of glycerol to a final concentration of approximately 25%. When cryo-protecting the crystal used for the structure of HD<sub>Φ</sub> bound to TAATCC (PDB code 2HOS), 10% (v/v) 3-methyl-2-oxazolidinone was included in the cryo-protectant. Density at the crystal packing interface near Tyr25 of chain B has been modeled as 3-methyl-2-oxazolidinone.

## Data Collection and Refinement

Data were collected at the ALS beamline 8.3.1. Data were indexed, scaled and integrated with HKL2000 [34]. The starting model for HD<sub>Φ</sub> bound to TAATCC (PDB code 2HOS) was derived from the structure of HD<sub>i</sub> bound to the same DNA sequence (PDB code 2HDD, [15]) by removing all waters, replacing all mutated residues (45, 47 and 52) with glycine and setting the backbone occupancy of these residues to zero. Rigid body refinement followed by all atom refinement was performed using CNS [35]. At this stage, density consistent with the mutated residues was clear and these residues were modeled into the structure. Further refinement with TLS parameters was performed using Refmac [36] and waters were added using Coot [37]. In the 2HOS structure, five residues were each modeled in two conformations (Chain A: R18, N21, N23, S35 and Chain B: N21). Alternate conformations were only modeled when suggested by strong difference ( $F_o - F_c$ ) density and supported

by an omit map. 2HOS with no waters and a single conformation for all residues was used as the initial model for HD<sub>ϕ</sub> bound to TAA1CC (PDB code 2HOT). After initial refinement with Refmac, the alkynyl oxazolidinone modification at T14 was clear. Modeling of the oxazolidinone modification into the structure was followed by additional cycles of refinement and addition of waters. No residues were modeled with alternate conformations in the 2HOT structure. Structure graphics were generated using Pymol [38]. CNS was used to generate a simulated-annealing composite omit map from the 2HOT coordinates (Figure 2, panel b).

### Accession Codes

Structure factors and final coordinates have been deposited in the RCSB PDB with ID codes 2HOT and 2HOS for HD<sub>ϕ</sub> bound to TAA1CC and TAATCC respectively.

### References

- 1) Bishop, A. C., Shah, K., Liu, Y., Witucki, L., Kung, C., and Shokat, K. M. (1998) Design of allele-specific inhibitors to probe protein kinase signaling, *Curr. Biol.* 8, 257–266.
- 2) Bishop, A. C., Buzko, O., and Shokat, K. M. (2001) Magic bullets for protein kinases, *Trends Cell Biol.* 11, 167–172.
- 3) Bishop, A. C., Ubersax, J. A., Petsch, D. T., Matheos, D. P., Gray, N. S., Blethrow, J., Shimizu, E., Tsien, J. Z., Schultz, P. G., Rose, M. D., Wood, J. L., Morgan, D. O., and Shokat, K. M. (2000) A chemical switch for inhibitor-sensitive alleles of any protein kinase, *Nature* 407, 395–401.

- 4) Hwang, Y. W., and Miller, D. L. (1987) A mutation that alters the nucleotide specificity of elongation factor Tu, a GTP regulatory protein, *J. Biol. Chem.* 262, 13081–13085.
- 5) Bishop, A., Buzko, O., Heyeck-Dumas, S., Jung, I., Kraybill, B., Liu, Y., Shah, K., Ulrich, S., Witucki, L., Yang, F., Zhang, C., and Shokat, K. M. (2000) Unnatural ligands for engineered proteins: new tools for chemical genetics, *Annu. Rev. Biophys. Biomol Struct.* 29, 577–606.
- 6) Weijland, A., Parlato, G., and Parmeggiani, A. (1994) Elongation factor Tu D138N, a mutant with modified substrate specificity, as a tool to study energy consumption in protein biosynthesis, *Biochemistry* 33, 10711–10717.
- 7) Weijland, A., and Parmeggiani, A. (1993) Toward a model for the interaction between elongation factor Tu and the ribosome, *Science* 259, 1311–1314.
- 8) Atwell, S., Ultsch, M., De Vos, A. M., and Wells, J. A. (1997) Structural plasticity in a remodeled protein-protein interface, *Science* 278, 1125–1128.
- 9) Greisman, H. A., and Pabo, C. O. (1997) A general strategy for selecting high-affinity zinc finger proteins for diverse DNA target sites, *Science* 275, 657–661.
- 10) Pabo, C. O., Peisach, E., and Grant, R. A. (2001) Design and selection of novel Cys2His2 zinc finger proteins, *Annu. Rev. Biochem.* 70, 313–340.
- 11) Segal, D. J., Dreier, B., Beerli, R. R., and Barbas, C. F., 3rd. (1999) Toward controlling gene expression at will: selection and design of zinc finger domains recognizing each of the 5'-GNN-3' DNA target sequences, *Proc. Natl. Acad. Sci. U. S. A.* 96, 2758–2763.
- 12) Kortemme, T., and Baker, D. (2004) Computational design of protein-protein interactions, *Curr. Opin. Chem. Biol.* 8, 91–97.

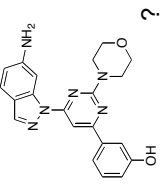
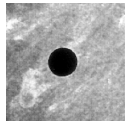
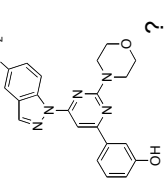
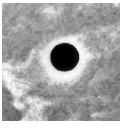
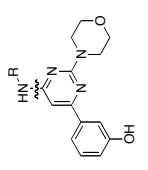
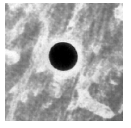
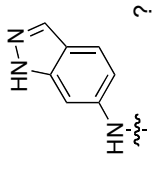
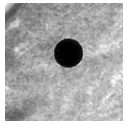
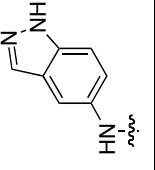
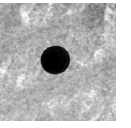
- 13) Allen, J. J., Lazerwith, S. E., and Shokat, K. M. (2005) Bio-orthogonal affinity purification of direct kinase substrates, *J. Am. Chem. Soc.* 127, 5288–5289.
- 14) Gehring, W. J., Affolter, M., and Burglin, T. (1994) Homeodomain proteins, *Annu. Rev. Biochem.* 63, 487–526.
- 15) Tucker-Kellogg, L., Rould, M. A., Chambers, K. A., Ades, S. E., Sauer, R. T., and Pabo, C. O. (1997) Engrailed (Gln50→Lys) homeodomain-DNA complex at 1.9 Å resolution: structural basis for enhanced affinity and altered specificity, *Structure* 5, 1047–1054.
- 16) Clarke, N. D., Kissinger, C. R., Desjarlais, J., Gilliland, G. L., and Pabo, C. O. (1994) Structural studies of the engrailed homeodomain, *Protein Sci.* 3, 1779–1787.
- 17) Fraenkel, E., Rould, M. A., Chambers, K. A., and Pabo, C. O. (1998) Engrailed homeodomain-DNA complex at 2.2 Å resolution: a detailed view of the interface and comparison with other engrailed structures, *J. Mol. Biol.* 284, 351–361.
- 18) Kissinger, C. R., Liu, B. S., Martin-Blanco, E., Kornberg, T. B., and Pabo, C. O. (1990) Crystal structure of an engrailed homeodomain-DNA complex at 2.8 Å resolution: a framework for understanding homeodomain-DNA interactions, *Cell* 63, 579–590.
- 19) Ades, S. E., and Sauer, R. T. (1994) Differential DNA-binding specificity of the engrailed homeodomain: the role of residue 50, *Biochemistry* 33, 9187–9194.
- 20) Simon, M. D., and Shokat, K. M. (2004) Adaptability at a protein-DNA interface: re-engineering the engrailed homeodomain to recognize an unnatural nucleotide, *J. Am. Chem. Soc.* 126, 8078–8079.
- 21) Grant, R. A., Rould, M. A., Klemm, J. D., and Pabo, C. O. (2000) Exploring the

- role of glutamine 50 in the homeodomain-DNA interface: crystal structure of engrailed (Gln50→Ala) complex at 2.0 Å, *Biochemistry* 39, 8187–8192.
- 22) Ades, S. E., and Sauer, R. T. (1995) Specificity of minor-groove and major-groove interactions in a homeodomain-DNA complex, *Biochemistry* 34, 14601–14608.
- 23) He, J., and Seela, F. (2002) Propynyl groups in duplex DNA: stability of base pairs incorporating 7-substituted 8-aza-7-deazapurines or 5-substituted pyrimidines, *Nucleic Acids Res.* 30, 5485–5496.
- 24) Simon, M. D., Sato, K., Weiss, G. A., and Shokat, K. M. (2004) A phage display selection of engrailed homeodomain mutants and the importance of residue Q50, *Nucleic Acids Res.* 32, 3623–3631.
- 25) Sato, K., Simon, M. D., Levin, A. M., Shokat, K. M., and Weiss, G. A. (2004) Dissecting the Engrailed homeodomain-DNA interaction by phage-displayed shotgun scanning, *Chem. Biol.* 11, 1017–1023.
- 26) Banerjee-Basu, S., and Baxevanis, A. D. (2001) Molecular evolution of the homeodomain family of transcription factors, *Nucleic Acids Res.* 29, 3258–3269.
- 27) Clarke, N. D. (1995) Covariation of residues in the homeodomain sequence family, *Protein Sci.* 4, 2269–2278.
- 28) Stollar, E. J., Mayor, U., Lovell, S. C., Federici, L., Freund, S. M., Fersht, A. R., and Luisi, B. F. (2003) Crystal structures of engrailed homeodomain mutants: implications for stability and dynamics, *J. Biol. Chem.* 278, 43699–43708.
- 29) Matthews, B. W., Nicholson, H., and Becktel, W. J. (1987) Enhanced protein thermostability from site-directed mutations that decrease the entropy of unfolding, *Proc. Natl. Acad. Sci. U. S. A.* 84, 6663–6667.

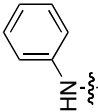
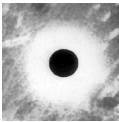
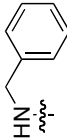
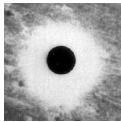
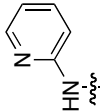
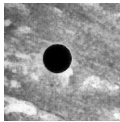
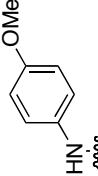
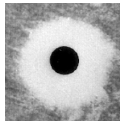
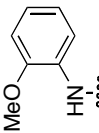
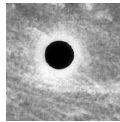
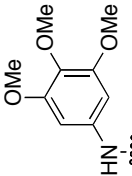
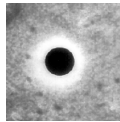
- 30) Serrano, L., Neira, J. L., Sancho, J., and Fersht, A. R. (1992) Effect of alanine versus glycine in alpha-helices on protein stability, *Nature* 356, 453–455.
- 31) John, D. M., and Weeks, K. M. (2000) van't Hoff enthalpies without baselines, *Protein Sci.* 9, 1416–1419.
- 32) Motulsky, H., and Christopoulos, A. (2004) *Fitting Models to Biological Data Using Linear and Nonlinear Regression: A Practical Guide to Curve Fitting*, Oxford University Press, New York, NY.
- 33) (2004) *Statistics Toolbox User's Guide*, The Mathworks, Natick, MA.
- 34) Otwinowski, Z. and Minor, W. (2003) Processing of X-ray diffraction data collected in oscillation mode, *Methods Enzymol.* 276, 307–326.
- 35) Brunger, A. T., Adams, P. D., Clore, G. M., DeLano, W. L., Gros, P., Grosse-Kunstleve, R. W., Jiang, J. S., Kuszewski, J., Nilges, M., Pannu, N. S., Read, R. J., Rice, L. M., Simonson, T., and Warren, G. L. (1998) Crystallography & NMR system: A new software suite for macromolecular structure determination, *Acta Crystallogr. D Biol. Crystallogr.* 54, 905–921.
- 36) Winn, M. D., Isupov, M. N., and Murshudov, G. N. (2001) Use of TLS parameters to model anisotropic displacements in macromolecular refinement, *Acta Crystallogr. D Biol. Crystallogr.* 57, 122–133.
- 37) Emsley, P., and Cowtan, K. (2004) Coot: model-building tools for molecular graphics, *Acta Crystallogr. D Biol. Crystallogr.* 60, 2126–2132.
- 38) DeLano, W. L. (2002) *The PyMOL Molecular Graphics System*, <http://www.pymol.org>.

# **Appendix**

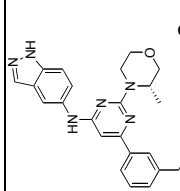
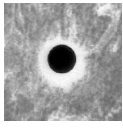
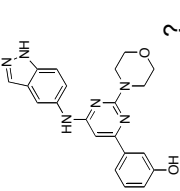
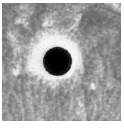
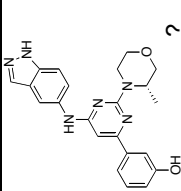
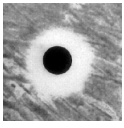
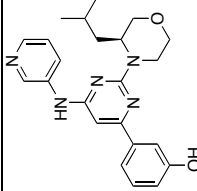
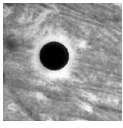
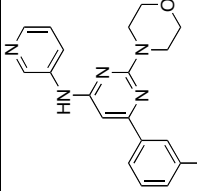
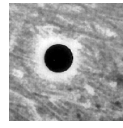
## **Morpholino-Pyridine Inhibitors of the PI3-K Family**

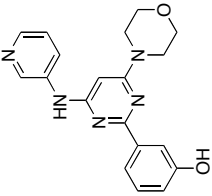
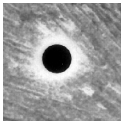
Name	Structure or R	M+H	IC <sub>50</sub> μM							Yeast Halo (YRP)
			p110α	p110β	p110δ	p110γ	DNA-PK	mTOR		
MF11a		389.1	0.056	0.62	0.16	0.66	0.055	>10		
MF14a		389.1	0.068	0.79	0.19	1.0	0.12	1.3		
MF9		310.2	0.042	0.18	0.39	0.72	0.158	0.77		
MF11b		389.1	0.049	0.29	0.11	3.8	0.13	>10		
MF14b		389.1	0.025	0.45	0.78	1.9	0.082	0.35		



Name	Structure or R	M+H	IC <sub>50</sub> $\mu$ M						Yeast Halo (YRP)
			p110 $\alpha$	p110 $\beta$	p110 $\delta$	p110 $\gamma$	DNA-PK	mTOR	
73-1		349.2							
73-2		363.1							
73-5		350.0	0.032	0.27	0.18	2.7	0.10	0.40	
73-6		379.1	0.165	0.23	0.44	6.3	0.36	1.9	
73-7		379.1	0.205	2.0	0.71	8.4	0.37	4.7	
73-8		439.1							

Name	Structure or R	M+H	IC <sub>50</sub> $\mu$ M							Yeast Halo (YRP)
			p110 $\alpha$	p110 $\beta$	p110 $\delta$	p110 $\gamma$	DNA-PK	mTOR		
73-9		410.1	0.369	1.7	0.38	4.5	0.43	4.0		
73-10		400.1	0.429	3.0	0.25	1.3	0.33	1.8		
73-12		425.2	2.8	9.6	1.1	>10	1.7	>10		
MF16		378.1	0.251	0.84	0.74	2.5	0.38	1.3		
MF22		403.1	0.086	0.98	0.3	1.1	0.52	2.6		

Name	Structure or R	M+H	IC <sub>50</sub> $\mu$ M							Yeast Halo (YRP)
			p110 $\alpha$	p110 $\beta$	p110 $\delta$	p110 $\gamma$	DNA-PK	mTOR		
MF23		417.1	0.113	1.5	0.4	2.8	1.5	2.8		
MF24		389.1	0.073	1.0	0.42	0.84	0.110	0.85		
MF25		403.1	0.13	1.4	0.44	2.0	0.314	0.47		
MF33		406.6	6.6	2.3	1.7	>10	>10	13		
MF34a		350.5	0.042	0.18	0.39	0.72	0.158	0.77		

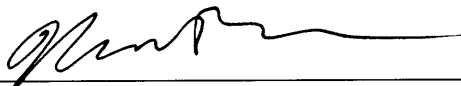
Name	Structure or R	M+H	IC <sub>50</sub> $\mu$ M							Yeast Halo (YRP)
			p110 $\alpha$	p110 $\beta$	p110 $\delta$	p110 $\gamma$	DNA-PK	mTOR		
MF34b		350.5	0.029	0.91	0.63	2.7	0.156	0.47		

**Publishing Agreement**

*It is the policy of the University to encourage the distribution of all theses, dissertations, and manuscripts. Copies of all UCSF theses, dissertations, and manuscripts will be routed to the library via the Graduate Division. The library will make all theses, dissertations, and manuscripts accessible to the public and will preserve these to the best of their abilities, in perpetuity.*

***Please sign the following statement:***

*I hereby grant permission to the Graduate Division of the University of California, San Francisco to release copies of my thesis, dissertation, or manuscript to the Campus Library to provide access and preservation, in whole or in part, in perpetuity.*



\_\_\_\_\_  
Author Signature

8/31/09

\_\_\_\_\_  
Date